
Electronic Theses and Dissertations, 2004-2019

2015

Towards High-Flux Isolated Attosecond Pulses with a 200 TW CPA

Eric Cunningham
University of Central Florida

 Part of the [Electromagnetics and Photonics Commons](#), and the [Optics Commons](#)
Find similar works at: <https://stars.library.ucf.edu/etd>
University of Central Florida Libraries <http://library.ucf.edu>

This Doctoral Dissertation (Open Access) is brought to you for free and open access by STARS. It has been accepted for inclusion in Electronic Theses and Dissertations, 2004-2019 by an authorized administrator of STARS. For more information, please contact STARS@ucf.edu.

STARS Citation

Cunningham, Eric, "Towards High-Flux Isolated Attosecond Pulses with a 200 TW CPA" (2015). *Electronic Theses and Dissertations, 2004-2019*. 1450.
<https://stars.library.ucf.edu/etd/1450>

TOWARDS HIGH-FLUX ISOLATED ATTOSECOND PULSES WITH A 200 TW CPA

by

ERIC CUNNINGHAM
B.S. Brigham Young University, 2009
M.S. Brigham Young University, 2011

A dissertation submitted in partial fulfillment of the requirements
for the degree of Doctor of Philosophy
in CREOL, the College of Optics & Photonics
at the University of Central Florida
Orlando, Florida

Fall Term
2015

Major Professor: Zenghu Chang

© 2015 Eric Cunningham

ABSTRACT

Attosecond pulses have been developed as a means for investigating phenomena that proceed on the order of the atomic unit of time (24 as). Unfortunately, these extreme ultraviolet (XUV) pulses by themselves contain too few photons to initiate nonlinear dynamics or dress states in an attosecond pump–attosecond probe scheme. As a result, most attosecond experiments thus far have featured complementary near infrared (NIR) femtosecond lasers for instigating electron dynamics. In order to access the benefits of all-attosecond measurements and open attosecond physics to new fields of exploration, the photon flux of these pulses must be increased.

One way to boost the attosecond pulse energy is to scale up the energy of the NIR pulse responsible for driving high-harmonic generation (HHG). With generalized double optical gating (GDOG), isolated attosecond pulses can be generated with *multi*-cycle laser systems, wherein the pulse energy can be boosted more easily than in the *few*-cycle laser systems required by other gating methods. At the Institute for the Frontier of Attosecond Science and Technology (IFAST), this scalability was demonstrated using a 350 mJ, 15 fs (10 TW) Ti:sapphire laser, which was used to generate a 100 nJ XUV continuum. This represented an order-of-magnitude improvement over typical attosecond pulse energies achievable by millijoule-level few-cycle lasers.

To obtain the microjoule-level attosecond pulse energy required for performing all-attosecond experiments, the attosecond flux generated by the IFAST 10 TW system was still deficient by an order of magnitude. To this end, the laser system was upgraded to provide joule-level output energies while maintaining pulse compression to 15 fs, with a targeted peak power of 200 TW. This was accomplished by adding an additional Ti:sapphire amplifier to the existing 10 TW system and implementing a new pulse compression system to accommodate the higher pulse energy.

Because this system operated at a 10 Hz repetition rate, stabilization of the carrier-envelope phase

(CEP) – important for controlling attosecond pulse production – could not be achieved using traditional methods. Therefore, a new scheme was developed, demonstrating the first-ever control of CEP in a chirped-pulse amplifier (CPA) at low repetition rates.

Finally, a new variation of optical gating was proposed as a way to improve the efficiency of the attosecond pulse generation process. This method was also predicted to allow for the generation of isolated attosecond pulses with longer driving laser pulses, as well as the extension of the high-energy photon cut-off of the XUV continuum.

To E. J.

ACKNOWLEDGMENTS

The work of this thesis would not have been possible without the contributions of countless individuals.

First, I acknowledge my advisor, Dr. Zenghu Chang.

I acknowledge the impact of many group members, including Dr. Yi Wu, Dr. Kun Zhao, Dr. Michael Chini, Dr. Xiaowei Wang, Dr. Qi Zhang, Dr. Yan Cheng, Dr. Xiaoming Ren, Dr. Yanchun Yin, Jie Li, Yang Wang, Jian Zhao, Tianyi Guo, Wenxu Zhang, Yiduo Zhan, Huaping Zang, Adrian Tatulian, Jing Wu, and Matthew Suttinger.

I acknowledge the leadership of the CREOL and physics department faculty, especially my committee members Dr. M.J. Soileau, Dr. Bahaa Saleh, and Dr. Haripada Saha.

I acknowledge the support staff of UCF, including (but certainly not limited to) Dave Bradford, Jessica Brooks, Monika Crittenden, Deon Frank, Rachel Franzetta, Sara Reese, Elizabeth Rivera, Denise Whiteside, Richard Zotti, and all members at the UCF Creative School for Children.

I acknowledge the tremendous support of the CREOL, UCF, and Orlando communities at large.

I acknowledge the immeasurable role of friends and family members, especially my parents and my late wife.

TABLE OF CONTENTS

LIST OF FIGURES	xii
CHAPTER 1: INTRODUCTION	1
1.1 An Historical Glance at the Need for Higher Optical Power	1
1.1.1 Flash Photolysis	1
1.1.2 The First Laser	3
1.2 Attosecond Physics	5
1.3 Dissertation Outline	7
CHAPTER 2: A 200 TW Ti:SAPPHIRE LASER	9
2.1 General Design Considerations	9
2.1.1 History and Concept of Chirped Pulse Amplification	9
2.1.2 Spectrum and Phase Correction in CPA Systems	12
2.1.2.1 Specialty Stretcher Construction	13
2.1.2.2 Gain-Competition Reduction	14
2.1.2.3 Gain-Reduction Competition	16
2.1.2.4 Spatial Light Modulation	18

2.1.2.5	Spectral Filtration	22
2.1.3	Transverse Lasing	25
2.2	IFAST 10 TW Laser [148]	27
2.2.1	Motivation	27
2.2.2	Laser Architecture	28
2.2.3	HHG from the IFAST 10 TW Laser	31
2.3	IFAST 200 TW Laser	35
2.3.1	200 TW Pulse Amplification	40
2.3.1.1	Ti:Sapphire Amplifier	40
2.3.1.2	Pumping Configuration	42
2.3.1.3	Index Matching	46
2.3.2	200 TW Pulse Compression	48
2.3.2.1	Grating Compressor	48
2.3.2.2	Plasma Cleaning	49
2.3.2.3	Spectral Shaping	50
CHAPTER 3: CARRIER-ENVELOPE PHASE CONTROL AT 10 Hz		55
3.1	Introduction to Carrier-Envelope Phase	55

3.1.1	Fundamental Concept	55
3.1.2	Influence on Physical Phenomena	56
3.2	Standard CEP Measurement and Stabilization Techniques	57
3.2.1	Oscillator Pulses (80 MHz)	59
3.2.2	Amplified Pulses (1 kHz)	60
3.3	Stabilization of the CEP at 10 Hz	62
3.3.1	Difficulty of Sub-kHz CEP Control	62
3.3.2	The “CEP Probe” Technique	63
3.4	CEP Control of the IFAST 10 TW Laser	64
3.4.1	Application of the CEP Probe Technique	64
3.4.2	Effect of CEP on Gated HHG	67
3.4.3	Difficulty of f-to-2f with 10 Hz Beam	67
3.5	CEP Control of the IFAST 200 TW Laser	69
CHAPTER 4: OPTICAL GATING WITH ASYMMETRIC FIELDS		71
4.1	Common Types of Optical Gating	71
4.1.1	Polarization Gating (PG)	72
4.1.2	Double Optical Gating (DOG)	74

4.1.3	Generalized Double Optical Gating (GDOG)	76
4.2	Asymmetric Gating	77
4.2.1	Physical Apparatus and Gating Parameters	78
4.2.2	Effect on Polarization Gate Position t_c	81
4.2.3	Effect on Pulse Separation T_d	83
4.2.4	Effect on HHG-Producing Field Amplitude $E_{drive}(t = t_c)$	84
4.2.5	Ionization Simulations	87
4.2.5.1	Longer Driving Pulse Duration	89
4.2.5.2	Improved Phase Matching	90
4.2.5.3	Higher Saturation Intensity	91
4.3	Simulating HHG from Asymmetric Fields in the Low-Ionization Regime	92
4.3.1	Simulation Results – Frequency Domain	93
4.3.2	Simulation Results – Time Domain	95
CHAPTER 5: OUTLOOK		101
5.1	Improve Pulse Energy and Stability Using a 4 J, Diode-Pumped Pump Laser	101
5.2	Attosecond Pulse Generation	102
5.3	Frequency-Domain Optical Parametric Amplification (FOPA)	105

APPENDIX A: NON-TIME-AVERAGED OPTICS FOR SUB-CYCLE INTERESTS . . . 108

APPENDIX B: GENERAL GATING FIELDS 115

APPENDIX C: COPYRIGHT PERMISSIONS 121

LIST OF REFERENCES 169

LIST OF FIGURES

Figure 1.1: Diagram of the experimental arrangement for performing flash photolysis. Adapted from [4] with permission of The Royal Society of Chemistry.	2
Figure 1.2: Bimolecular disappearance of Chloric Oxide (ClO). Adapted from [5] with permission of The Royal Society of Chemistry.	3
Figure 1.3: Energy levels of ruby. The two strongest lines correspond to S_{21} . Reprinted with permission from [11]. Copyright 1960 by the American Physical Society.	4
Figure 1.4: Apparatus for pulsed excitation of ruby. (Actual size, approximately 2×1 in. o.d.). Reprinted with permission from [13]. Copyright 1961 by the American Physical Society.	5
Figure 1.5: Example of a femtosecond pump–attosecond probe setup investigating helium [23].	6
Figure 2.1: The first demonstration of chirped pulse amplification. Reprinted from [48], with permission from Elsevier.	11
Figure 2.2: Examples of stretchers designed to reduce higher-order phase errors.	13
Figure 2.3: Elimination of gain competition via a spatially-dispersed resonator. Adapted from [81] with kind permission from Springer Science and Business Media.	14
Figure 2.4: Gain curve-flattened amplification using a spatially-modulated pump [82].	15

Figure 2.5: Multi-pump, spatially-dispersed, regenerative Ti:S amplifier. Reprinted from [83], with permission from Elsevier.	15
Figure 2.6: Multi-pump, spatially-dispersed, multi-pass Ti:S amplifier [84].	16
Figure 2.7: Negative and positive chirped pulse amplification (NPCPA). Adapted from [85] with kind permission from Springer Science and Business Media.	17
Figure 2.8: Shaping with opaque mask and dispersive material in a compressor [89].	18
Figure 2.9: Typical implementation of a liquid crystal spatial light modulator [92].	19
Figure 2.10: Depiction of a continuous-electrode LC-SLM [105].	20
Figure 2.11: Microlens array inside a zero-dispersion stretcher [106]. (© 1996 IEEE)	20
Figure 2.12: Two alternative transmissive elements used in a stretcher for pulse shaping.	21
Figure 2.13: Two typical reflective elements used to correct phase errors in a laser pulse.	21
Figure 2.14: Spectral filtering via etalon, spatial mask, and birefringent plate [91].	22
Figure 2.15: Spectral shaping using an AOPDF. Adapted from [131] with kind permission from Springer Science and Business Media.	24
Figure 2.16: Spectral shaping using an AOPGCF [135].	24
Figure 2.17: Key characteristics of the IFAST 10 TW laser system generating 15 fs. Reprinted with permission from [148]. Copyright 2013, AIP Publishing LLC.	29
Figure 2.18: Single-shot FROG trace of the IFAST 10 TW laser. Reprinted with permission from [148]. Copyright 2013, AIP Publishing LLC.	31

Figure 2.19: End station and HHG scheme for the IFAST 10 TW laser. Reprinted with permission from [148]. Copyright 2013, AIP Publishing LLC.	32
Figure 2.20: Beam profile at the focus of the IFAST 10 TW laser. Reprinted with permission from [148]. Copyright 2013, AIP Publishing LLC.	33
Figure 2.21: Generation of a 100 nJ XUV continuum capable of supporting 230 as pulses. Reprinted with permission from [148]. Copyright 2013, AIP Publishing LLC.	34
Figure 2.22: Early construction of the 200 TW amplifier at the IFAST lab.	35
Figure 2.23: Hollow-core fiber using a flexible fused silica waveguide.	37
Figure 2.24: The third-stage Ti:sapphire-based amplifier of the IFAST 200 TW laser system.	41
Figure 2.25: Broadband response of the third-stage amplifier in an early gain measurement.	41
Figure 2.26: Representation of the third-stage amplifier layout at the IFAST lab. At the time of writing, four PRO350 systems (represented by the green boxes in the top-middle) were available.	42
Figure 2.27: Relay imaging preserves the smooth pump profile output from the laser head.	43
Figure 2.28: Beam profiles of three pump beams (left) and amplified beam (right).	44
Figure 2.29: Utility closets constructed to house power supplies of the pump lasers for the IFAST 200 TW system.	45
Figure 2.30: Index-matched, ASE-absorbing cladding for suppressing parasitic lasing. . .	47
Figure 2.31: The grating compressor was designed to output 3 J, 15 fs pulses.	48

Figure 2.32: Pulse spectrum after various stages of the IFAST 200 TW system.	49
Figure 2.33: Recovery of a carbon-contaminated quartz plate before (left), during (center), and after (right) RF plasma cleaning.	50
Figure 2.34: A LCoS-SLM corrects phase errors to help with pulse compression. (Cour- tesy of Boulder Nonlinear Systems.)	52
Figure 2.35: FROG measurement of pulses compressed by the IFAST 200 TW compressor and LCoS-SLM.	54
Figure 3.1: The CEP describes the position of the electric field beneath the pulse envelope.	56
Figure 3.2: Attosecond flux from a two-color sub-cycle gate with (a) $\phi_{CE} = 0$ and (b) $\phi_{CE} = \pi/2$. Reprinted with permission from [181]. Copyright 2010 by the American Physical Society.	57
Figure 3.3: F-to-2f interferometry with oscillator pulses. Copyright 2010 Wiley. Used with permission from [205].	60
Figure 3.4: F-to-2f interferometry with amplified pulses.	61
Figure 3.5: Scheme for locking the CEP of the IFAST 1 kHz system.	61
Figure 3.6: The CEP probe provides phase information relevant to both beams.	63
Figure 3.7: Scheme for locking the CEP of the IFAST 10 Hz system.	64
Figure 3.8: Repeating structures in a 6π CEP scan of the gated HHG spectrum in argon. .	68
Figure 3.9: In-loop measurement of the 1 kHz probe beam through the 200 TW system. .	70

Figure 3.10: Demonstration of the CEP locking of the probe beam through the IFAST 200 TW compressor over a full work day. Notice the relative stability in the lab during the lunch hour.	70
Figure 4.1: Birefringent optics for polarization gating (PG): one multi-order full-wave plate and one zero-order half-wave plate.	73
Figure 4.2: Attosecond pulse spacing is only half as much when produced (a) with a fundamental field versus (b) with a fundamental field augmented by its second harmonic.	74
Figure 4.3: Birefringent optics for double optical gating (DOG): one multi-order full-wave plate and one zero-order half-wave plate comprised of a multi-order full-wave plate and a multi-order quarter-wave second-harmonic crystal. . . .	75
Figure 4.4: Birefringent optics for generalized double optical gating (GDOG): one multi-order full-wave plate, one Brewster window, and one zero-order half-wave plate comprised of a multi-order full-wave plate and a multi-order quarter-wave second-harmonic crystal.	76
Figure 4.5: Examples of symmetric and asymmetric gating fields [221]. (© 2015 IEEE) .	77
Figure 4.6: Birefringent optics for asymmetric generalized double optical gating [221]. (© 2015 IEEE)	78
Figure 4.7: An example of polarization-gated few-cycle pulses, demonstrating the cases of $\theta_1 = \cot^{-1}(1/2)$ (top row, 2:1 ratio), $\theta_1 = \cot^{-1}(1)$ (middle row, 1:1 ratio), and $\theta_1 = \cot^{-1}(1/2)$ (bottom row, 1:2 ratio) and their effect on the electric field, polarization gate, and ellipticity.	82

Figure 4.8: Scaling factors required to maintain a constant driving field intensity inside the polarization gate as the field asymmetry is changed [221]. (© 2015 IEEE)	85
Figure 4.9: Scaling factors required to maintain a constant driving field intensity inside the polarization gate as the field ellipticity is changed [221]. (© 2015 IEEE)	86
Figure 4.10: Predicted ionization rates in argon with GDOG and AGDOG _{3:1} fields ($\lambda = 800$ nm, $\tau_p = 20$ fs, $\epsilon = 0.5$, $I_{gate} = 2.19 \times 10^{14}$ W/cm ²) [221]. (© 2015 IEEE)	88
Figure 4.11: Predicted ionization rates in argon with different gating schemes as a function of pulse duration ($\epsilon = 1$ (PG, DOG) or $\epsilon = 0.5$ (GDOG, AGDOG), $\lambda = 800$ nm, $I_{gate} = 2.8 \times 10^{14}$ W/cm ²) [221]. (© 2015 IEEE)	89
Figure 4.12: The XUV cut-off energy associated with the highest polarization gate intensity that did not result in ionization surpassing the criteria for phase matching ($\epsilon = 1$ (PG, DOG) or $\epsilon = 0.5$ (GDOG, AGDOG), $\lambda = 800$ nm) [221]. (© 2015 IEEE)	90
Figure 4.13: The XUV cut-off energy associated with the highest polarization gate intensity that did not result in ionization surpassing the criteria for saturation ($\epsilon = 1$ (PG, DOG) or $\epsilon = 0.5$ (GDOG, AGDOG), $\lambda = 800$ nm) [221]. (© 2015 IEEE)	91
Figure 4.14: Single-atom (bottom) and 3D macroscopic (top) harmonic spectra generated by polarization gating fields with different field ratios.	94

Figure 4.15: Driving field extrema surrounding the polarization gate for different field ratios. While the envelope of all three fields (dotted lines) were normalized at the center of the polarization gate, the fields themselves (solid lines) differed in magnitude because of the field asymmetry.	94
Figure 4.16: The temporal profile of the isolated attosecond pulses corresponding to the macroscopic HHG spectra plotted in the top panel in Fig. 4.14.	96
Figure 4.17: The temporal profile of twenty harmonic-wide ranges of the macroscopic spectrum in the top panel of Fig. 4.14 corresponding to $\theta_1 = \cot^{-1}(2)$ (red curve). Each range was centered at the harmonic order specified at the right of each panel (H40, ... , H120). The satellite pulse was only apparent when selecting the lowest-order harmonic region.	98
Figure 4.18: The effect of a 1400 nm-thick zirconium filter on the macroscopic spectrum in the top panel of Fig. 4.14 for the case of $\theta_1 = \cot^{-1}(2)$ (red curve).	99
Figure 4.19: The temporal profiles of the attosecond pulses corresponding to the HHG spectra shown in Fig. 4.18.	100
Figure 5.1: Proposed scheme for beam propagation after the pulse compressor.	102
Figure 5.2: The IFAST 200 TW amplifier (center), compressor (top), focusing beamline (front edge), and end station (left).	104
Figure 5.3: Block diagram of the proposed scheme for the FOPA laser system.	105
Figure 5.4: The principle of frequency-domain optical parametric amplification [230].	106

CHAPTER 1: INTRODUCTION

1.1 An Historical Glance at the Need for Higher Optical Power

Breakthroughs in the modern-day study of atomic and molecular dynamics have often been made possible by the advancement of high-power optical sources.

1.1.1 Flash Photolysis

In 1947, the Faraday Society held a series of talks and discussions on “The Labile Molecule”. Of primary interest was the topic of free radicals: highly reactive atoms or compounds that are key to many important chemical processes. At the time, few free radicals had been thoroughly measured due in part to their volatility: only certain more-stable specimens could be confined in high enough concentrations to be properly studied ($>10^{-5}$ mol/l required), but this stability also made them less interesting and less important subjects of investigation. More relevant free radicals could only be produced in very low concentrations – on the order of 10^{-7} – 10^{-10} mol/l. On this matter, the introductory address stated: “The direct physical methods of measurement simply cannot reach these magnitudes, far less make accurate measurements in a limited period of time, e.g. 10^{-3} sec.” [1,2].

Within the next five years, British chemists Ronald G. W. Norrish and George Porter had created a new method that improved on both of these obstacles, producing higher concentrations of free radicals and performing accurate time-resolved measurements on the millisecond time scale. Their new technique, first published in *Nature* in 1949, was called flash photolysis: A meter-long cell filled with a gas mixture was placed next to a flash tube, which was modified to drastically increase the discharge pump energy from ~ 100 J to as high as 10 kJ [3]. The great burst of energy from

the lamp was sufficient to produce high concentrations of free radicals in the gas mixture, which could be probed using the flash of a second lamp passing longitudinally through the cell and into a spectrometer (shown in Fig. 1.1) [4]. By controlling the delay between the pump flash and the probe flash, the disappearance of the free radicals could be mapped out over time, as suggested in Fig. 1.2 [5]. The flash photolysis technique was quickly adapted by the rest of the field, leading to many significant investigations into chemical dynamics occurring on the millisecond (10^{-3} s) and microsecond (10^{-6} s) scale. This helped earn Norrish and Porter a share of the 1967 Nobel Prize in Chemistry “for their studies of extremely fast chemical reactions, effected by disturbing the equilibrium by means of very short pulses of energy” [6].

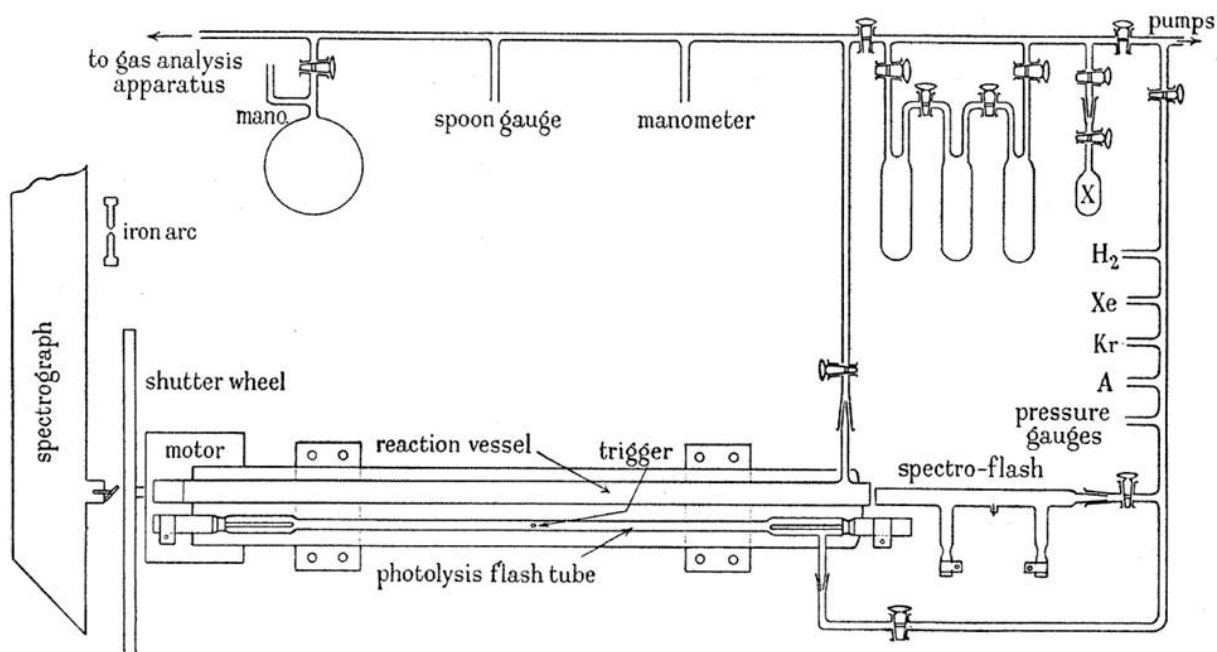


Figure 1.1: Diagram of the experimental arrangement for performing flash photolysis. Adapted from [4] with permission of The Royal Society of Chemistry.

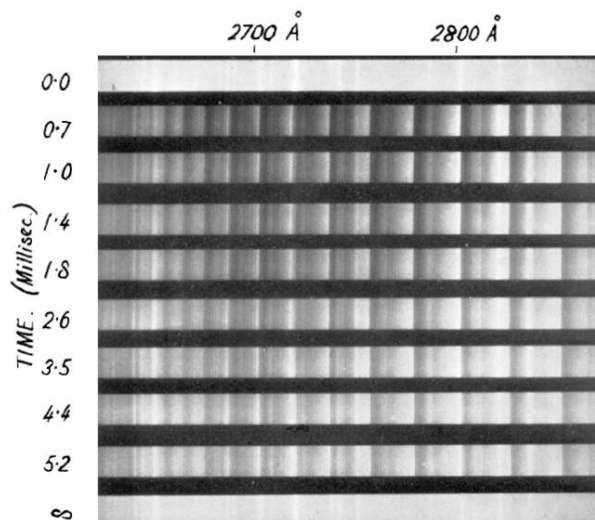


Figure 1.2: Bimolecular disappearance of Chloric Oxide (ClO). Adapted from [5] with permission of The Royal Society of Chemistry.

1.1.2 The First Laser

Of course, concurrent with this research was the development of other scientifically-useful radiation sources: masers and lasers. Precursory work on the maser was first published in 1954 [7, 8], and the earliest records of optical maser designs began to appear in 1957 [9]. Looking forward to the laser's applicability as a high-power source for scientific investigation, Arthur Schawlow expressed his vision for the future in 1959 [10]:

If a plane wave output of, say, 1 milliwatt can be concentrated into a spot of 10^{-8} cm², the power density achieved will be 10^5 watts per cm² at the focus. ... Such a large field, even though very localized, might be sufficient to show nonlinear effects either in its interaction with matter or with other light waves.

Before the first-ever laser action could be realized in Theodore Maiman's pink ruby, however, limitations arising from insufficient pump power needed to be overcome (see Fig. 1.3).

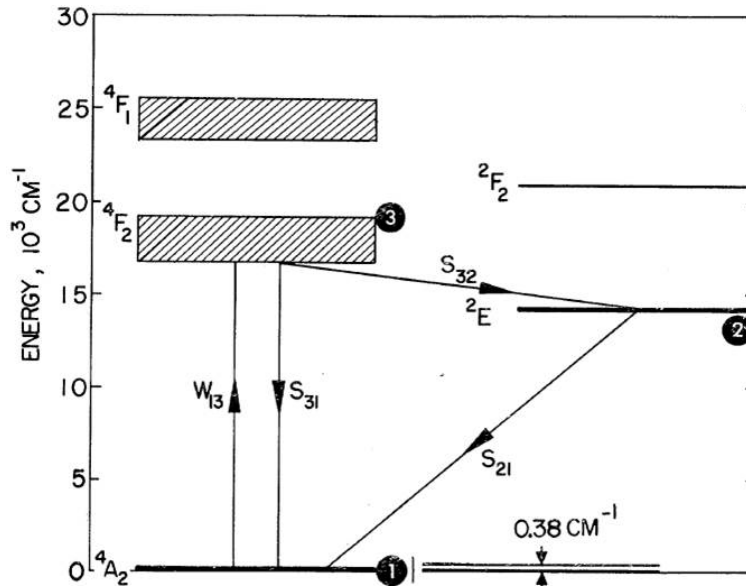


Figure 1.3: Energy levels of ruby. The two strongest lines correspond to S_{21} . Reprinted with permission from [11]. Copyright 1960 by the American Physical Society.

Inducing a population inversion in pink ruby seemed unlikely at first: Schawlow dismissed the medium completely, suggesting that “the two strongest lines (at 6919 Å and 6934 Å) go to the ground state, so that they will always have more atoms in their lower state, and are not suitable for maser action” [10]. Even in April 1960 – only one month before his historic achievement! – Maiman reported only a 3% change in pink ruby’s ground-state population when optically pumped [11]. A key alteration to this optical pumping configuration eventually made the difference: “due to the need for high source intensities to produce stimulated emission in ruby”, Maiman switched to a high-power xenon flash lamp, and lasing was first observed in May 1960 [12–14]. A diagram of this laser is shown in Fig. 1.4.

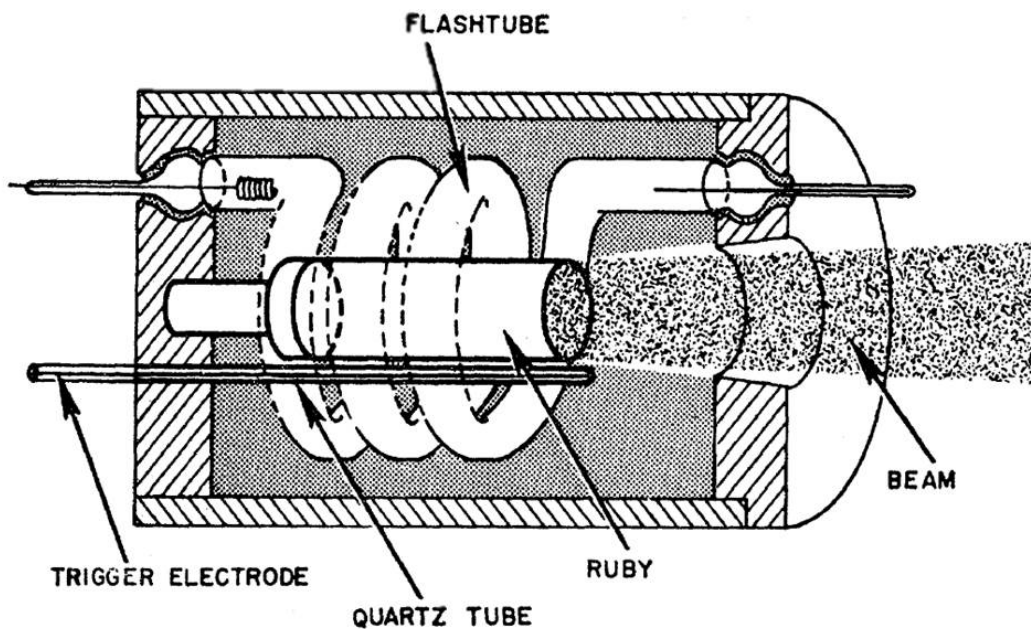


Figure 1.4: Apparatus for pulsed excitation of ruby. (Actual size, approximately 2×1 in. o.d.). Reprinted with permission from [13]. Copyright 1961 by the American Physical Society.

Maiman's success was the first of many technological breakthroughs that facilitated new methods for studying atoms and molecules. The significance of this development was commemorated in 1981, when Schawlow and Bloembergen were awarded shares of the Nobel Prize in Physics "for their contribution to the development of laser spectroscopy" [15].

1.2 Attosecond Physics

While the first laser pulse lasted several hundred microseconds [16], laser advancements such as Q-switching [17] and mode-locking [18] soon allowed for laser pulses reaching nanosecond (10^{-9} s), picosecond (10^{-12} s), and even femtosecond (10^{-15} s) time scales. These pulses, like the revolutionary pump and probe outbursts in the flash photolysis method, were also used to initiate and measure atomic and molecular dynamics with a higher temporal resolution than ever

before [19]. The significance of the discoveries resulting from these new ultrafast pulses was found deserving of the 1999 Nobel Prize in Chemistry, presented to Ahmed Zewail “for his studies of the transition states of chemical reactions using femtosecond spectroscopy” [20].

Within the next few years, a new level of temporal resolution became available for pump–probe spectroscopy, as pulses with attosecond (10^{-18} s) durations were demonstrated for the first time in 2001 [21]. While attosecond pulses have proven to be valuable for studying electron dynamics [22], their usefulness so far has been largely limited to femtosecond pump–attosecond probe schemes (an example of which is shown in Fig. 1.5). This is because typical attosecond pulses are usually limited to pulse energies on the nanojoule level, which by itself is too weak to serve as both the pump and the probe of a system. Because attosecond pulses are not strong enough to drive electron dynamics themselves, past experiments have relied upon stronger femtosecond pulses even though they do not possess the same level of temporal confinement.

To make new breakthroughs in attosecond physics, the attosecond pulse flux must increase so as to enable all-attosecond measurements.

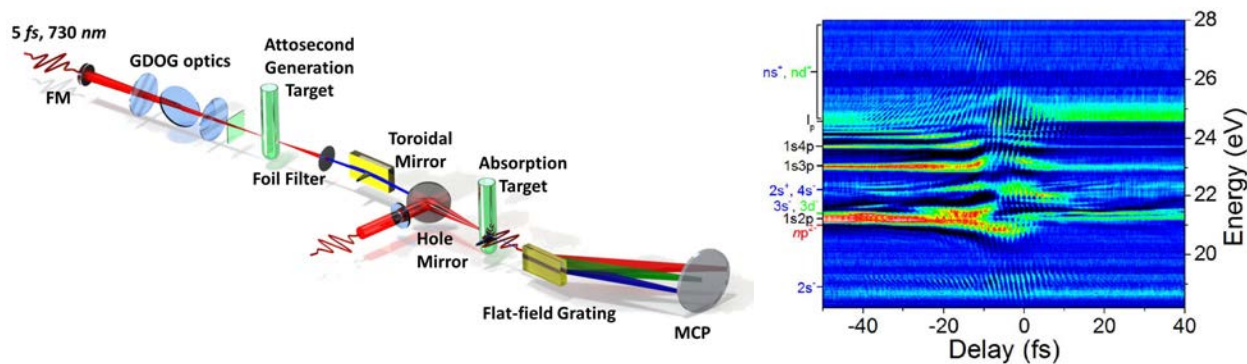


Figure 1.5: Example of a femtosecond pump–attosecond probe setup investigating helium [23].

1.3 Dissertation Outline

With the overarching goal of generating isolated attosecond pulses with 1 μJ of energy, this dissertation primarily concerns itself with the development of the driving laser system capable of driving a high-flux isolated attosecond pulse source at the Institute for the Frontier of Attosecond Science and Technology (IFAST) at the University of Central Florida.

After a brief introduction to chirped pulse amplification (CPA), Chapter 2 describes the design and performance of the IFAST 10 TW CPA system, which was used to generate an extreme ultraviolet (XUV) continuum with a pulse energy of 100 nJ. This is followed by a discussion of the implemented system upgrade for increasing the laser's peak power from 10 TW to 200 TW, with the intention being to scale the attosecond pulse flux to the microjoule regime.

Even isolated attosecond pulses with the *potential* for high flux would be unfit for all-attosecond measurements if the carrier-envelope phase (CEP) of the driving laser were not stabilized, as resulting fluctuations in the attosecond pulse parameters would be unacceptable when using the pulses to pump and probe a quantum system or to initiate nonlinear XUV dynamics. Unfortunately, locking the CEP of a sub-kHz laser is not straightforward: phase feedback arriving at the repetition rate of the laser comes too infrequently to compensate the CEP noise arising from vibrations in the pulse stretcher and compressor. Chapter 3 details a new method capable of controlling the CEP of low-repetition-rate CPA systems, and results with the 10 TW system and the 200 TW system are presented.

Finally, Chapter 4 examines the gating schemes used for generating isolated attosecond pulses, and a new variation on these previous techniques is suggested. A decrease in pre-gate ionization is expected using the proposed method as compared to other common schemes. This innovation is predicted to help increase attosecond flux by improving phase matching and extending the high-

energy photon cutoff, and it also opens the possibility of isolated attosecond pulse production with longer, more common driving laser pulse durations.

Chapter 5 concludes this dissertation with a discussion of future work.

CHAPTER 2: A 200 TW Ti:SAPPHIRE LASER

2.1 General Design Considerations

The primary objective towards reaching microjoule-level attosecond pulses in the IFAST lab is upgrading a previously-constructed 10 TW system to be capable of reaching peak powers of 200 TW (3 J in 15 fs). Before discussing the 10 TW and 200 TW systems, first some background information is provided that introduces a number of the basic concepts encountered when constructing laser systems with peak powers in excess of 10 TW.

2.1.1 History and Concept of Chirped Pulse Amplification

Similar to how the laser was developed borrowing concepts from the maser, the historical roots of chirped pulse amplification (CPA) can be traced back to shaping techniques used with radar pulses in the mid-twentieth century. At the time, two constraints of a typical radar system were 1) the limit of the detection range, as determined by the energy of the radar pulses, and 2) the limit of the detection resolution, as determined by the temporal duration of the radar pulses. To improve the detection range, the pulse energy could be increased; unfortunately, this led to a deterioration in detection resolution, as longer pulses were needed to prevent equipment damage from increasing peak powers. To solve this problem, a radar pulse was instead transmitted with a “chirp”, meaning that a strong non-zero phase relationship was applied between the individual frequency constituents of the radio pulse. This resulted in a pulse with a long, non-bandwidth-limited pulse duration that could be safely amplified to higher pulse energies, thus improving the detection range. When the “echo” signal of the radar pulse returned, a complementary phase was applied in order to temporally compress, or “de-chirp”, the radar pulse to a short duration, thus also improving the

detection resolution [24, 25].

While the chirping and de-chirping of radio pulses could be accomplished using electronics, methods for de-chirping materially-dispersed optical pulses were not developed until after the advent of the laser; several such techniques include the Gires-Tournois Interferometer in 1964 [26–28], the Bragg diffraction compressor in 1967 [29], the bulk compressor (bromobenzene) in 1968 [30], the grating compressor in 1969 [31], the alkali-metal vapor compressor in 1971 [32], the prism compressor in 1985 [33], and the chirped mirror compressor in 1994 [34]. The general function of these techniques is the same as the radar-chirping electronics: a fixed, frequency-dependent phase is applied across the spectral bandwidth of the optical pulse, thereby allowing a degree of control over its temporal profile.

Early on, these techniques were often applied in re-compressing a pulse to a width shorter than its original durations after using self-phase modulation in a fiber or frequency sweeping in an electro-optic crystal to broaden the spectrum of the initial pulse [30, 35–43]. This technique still finds use in increasing the bandwidth of seed and amplified pulses for generating few-cycle pulses [44–47]. In most of these cases, the magnitude of the positive material chirp was relatively small, and the chirped elements were simply used at the end of the laser system for dispersion control to achieve pulse durations close to the new bandwidth limit.

Unlike these earlier efforts which simply used dispersion control to re-compress the *final* optical pulse, chirped pulse amplification is more similar to the chirped radar technique, likewise calling for additional pre-chirping of the *initial* optical pulse so it can be amplified to high energy without damaging or accruing nonlinear effects in the gain medium. As was the case with chirped radar, the large total chirp of the optical pulses can be compensated in order to produce short temporal pulse durations. For these optical pulses, the compressive de-chirping can lead to peak powers that are orders of magnitude higher than the damage threshold of the amplifier, which would otherwise

impose a limit on the laser system's highest level of performance.

When chirped pulse amplification was first implemented in 1985, a >1 km fiber was used to significantly stretch the pulse before it was amplified in a neodymium glass amplifier and compressed by a grating pair [48]. This is captured in Fig. 2.1. Around the same time, non-material-based *positive*-dispersion systems were under development: it was shown that a lens pair inserted between a pair of gratings or prisms – often called a “4-f stretcher” – could reverse the typical sign of the dispersion [49–52]. These advancements led to the first proposal of chirped pulse amplification as it is commonly implemented in ultrafast laser laboratories, using diffraction gratings for both the pulse stretcher and compressor [53]. All the same, fiber stretchers continued to be used in CPA setups, often in conjunction with prism pairs to compensate for dispersion in (for example) regenerative amplifiers [54,55].

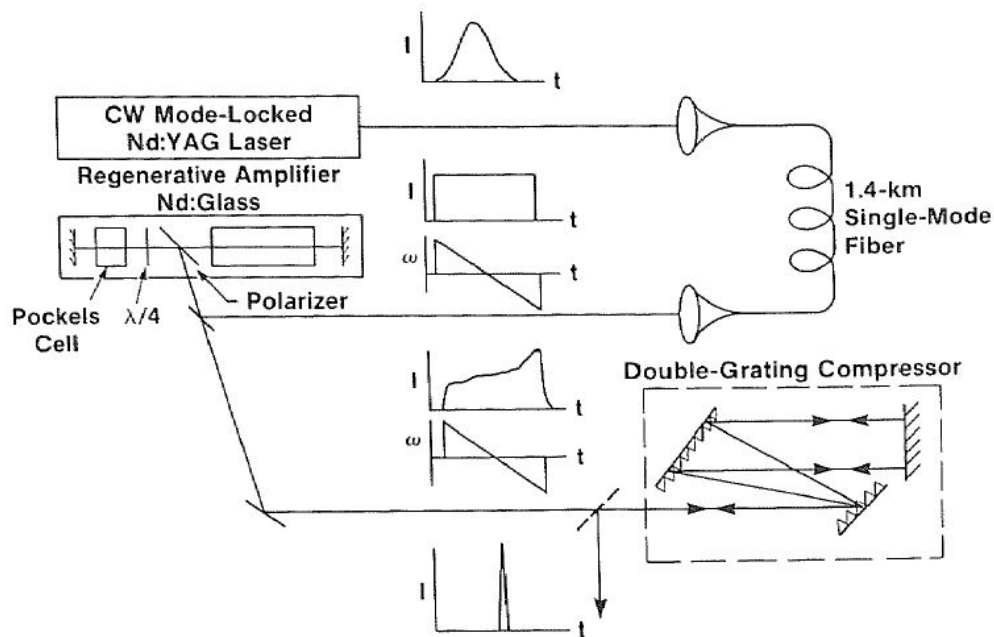


Figure 2.1: The first demonstration of chirped pulse amplification. Reprinted from [48], with permission from Elsevier.

2.1.2 *Spectrum and Phase Correction in CPA Systems*

According to Fourier optics, the temporal duration of a laser pulse is directly related to 1) the frequency bandwidth of the pulse and 2) the relative phases between those frequencies. In order to attain the shortest-possible pulse, 1) the spectrum must be as broad as possible and 2) the phase must be as uniform as possible. These two conditions, however, are often undermined by the typical operation of amplifiers and other elements in CPA systems.

Pulse amplification can cause many unwanted changes to a laser's spectrum. For example, a gain medium with a wide gain bandwidth, such as titanium-doped sapphire (Ti:S) [56, 57], is required to produce an amplified pulse with a broad spectrum. However, the gain profile of such media are typically non-uniform, meaning that wavelengths near the peak of the gain curve are amplified more than wavelengths in the wings of the spectrum. This leads to a phenomenon called “gain narrowing”, an effectual contraction of the amplified wavelength spread that places a limitation on the pulse duration [58–60]. Similarly, if the wavelength of the peak of the gain curve and the input spectrum do not match, the peak wavelength of the output spectrum shifts towards the peak of the gain curve – an effect known as “gain pulling”. Additional changes to the spectrum may also occur due to the chirp of the pulse, as the wavelengths arriving at the amplification medium first experience higher gain than the latter wavelengths due to gain saturation. In titanium-doped sapphire, these detrimental effects must be addressed in order to reduce the amplified pulse duration below ~ 25 fs [61].

In terms of the second Fourier condition, a pulse propagating through a CPA system accrues phase errors and aberrations that distort the pulse's phase. High-order errors arise as various wavelengths of the pulse travel differently through system materials. Other phase errors occur from the misalignment, inhomogeneities, surface roughness, or aberrations of optical elements. All phase errors must be addressed collectively to achieve a bandwidth-limited pulse duration.

These spectrum and phase concerns can be approached in a number of ways, as described in the following sections.

2.1.2.1 Specialty Stretcher Construction

Higher-order phase problems are most fundamentally addressed by the chirping elements of the CPA system itself. While the primary purpose of the stretcher and compressor is to provide controllable positive and negative dispersion (usually in that order), the design and alignment of these CPA subsystems can themselves introduce higher-order phase terms and aberrations which detrimentally impact the laser pulse [62]. As a result, many stretcher and compressor configurations have been devised that prevent new phase problems and even reduce phase errors from the rest of the system [45, 63–71]. Examples include grism-based stretchers and compressors (Fig. 2.2(a)) [72, 73], mixed-grating stretchers and compressors [74–76], aberration-free Offner-type stretchers (Fig. 2.2(b)) [71, 77–79], and phase-corrected chirped mirrors [80].

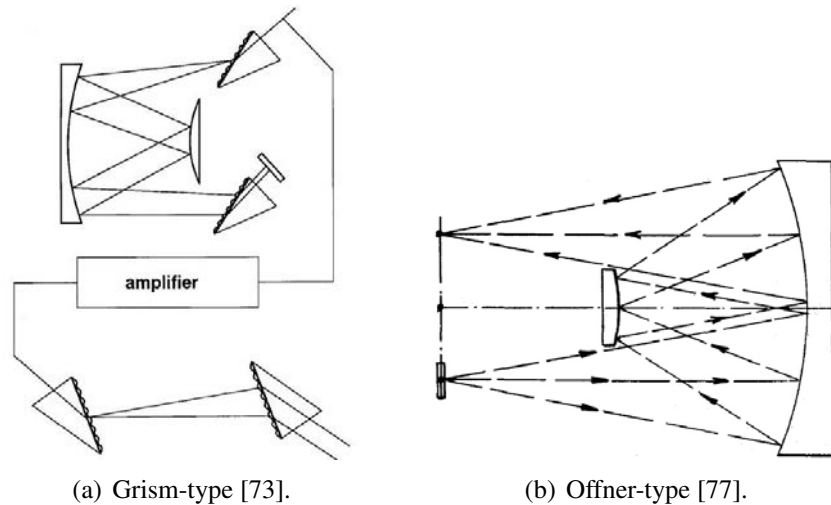


Figure 2.2: Examples of stretchers designed to reduce higher-order phase errors.

2.1.2.2 Gain-Competition Reduction

Design considerations for the amplifier can also alleviate distortions in the spectrum that arise from gain. To reduce the competition for gain between the laser's individual wavelengths, for example, special propagation configurations have been formulated to allow each wavelength to see its own gain separately. These setups, in some cases, can eliminate the phenomena of gain narrowing, gain pulling, and gain saturation altogether.

One such demonstration is the spatially-dispersed resonator, as shown in Fig. 2.3 [81]. Because of the intra-cavity prism pair, each wavelength propagates along its own trajectory through the entire resonator, including the gain medium. In this way the effects of gain saturation are avoided.

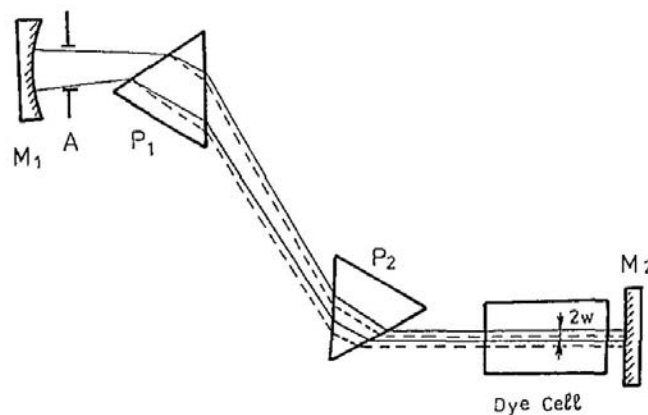


Figure 2.3: Elimination of gain competition via a spatially-dispersed resonator. Adapted from [81] with kind permission from Springer Science and Business Media.

Such a setup can also eliminate the effects of gain narrowing and gain pulling if the gain medium is pumped non-uniformly, as in Fig. 2.4 [82]. Wavelengths near the peak of the material gain curve can be allocated less energy than wavelengths in the wings of the curve through judicious spatial variation of the pump energy. This can flatten the overall gain curve. A similar technique based on parametric amplification rather than stimulated emission is mentioned in Sec. 5.3.

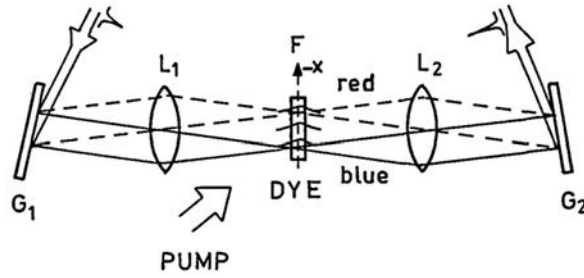


Figure 2.4: Gain curve-flattened amplification using a spatially-modulated pump [82].

In practice, the localized variation of the pump energy is sometimes achieved by pumping the gain medium with multiple pump lasers. The intersection of these laser profiles is chosen to overlap in the regions of the gain medium through which the less-efficient wavelengths propagate. These wavelengths in the wings of the gain curve thus experience a similar gain to that of the “peak gain” wavelengths, which do not propagate through the high-energy regions corresponding to the overlapping pump beams [83, 84]. Figures 2.5 and 2.6 show examples of a spatially-dispersed regenerative Ti:S amplifier and multi-pass Ti:S amplifier, respectively, using this multi-pump method.

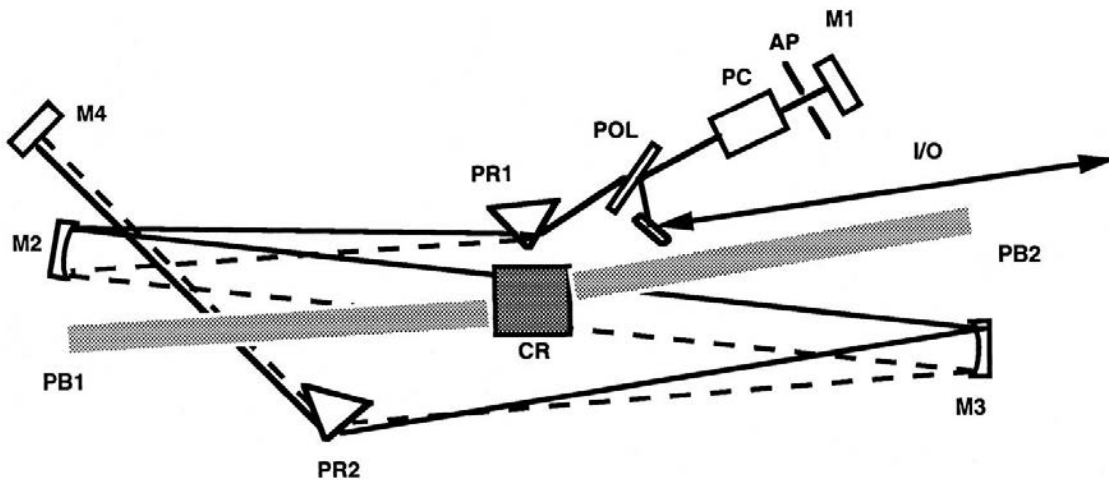


Figure 2.5: Multi-pump, spatially-dispersed, regenerative Ti:S amplifier. Reprinted from [83], with permission from Elsevier.

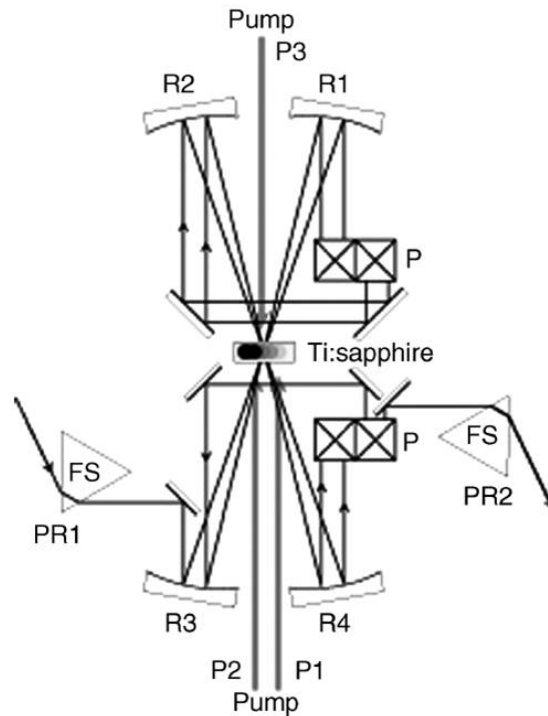


Figure 2.6: Multi-pump, spatially-dispersed, multi-pass Ti:S amplifier [84].

2.1.2.3 Gain-Reduction Competition

While each of the gain effects mentioned above distorts the input laser spectrum, each effect occurs in a different way. The schemes mentioned in this section provide spectral shaping by setting one gain effect at odds with another, causing a beneficial competition between the two.

One such scenario, called negatively and positively chirped pulse amplification (NPCPA), uses gain saturation in each amplification stage to mitigate spectral distortions. As seen in Fig. 2.7, the laser pulse is first chirped *negatively* and amplified before being chirped *positively* and amplified. Because of gain saturation, the first amplification stage favors the *short* wavelengths and the second amplification stage favors the *long* wavelengths. These two effects largely balance each other and lead to a broader, more-symmetric spectrum [85].

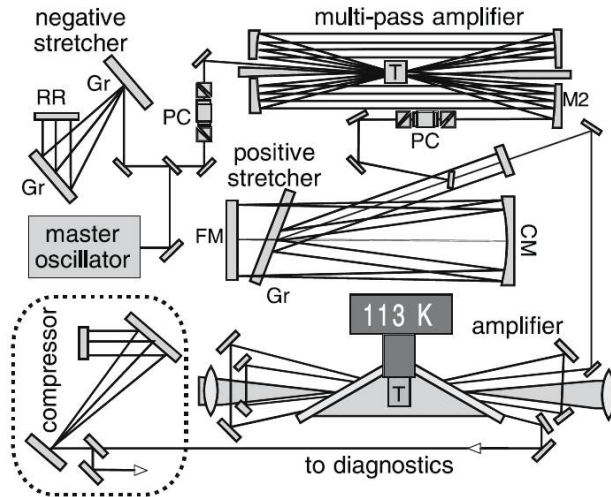


Figure 2.7: Negative and positive chirped pulse amplification (NPCPA). Adapted from [85] with kind permission from Springer Science and Business Media.

Another method counter-balances two gain-pulling effects by including two different gain media in the same regenerative amplifier. Each type of neodymium-doped glass has its own gain curve, with the two peaks located at different wavelengths. For an input spectrum centered at a wavelength *between* these two peaks, the gain-pulling effect pulls the peak of the spectrum in opposite directions as the pulse is amplified. The pump power for each glass amplifier can be tuned to balance the spectral pulling from either side, thus providing a smoother, broader overall gain profile [86, 87].

Finally, the long wavelength injection (LWI) method takes advantage of a competition between gain saturation and gain pulling. Under typical CPA operation, gain saturation favors longer wavelengths because they comprise the leading edge of the pulse. Comparatively, the peak of the gain curve is often found at lower wavelengths, meaning that gain pulling shifts the spectrum in the opposite direction. Therefore, if the input spectrum is tuned such that its peak lies well beyond the center of the gain profile, then gain saturation preferentially amplifies the *long* wavelength side and gain pulling preferentially amplifies what is tuned to be the *short* wavelength side. As a result, each effect favors a different part of the spectrum, and the overall gain is more uniform [88].

2.1.2.4 Spatial Light Modulation

It is straightforward to treat the individual components of the laser's phase and spectrum when the wavelengths are spatially dispersed. As a result, many spectral- and phase-correction *devices* in CPA lasers are located in a stretcher or compressor. In the simplest of cases, an opaque spatial mask can block unwanted frequencies, or a dispersive material can delay the phases of covered frequencies [66, 89–91]. As an example of its usefulness, the overall gain curve of a regenerative amplifier can be leveled by adding loss to the wavelengths near the peak gain (e.g. using a well-placed needle), thus reducing the effects of gain narrowing [67]. Figure 2.8 shows one of the earliest applications of this rudimentary pulse-shaping technique.

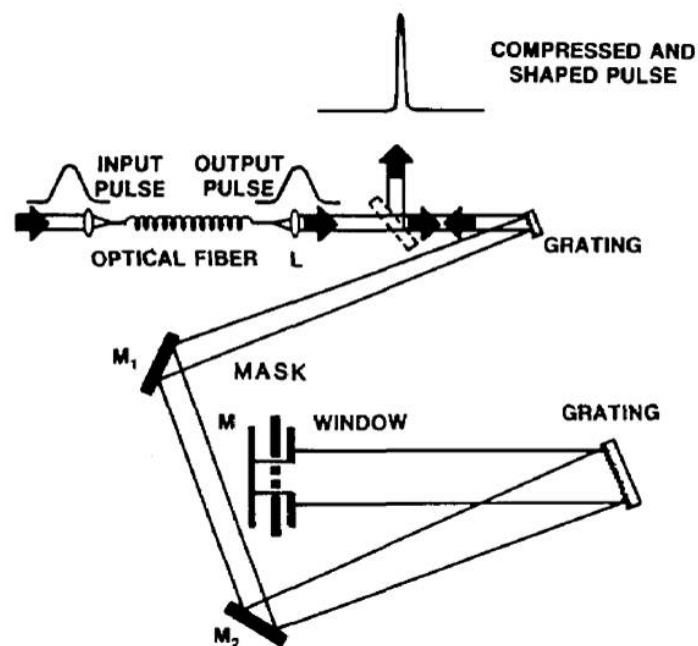


Figure 2.8: Shaping with opaque mask and dispersive material in a compressor [89].

A more versatile tool is the liquid crystal spatial light modulator (LC-SLM), an example of which is captured in Fig. 2.9. This array of liquid crystal cells, placed at the Fourier plane of a stretcher or compressor, can perform both phase and amplitude manipulation, and its values can be dynamically assigned (as opposed to the permanent nature of an etched mask) [92, 93]. Multiple LC-SLMs can be used together to improve control over the spectrum [94–96], the individual corrections being determined by specialized algorithms [97, 98] and even experimental feedback [99, 100]. These corrections, while beneficial, cannot always optimize an entire CPA system alone, so LC-SLMs are sometimes used cooperatively with other corrective devices [46, 101–103].

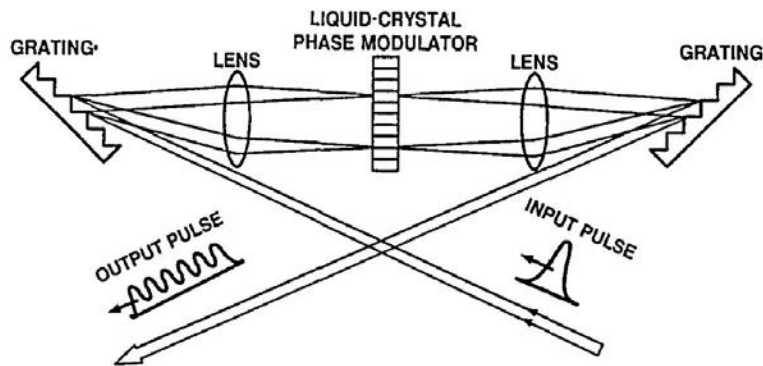


Figure 2.9: Typical implementation of a liquid crystal spatial light modulator [92].

While a traditional LC-SLM can have thousands of cells [104], the pixelated nature of the array can lead to some undesirable effects. One inventive solution is the continuous-electrode LC-SLM shown in Fig. 2.10. Instead of an array of liquid crystal cells, this device uses a single cell with an included layer of the photoconductor BSO. By illuminating the BSO with wavelengths below 550 nm, its conductivity can be adjusted. Therefore, a quartz lamp imaged through an LC TV (i.e. to give the variation desired) onto the BSO changes its conductivity locally, which in turn alters the field applied to different regions of the liquid crystal. This produces the same corrective behavior as a traditional LC-SLM, except without the effects of pixelation [105].

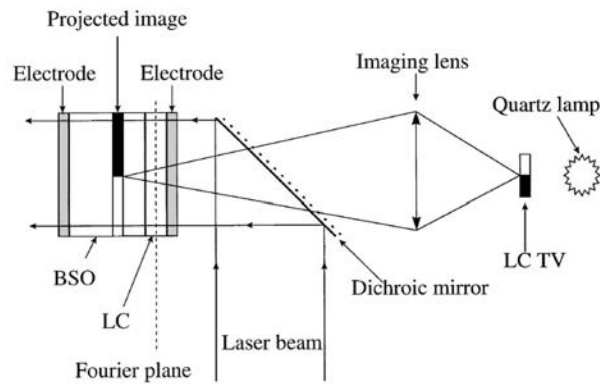


Figure 2.10: Depiction of a continuous-electrode LC-SLM [105].

It is worthwhile to note that the effect of pixelation can also be reduced using a microlens array, which focuses the incident light through the available modulation cells. This spacing also creates enough room to use larger manipulation devices, such as electro-optic modulators [106].

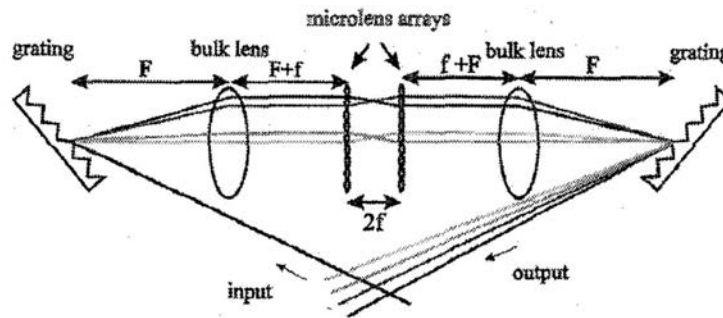


Figure 2.11: Microlens array inside a zero-dispersion stretcher [106]. (© 1996 IEEE)

Besides liquid crystal systems, other transmissive devices can also be added to the pulse stretcher or compressor to regulate the spectrum and phase. For example, a hologram can be used to shape a pulse's amplitude and phase to achieve a desired output profile (Fig. 2.12(a)) [107]. An acousto-optic modulator (AOM) can also address the spectrum (Fig. 2.12(b)), as the diffraction of each wavelength can be influenced according to the arbitrarily-shaped acoustic waveform. This provides the dynamic manipulation of an LC-SLM without the pixelation [108, 109].

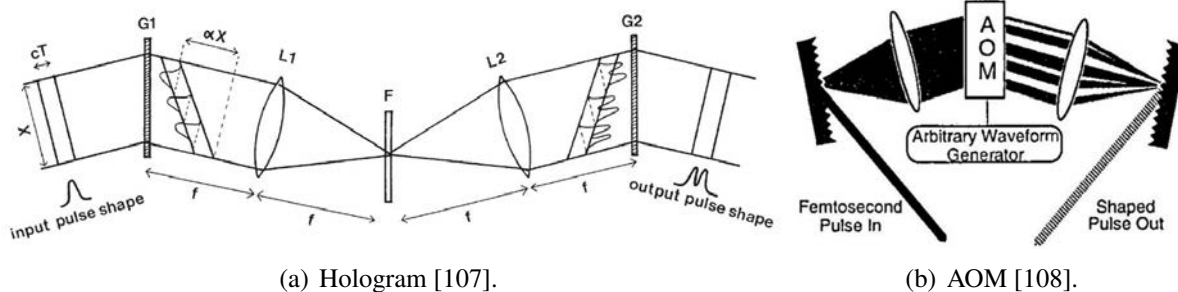
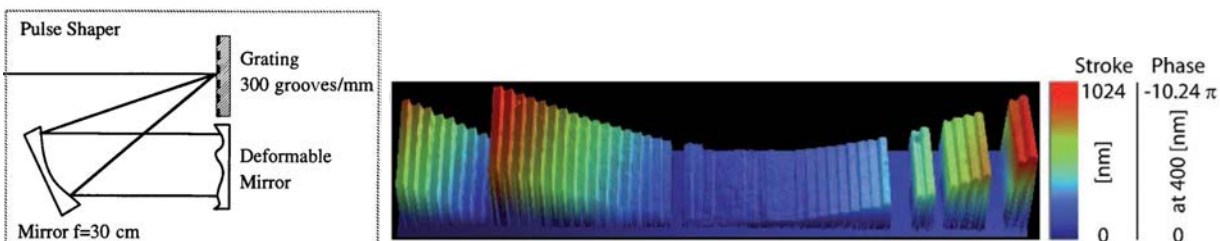


Figure 2.12: Two alternative transmissive elements used in a stretcher for pulse shaping.

In addition to these transmissive devices, reflective modulators have also been developed for use in compressors or stretchers with folded geometries. For example, the surface of a mirror can be deformed longitudinally such that different wavelengths of a retro-reflected, spatially-dispersed laser pulse travel different distances. This introduces a relative phase shift which can be controlled by the distortion depths of the reflective surface. This technique is typically performed by two different types of devices: 1) micro-machined deformable mirrors (MMDMs), which employ programmable arrays of actuators that can electrostatically deform a single, continuous reflective membrane [110–113] and 2) micro-electro-mechanical systems (MEMS) mirrors, which are composed of many densely-arranged, individually-controllable micro-mirrors [114–116].



(a) Shaping with a MMDM [110]. (b) Electron microscope image of one type of MEMS mirror [115].

Figure 2.13: Two typical reflective elements used to correct phase errors in a laser pulse.

2.1.2.5 Spectral Filtration

Naturally, the wavelengths of a laser need not be dispersed spatially to be modified. As opposed to the spatially-sensitive modulation devices just mentioned, it is often easier to use basic spectral filters that are readily placed into a laser system without the need for much alignment or calibration. Of course, there *are* other spectral filters that sacrifice simplicity for dynamic operational control; two such filters – the acousto-optic programmable dispersive filter (AOPDF) and the acousto-optic programmable gain control filter (AOPGCF) – are discussed at the end of this section.

The setup in Fig. 2.14 shows a regenerative amplifier with three different types of filters commonly used for spectral shaping: a thin etalon, a spatial mask (discussed in Sec. 2.1.2.4), and a birefringent plate. These methods are favorable due to their simplicity. Etalons can be tuned such that wavelengths near the peak of the gain curve experience destructive interference, thus leading to a flattening of the round-trip gain curve [45, 67–70, 75, 91, 101, 117–120]. The birefringent plate works similarly, as different wavelengths experience different amounts of phase retardation; an intra-cavity polarizer can introduce wavelength-specific loss accordingly [71, 91, 120, 121].

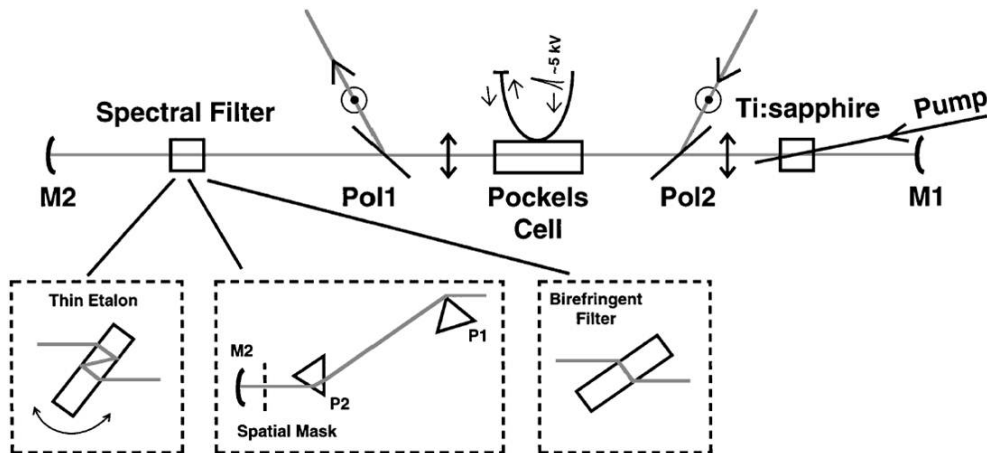


Figure 2.14: Spectral filtering via etalon, spatial mask, and birefringent plate [91].

Other spectral filters are simply multilayer dielectric stacks that are painstakingly designed to have extra loss corresponding to the peak gain wavelength. Optical elements performing these duties include gain-narrowing compensation filters [80, 102, 122–125], partial mirror coatings [103, 126], and variable-reflectivity or gain-flattening mirrors [127].

It is worthwhile to note that similar measures are taken to *preserve* the wavelengths in the *wings* of the spectrum, where the reflective performance of many dielectric mirrors begins to suffer. Such techniques include the design of super broadband mirrors [47, 101, 102, 119, 125] and the use of mirrorless amplifiers [101].

As stated earlier, not all spectral filters are static optical elements. The acousto-optic programmable dispersive filter (AOPDF) shapes the spectrum of a chirped laser pulse through selective diffraction of its individual wavelengths. These frequency components penetrate to different depths within the acousto-optic crystal, where they interact with a portion of an acoustic wave with a predetermined amplitude. This amplitude dictates the laser diffraction efficiency, so the input spectrum can be modified by carefully choosing the acoustic wave amplitude at each penetration depth inside the crystal [47, 84, 125, 128–133]. This is shown in Fig. 2.15.

The acousto-optic programmable gain control filter (AOPGCF) is a device that operates under the same principles, but a narrow acoustic wave is generated instead. Therefore, only wavelengths near the peak of the gain curve are diffracted, as opposed to the AOPDF's diffraction of the entire spectrum. These diffracted wavelengths are blocked, leaving the transmitted spectrum with a hole. This loss can be tuned appropriately in order to produce a flat, amplified spectrum [133, 134]. Figure 2.16 shows the use of an AOPGCF in regulating the gain of a regenerative amplifier.

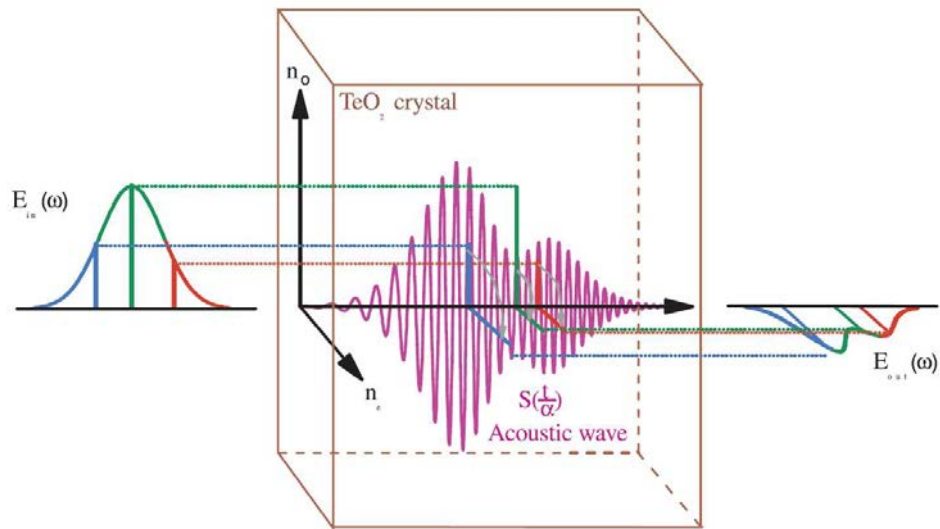


Figure 2.15: Spectral shaping using an AOPDF. Adapted from [131] with kind permission from Springer Science and Business Media.

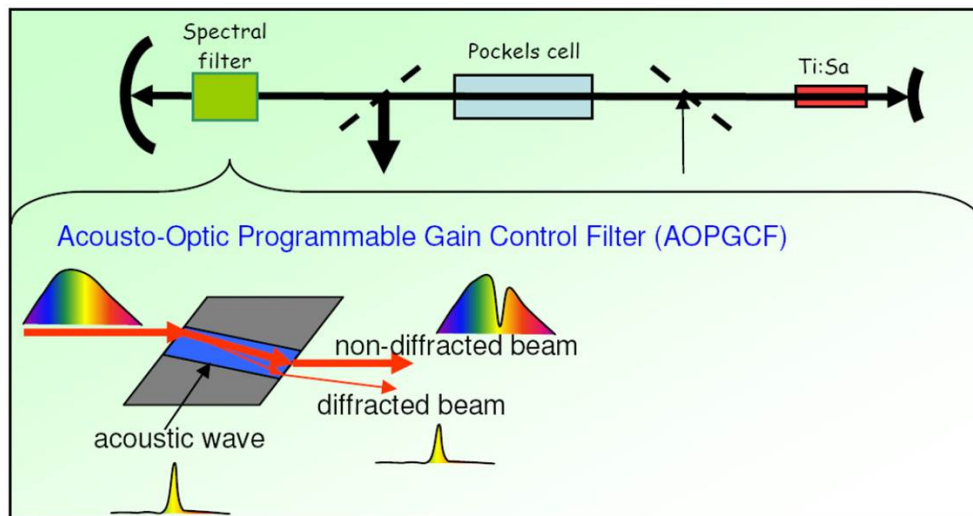


Figure 2.16: Spectral shaping using an AOPGCF [135].

2.1.3 Transverse Lasing

When attempting to amplify laser pulses to high energies, the gain medium's saturation fluence – the amount of energy that can be extracted per unit area of the amplifier before the available gain decreases by $1/e$ – dictates a major limitation to the total output pulse energy. This means that to produce higher and higher pulse energies, amplifiers must be used with larger and larger apertures. Besides the obvious practical constraints of trying to manufacture large gain media (e.g. large, laser-quality crystal growth) [136], a fundamental bottleneck to this aperture scaling is the onset of transverse lasing.

Transverse lasing, or parasitic oscillations, is a common problem for large-aperture, high-power, solid-state amplifiers which limits the final output power of the amplification process. When the radial size of the pump beam increases with the goal of increasing the energy output of the amplifier, the gain in the *transverse* direction correspondingly increases because laterally-emitted spontaneous emission experiences a longer optical path over which it can be amplified. If the transverse gain exceeds the transverse losses caused by the Fresnel reflections at the edge of the gain medium, transverse laser action results. These parasitics can quickly deplete the amplifier's population inversion, thereby clamping the gain available to the intended longitudinal amplification process. In this way the gain medium's aperture cannot be scaled further to increase energy output [137–139].

There are two main ways that transverse lasing can be controlled: one is to **increase the transverse losses**, and the other is to **decrease the transverse gain directly**. Both of these have the effect of increasing the transverse lasing threshold.

To **increase the transverse losses**, it is possible to use a ground finish around the edge of the amplifier to induce scattering losses or to engineer grooves and other structures into the edge of the amplifier to facilitate out-coupling of the parasitic oscillations [140]. Additionally, the strength of the

Fresnel reflections can be reduced by using anti-reflection coatings or index-matched claddings [141, 142] to transmit and then absorb lateral emissions.

There are several ways to **decrease the transverse gain directly** without at the same time affecting the performance of the amplifier too adversely. One method splits the pump energy amongst several pulses (or spreads it out in a relatively long pulse) such that the population inversion is not generated all at once; if the seed pulse extracts the energy from the amplifier *concurrent to* instead of *after* the gradual pumping process, the gain can be managed to remain below the transverse lasing threshold [143]. Another method involves using lower doping levels with thicker gain media or recycled pumping to maintain low levels of gain inside the amplifier [144, 145]; a similar effect can be achieved by simply tuning the polarization of the pump beam to take advantage of a lower absorption coefficient, thus mimicking a lightly-doped medium [146]. In general, it is also good practice to use flat-top pump beams so as to avoid the build-up of excess gain along the propagation axis of the amplifier [147].

2.2 IFAST 10 TW Laser [148]

2.2.1 Motivation

Isolated attosecond pulses are produced by high-harmonic generation (HHG) under one of several “gating” conditions, whereby the HHG spectrum is filtered or modified to produce an attosecond pulse-supporting extreme ultraviolet (XUV) broadband continuum. However, most of these gating schemes can only be realized using few-cycle driving near-infrared (NIR) pulses, which are typically restricted to output energies of ~ 1 mJ. Because of the low efficiency of the HHG process itself ($\sim 0.001\%$), isolated attosecond pulse energies from these systems are limited to < 10 nJ [149].

In order to produce *microjoule*-level attosecond pulses, a high-power (> 100 TW) laser must drive the generation process. Unfortunately, the only systems capable of delivering such peak powers also tend to feature pulse durations far too long – usually 30 fs or more because of the gain-narrowing effect – for use in common gating schemes. To close this gap without sacrificing peak power, the driving laser pulse duration must decrease, the gating scheme must tolerate longer pulse durations, or both.

To this end, a unique CPA system was constructed that offered high peak power (> 10 TW) while maintaining a pulse duration of 15 fs [148]. This was done by distributing the high total gain of $\sim 10^9$ between two CPA systems separated by a hollow-core fiber, which could regain the wings of the spectrum that would otherwise be irretrievably lost due to the gain-narrowing effect. In this unique way, pulses with hundreds of millijoules of pulse energy were generated with pulse durations short enough to be compatible with the generalized double optical gating (GDOG) technique for generating isolated attosecond pulses [150]. With this system, an XUV continuum of 100 nJ was produced, representing an important step towards scaling the isolated attosecond pulse energy to the microjoule level.

2.2.2 Laser Architecture

The general layout of this laser system is shown in Fig. 2.17(a). A 12-fs, nanojoule-level pulse from an oscillator was stretched in an Offner-type stretcher to 100 ps before passing through a Faraday isolator. The stretched pulse was then amplified from nanojoule- to millijoule-level in a single 14-pass Ti:sapphire-based amplifier. The crystal was pumped from each side by the beam-split output of a diode-pumped frequency-doubled Nd:YLF laser providing tens of millijoules of pulse energy at a 1 kHz repetition rate. A pulse tube cryogenic cooler attached to the amplifier was used to extract residual heat and reduce the thermal lens effect, thereby improving the beam quality. Due to the low temperature, the amplifier was housed in a chamber whose evacuated pressure was maintained by an ion pump. This assembly was mounted from the overhead frame in the IFAST laboratory to prevent the cryocooler vibrations from coupling into the optical table and affecting the stability of the optical mounts – a condition especially important for preserving carrier-envelope phase stability (discussed in Ch. 3).

Between the first and second seven passes of the 14-pass amplifier, the amplified spontaneous emission was reduced by a pulse cleaner comprised of a Pockels cell and two polarizers. After the second seven passes, the pulse underwent a final, single pass through another cryogenically-cooled Ti:sapphire amplifier before undergoing compression by means of a pair of reflective diffraction gratings with a groove density of 1200 l/mm. While gain-narrowing compensating filters were included in the 14-pass amplifier to alleviate the spectral effects of Ti:sapphire's non-uniform gain profile, the breadth of the spectrum still narrowed appreciably due to the high total gain of the system ($\sim 10^6$). This limited the pulse duration of the final output to >20 fs.

This bottleneck was overcome by propagating the pulse through a gas-filled hollow-core fiber (HCF) [151], which consisted of a rigid 150 cm-long glass capillary (O.D. 6 mm, I.D. 450 μm) resting in a straight v-groove inside a vacuum tube. The entire tube was evacuated and then back-

filled with neon gas to a static pressure of 1.4 bar. By propagating the 1.5 mJ, 20 fs pulse through this apparatus, self-phase modulation (SPM) recovered the wings of the spectrum lost to the gain-narrowing effect, as seen in Fig. 2.17(b).

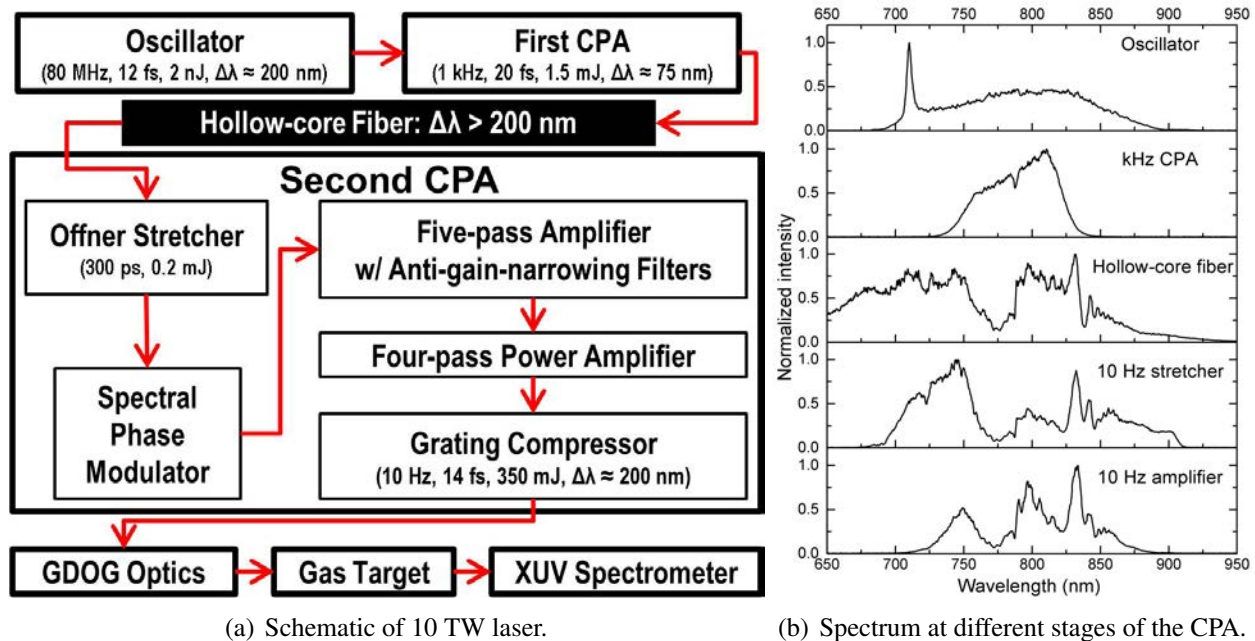


Figure 2.17: Key characteristics of the IFAST 10 TW laser system generating 15 fs. Reprinted with permission from [148]. Copyright 2013, AIP Publishing LLC.

To reach high peak powers, the broadband output of the HCF was first chirped to 300 ps in an Offner-type stretcher [152] that supported a bandwidth between 700 nm and 900 nm, as seen in Fig. 2.17(b). The stretcher itself consisted of two large spherical mirrors ($R = +1000$ mm and $R = -505$ mm) and a large reflective diffraction grating with a groove density of 1400 l/mm.

The first amplification stage consisted of four passes through a water-cooled, Brewster-cut Ti:sapphire crystal. Dual-sided pumping was provided by relay-imaged fractions of the output of a Q-switched frequency-doubled Nd:YAG laser (Quanta Ray PRO350) operating at a repetition rate of 10 Hz. The output energy of this amplifier was 30 mJ, and the spectrum was shaped by three gain-

narrowing compensating filters [126]. Lenses between different passes of the amplifier corrected for thermal lensing effects, and a telescope expanded the beam diameter to 10 mm before injection into the second amplifier.

The second amplification stage consisted of four passes through a water-cooled, flat-cut Ti:sapphire crystal ($\varnothing 15 \text{ mm} \times 10 \text{ mm}$). This crystal was pumped using the output of a PRO350 system with high M^2 factor and the remaining energy of the same PRO350 unit also used to pump the first amplifier. To maintain a smooth beam profile suitable for safe amplification, each pump beam passed through a beam homogenizer [145] before impinging upon either side of the crystal surface. Even with an output energy of 700 mJ, the spectrum still covered a range from 700 nm to 900 nm (Fig. 2.17(b)) and supported a transform-limited pulse duration of 12.2 fs.

To compress the pulse, a reflective grating pair with a groove density of 1400 l/mm was chosen. This setup was kept under vacuum to prevent the high peak powers from incurring damage and other nonlinear effects. The beam itself was expanded in a telescope before entering the vacuum chamber and passing through the pulse compressor, which had an efficiency of 50%. The gratings were tuned by observing the trace of a single-shot SHG FROG [153]. To help correct for higher-order phase errors, the pulse was addressed by a deformable mirror at the Fourier plane of a prism-based 4f-zero-dispersion stretcher [113] located after the Offner stretcher and before the first amplifier. The voltages for the twenty channels of the deformable mirror were optimized by an evolutionary algorithm that used the FROG traces as the fitness function. With this method, the pulse was compressed to a duration of 15.1 fs, as shown in Fig. 2.18. With a throughput of 350 mJ, this corresponded to a peak power of $>10 \text{ TW}$.

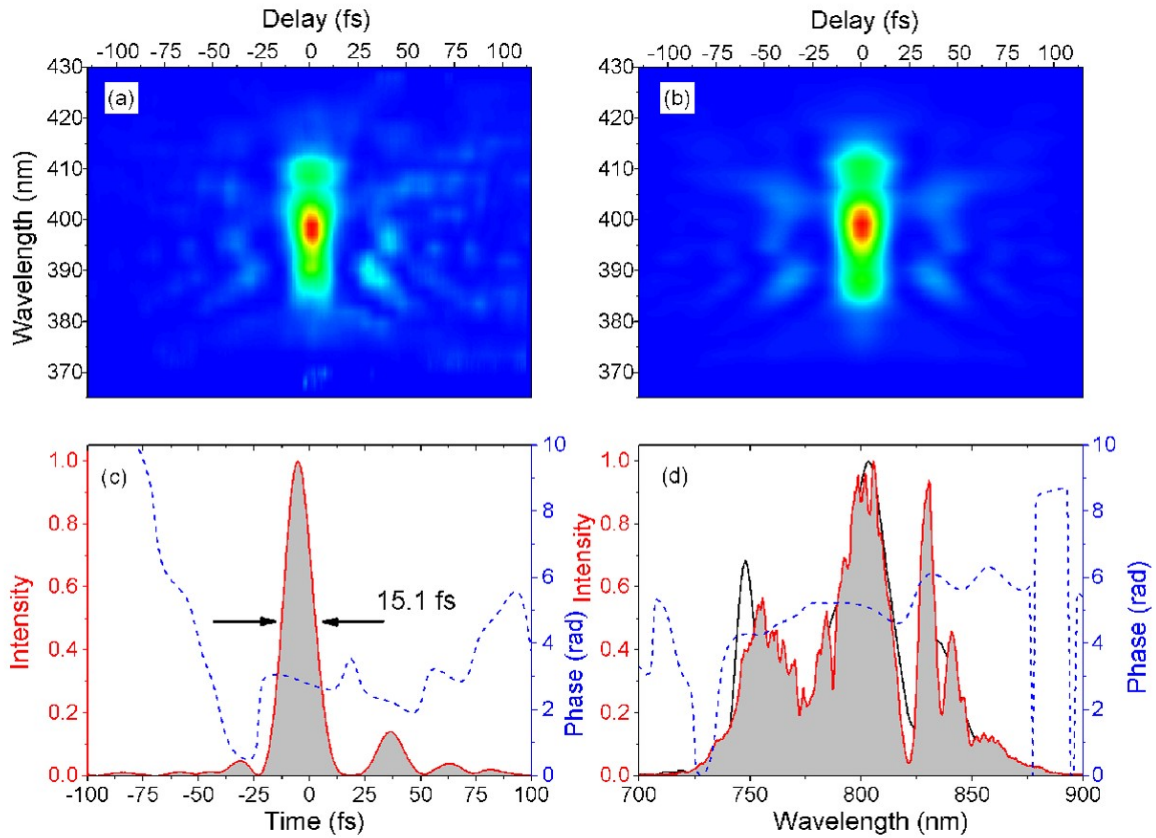


Figure 2.18: Single-shot FROG trace of the IFAST 10 TW laser. Reprinted with permission from [148]. Copyright 2013, AIP Publishing LLC.

2.2.3 HHG from the IFAST 10 TW Laser

Though too long for use with other gating schemes (see Ch. 4 for more information), the pulse was short enough for use with the generalized double optical gating (GDOG) technique. In short: compared to polarization gating, GDOG relaxes the constraint on the temporal width of the polarization gate; as a result, the delay between the two counter-rotating pulses can be decreased. This dramatically reduces the leading-edge parasitic ionization and thus allows for gated HHG with long initial pulse durations. This setup is shown in Fig. 2.19.

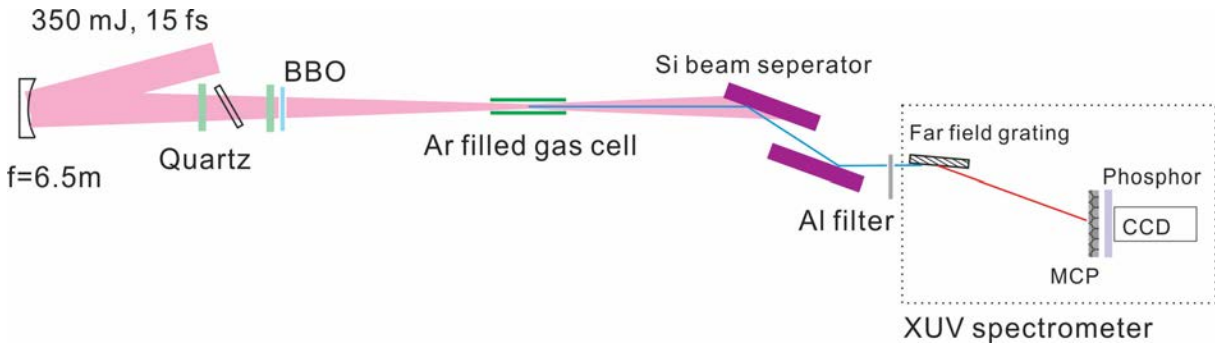


Figure 2.19: End station and HHG scheme for the IFAST 10 TW laser. Reprinted with permission from [148]. Copyright 2013, AIP Publishing LLC.

After the compressor, the pulse was directed to a concave mirror with a focal length of 6.5 m. As the beam gradually focused, it first passed through a full-order quartz plate with a thickness of $1070\ \mu\text{m}$ (used to set the polarization gate width to less than one cycle) and with the principal axes oriented at a 45° angle from the input polarization (used to generate $e-$ and $o-$ waves with equal magnitude). Next, three thin BK7 windows were used at Brewster's angle to transmit the gating field while partially reflecting the driving field, thereby determining the eventual ellipticity of the leading and trailing edges of the gating field. Finally, the beam was transmitted through a second quartz plate ($440\ \mu\text{m}$ thick) and a barium borate (BBO) crystal ($141\ \mu\text{m}$ thick) that combined to effectively form a zero-order quarter-wave plate with its principal axis oriented 45° from the principal axes of the first, full-order quartz plate. This generated the two-color field and also transformed the $e-$ and $o-$ waves from the first quartz plate into counter-rotating, elliptically-polarized pulses with the linear polarization gate at the center.

At the focus, the XUV pulse was generated in a gas cell filled with argon held at a backing pressure of 4 Torr. The beam size inside the 100 mm-long cell was $\sim 300\ \mu\text{m}$ in diameter (see Fig. 2.20) in order to prevent saturation of the target (i.e. $>97\%$ ionization by the cycles preceding the polarization gate).

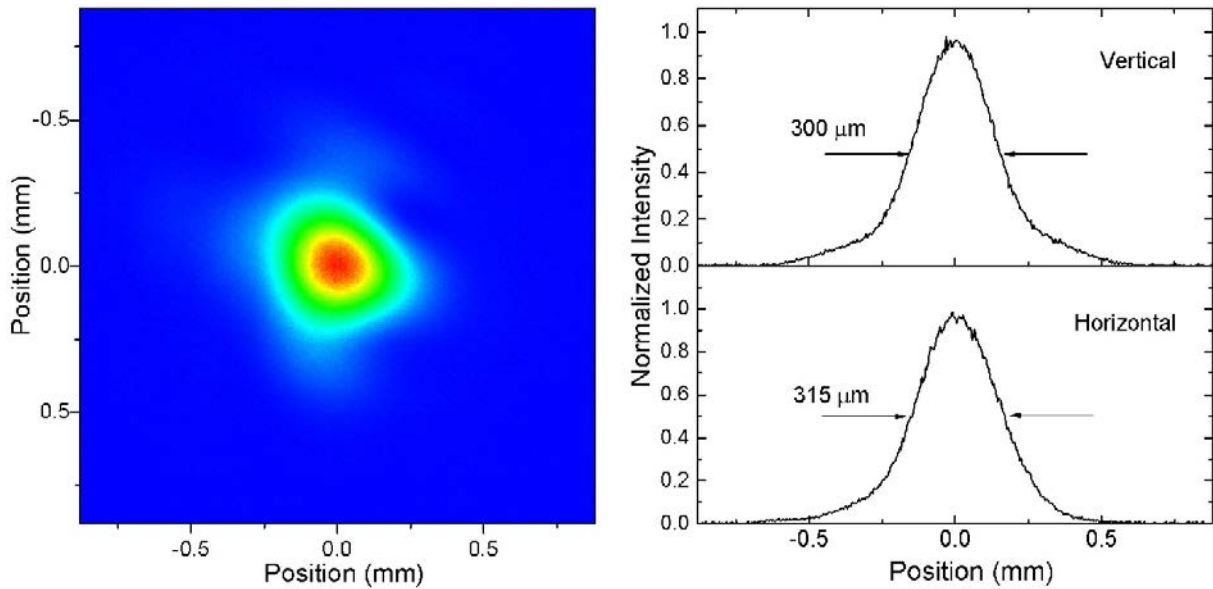


Figure 2.20: Beam profile at the focus of the IFAST 10 TW laser. Reprinted with permission from [148]. Copyright 2013, AIP Publishing LLC.

After the beam diverged from the focus, two silicon plates oriented at Brewster's angle for the infrared [154] were used to attenuate the residual infrared beam and reflect the XUV (up to only ~ 50 eV because of a sharp drop-off in reflectivity). The remaining infrared photons were extinguished with thin aluminum filters totaling 600 nm in thickness. The XUV pulse was characterized by an XUV spectrometer [155], which revealed odd harmonics when using the fundamental field, odd and even harmonics when using the two-color field, and an XUV continuum for every shot of the laser when using the GDOG field (see Fig. 2.21). This result, combined with the flux measurement from an XUV photodiode, indicated the generation of a 100 nJ XUV continuum capable of supporting 230 as pulses.

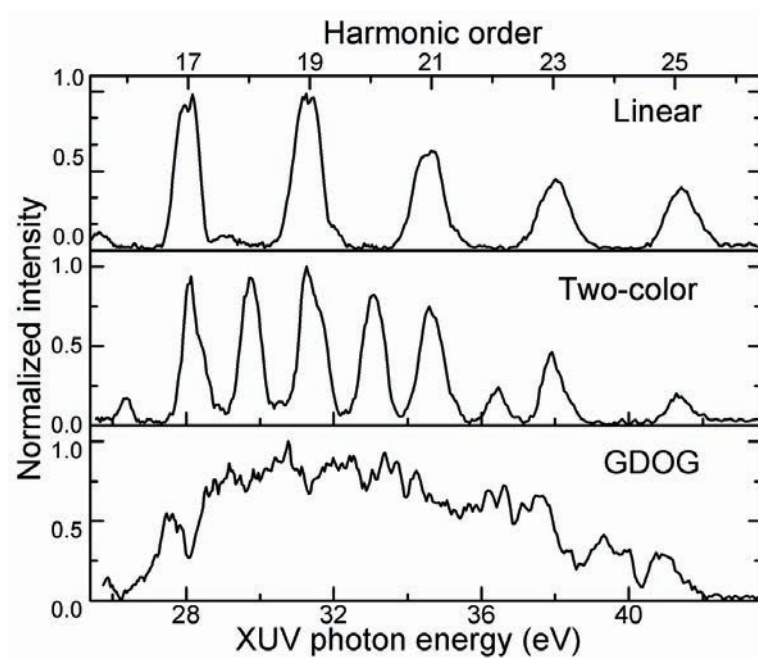


Figure 2.21: Generation of a 100 nJ XUV continuum capable of supporting 230 as pulses. Reprinted with permission from [148]. Copyright 2013, AIP Publishing LLC.

2.3 IFAST 200 TW Laser

While the IFAST 10 TW laser system was able to generate an XUV continuum with 100 nJ of photon flux, an additional order of magnitude is required for performing attosecond pump–attosecond probe experiments. Therefore, to scale the XUV pulse energy by a factor of ten, the driving pulse energy must also be scaled by a factor of ten without also lengthening the pulse duration. To this end, a new Ti:sapphire-based amplifier and compression scheme was designed and implemented to boost the compressed pulse energy by an additional factor of ten from ~ 300 mJ to ~ 3 J.

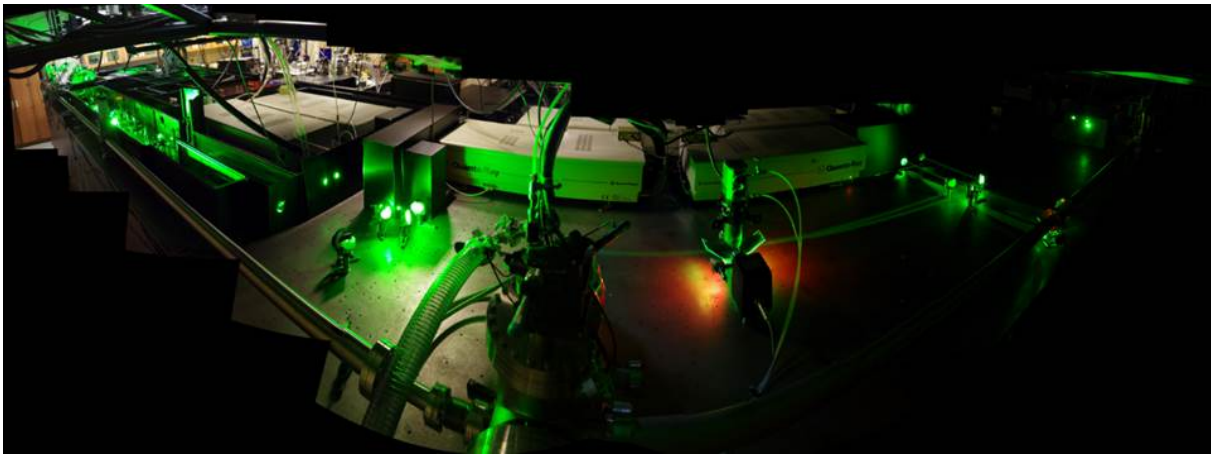


Figure 2.22: Early construction of the 200 TW amplifier at the IFAST lab.

Before discussing the third-stage amplifier and 200 TW grating compressor, it is important to point out several other changes that were made to the IFAST 10 TW system compared to how it was described in Sec. 2.2.2:

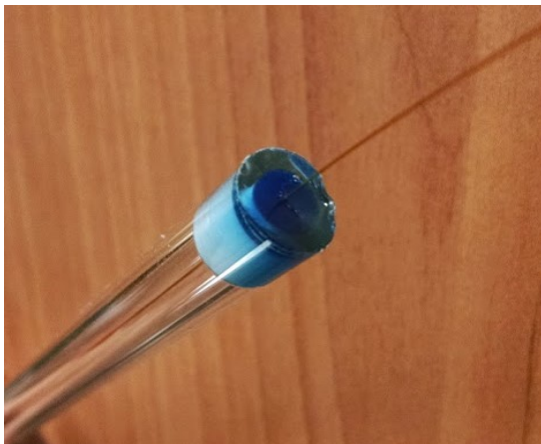
- In the front-end CPA operating at a 1 kHz repetition rate, the second, single-pass Ti:sapphire amplifier was removed, as the maximum energy input for the hollow-core fiber was attainable from the 14-pass first-stage amplifier directly.

- The roof mirrors in the 1 kHz compressor were replaced with broadband, high-damage threshold dielectric mirrors.
- The rigid hollow-core fiber assembly was replaced with a flexible hollow-core fiber setup. This apparatus consisted of a flexible, hollow, fused silica waveguide (O.D. 700 μm , I.D. 530 μm) that had been pulled until taught and then fastened at the ends of a 150 cm-long glass tube using two-part epoxy and teflon plugs with centered through-holes for the fiber (see Fig. 2.23(a)). To prepare the waveguide for laser use, each end was assembled as follows:
 1. After the fiber was cleaved near the face of the teflon plug, the end of the outer glass tube was outfitted with a snugly-fitting viton gasket that allowed the creation of a vacuum seal between the end of the glass tube and one side of a hole bored through a metal block.
 2. On the other side of this hole, a Kwik-Flange gasket created a seal between the metal block and a long, metal vacuum tube with a thin, glass, anti-reflection-coated window at the end for the transmission of laser light. On the input side, the tube length was 170 cm. On the exit side, the tube length was 130 cm.
 3. Holes machined in the lateral edge of the metal block were used for the connection of a gas line (on the laser-output side) or a vacuum line (on the laser-input side) to fill the fiber core with static pressure or a pressure gradient, which has been discussed previously as a way to reduce ionization and other detrimental effects in high-energy, high-throughput hollow-core compressors [156].
 4. To facilitate proper coupling of the laser through the waveguide, the metal block was mounted to a vertical translation stage, which itself was mounted atop a horizontal translation stage.

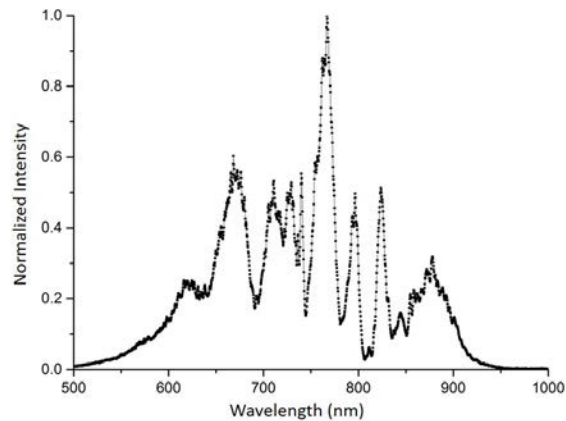
Between these two ends of the fiber, a thick metal bar was affixed to the two metal blocks to

add rigidity and stability to the assembly.

To maximize the signal between 700 nm and 900 nm, argon was fed into the gas line at a rate of 40 sccm using a mass flow controller. The vacuum line was activated so as to operate the setup under pressure gradient conditions. Using these parameters, an output of 1.25 mJ was achieved with an efficiency of $>70\%$. Figure 2.23(b) shows a sample spectrum from this hollow-core fiber setup.



(a) Uncleaved fiber.



(b) Spectrum of HCF output.

Figure 2.23: Hollow-core fiber using a flexible fused silica waveguide.

- The focusing element coupling the 1 kHz laser into the fiber was changed from a mirror to a lens of focal length 2 m.
- The diameter of the beam entering the Offner stretcher was increased by using a longer-focus collimating mirror after the hollow-core fiber. By increasing the area, it became possible to send the beam through the stretcher at the 1 kHz repetition rate without damaging the grating. This was convenient for CEP-locking purposes: because a high repetition rate is required for the CEP probe technique for locking the 10 Hz amplifier (see Sec. 3.3.2 for more details), it

was previously necessary to use a chopper wheel to protect the Offner stretcher from damage while operating the front-end CPA at 1 kHz.

- The large convex mirror in the Offner stretcher was changed from gold to dielectric to allow for higher input energies without damage. By also installing a new 1400 l/mm reflective diffraction grating, an overall efficiency of close to 50% was achieved.
- A new Q-switched frequency-doubled Nd:YAG laser was installed to pump the first Ti:sapphire amplifier, replacing the beam-split portion of the PRO350. This new system delivered 300 mJ of total energy to the crystal, with pump beams relay-imaged to either side of the crystal, just as before. The total energy output of the upgraded five-pass amplifier was 50 mJ.
- The second stage amplifier changed considerably as part of the system upgrade to 200 TW:
 - Because a new pump laser was installed to power the first amplifier, the full power of both PRO350 systems was available to pump the second amplifier. Moreover, the output of each of these PRO350 systems was factory-upgraded to 2 J/pulse. This increase in pump power, combined with the application of an index matching cladding for suppressing parasitic oscillations (discussed further in Sec. 2.3.1.3), allowed the output of the second stage amplifier to increase from 700 mJ to >1 J. The significance of this accomplishment is as follows: by increasing the gain of the second amplifier, the gain of the third amplifier need not be as high in order to reach pulse energies capable of achieving peak powers at the 100 TW level. Besides the direct, positive impact on the pulse parameters, a lower gain also typically implies that the amplifier can be operated at a higher efficiency, which is particularly important (i.e. cost-effective) when amplifying at the joule level.
 - The number of passes through the second Ti:sapphire crystal was decreased from four to three, and the arms of the multi-pass amplifier were shortened. This was done to

minimize the effect of thermal lensing and to keep the quality of the wavefront and beam profile as high as possible. This was important in generating a suitable seed for the third amplifier.

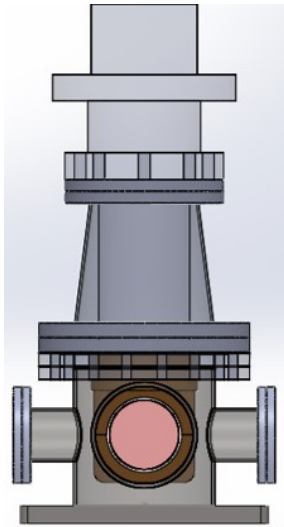
- While the pumping configuration still involved one beam incident to each side of the crystal, the profile of each beam was made as smooth as possible by using two-lens relay imaging (described in Sec. 2.3.1.2) *and* a beam homogenizer. The relay imaging was accomplished by means of two focusing lenses on either side of an evacuated tube, which was necessary to prevent the ionization of air at the inter-lens focus. The imaged beam passed through the beam homogenizer before arriving at the crystal. A focusing mirror was also included on either side of the crystal for pump recycling (i.e. the redirection of the unabsorbed, transmitted beams back to the crystal).
- Because beam homogenizers were used to pump the crystal as smoothly as possible, there was a significant amount of scatter in a narrow cone around the primary pump beam. Previously, this scatter had interacted with the indium foil between the crystal and the copper mount, generating particulates that led to damage of the crystal's anti-reflective coating. As part of the amplifier upgrade, a 2 mm-thick KV550 laminated longpass filter was mounted to each surface of the Ti:sapphire crystal with a hole cut in the center for unimpeded passage of the seed and pump beams. By absorbing the light incident outside the center-most region of the crystal, degradation of the crystal coating was prevented.

2.3.1 200 TW Pulse Amplification

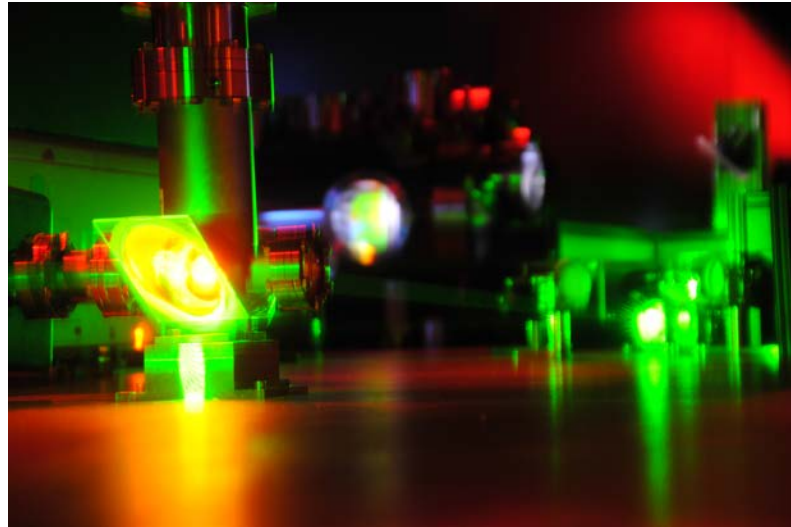
2.3.1.1 Ti:Sapphire Amplifier

The third amplifier was designed to support broadband amplification up to >5 J pulse energy. Physically, the amplifier crystal itself was 50 mm in diameter in order to accommodate the seed beam that was expanded to 20–25 mm in diameter by a telescope located after the second-stage amplifier. Because of the high pump energies, the doping of the crystal was kept relatively low to prevent the onset of parasitic lasing. As a result, a crystal thickness of 25 mm was employed, which still allowed a single-pass pump absorption of 92% despite the low Ti^{3+} concentration. The surfaces of the crystal were coated with a hard, broadband, anti-reflection coating to limit damage and reflection losses. The outer edge was placed in thermal contact with the cold finger of a cryogenic cooling system, which prevented the detrimental effects of thermal lensing. The entire apparatus was housed in an ion-pumped vacuum chamber with two large Brewster windows that allowed the entrance and exit of the pump and seed beams. The design and the implementation of this chamber are represented in Fig. 2.24(a) and Fig. 2.24(b), respectively.

Before the intended ultimate pump energy of the third-stage amplifier became available, the performance of the amplifier was tested using the on-hand pump energy. (Section 5.1 discusses the preparations for reaching the planned total pump energy of ~ 10 J.) In the first test, a 20 mm, 500 mJ seed pulse was amplified to 2.1 J after three passes through the unsaturated amplifier pumped by 5.5 J. While a subtle blue-shift in the spectrum resulted from the cryogenically-induced change to the gain profile, there was no gain narrowing effect on the amplified spectrum because the total gain was relatively low; the resulting spectrum shown in Fig. 2.25 was capable of supporting sub-15-fs pulse durations. At a later time when 6.6 J of pump energy was available, amplified pulse energies of 3.3 J were achieved using the same three-pass configuration.



(a) Chamber design.



(b) Third amplifier (front) with compressor chamber (back).

Figure 2.24: The third-stage Ti:sapphire-based amplifier of the IFAST 200 TW laser system.

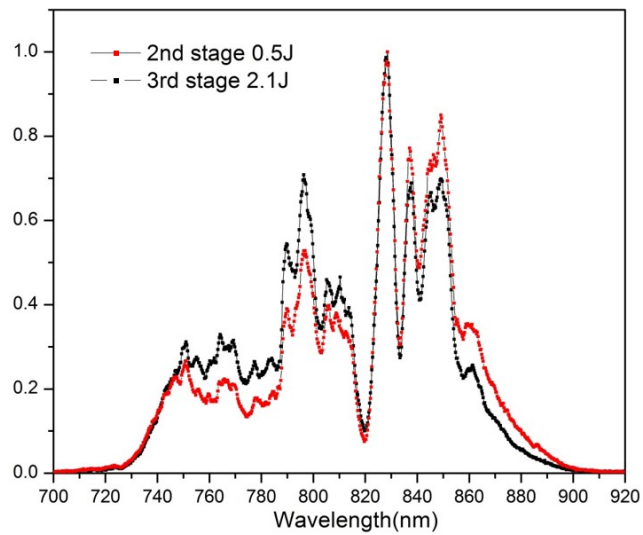


Figure 2.25: Broadband response of the third-stage amplifier in an early gain measurement.

2.3.1.2 Pumping Configuration

The proposed layout of the third-stage amplifier and its supporting pump lasers is depicted schematically in Fig. 2.26. The seed beam from the second-stage amplifier (red) enters from the bottom-left side before passing three times through the gray third-stage crystal chamber that is depicted near the center of the figure. The green boxes represent the six PRO350 systems used to pump the third-stage amplifier, with three lasers pumping each side of the Ti:sapphire crystal. At the time of writing, the four systems depicted in the top-middle of the schematic had already been installed and operated, with two pumps directed to either side of the amplifier. The two remaining systems – one on the far left edge and one in the bottom-right corner – will be installed at a later point in time (see Sec. 5.1). With 2 J/pulse from each PRO350 system, this pumping configuration will provide enough energy to reach the ultimate goal of 5-J amplified pulses before compression.

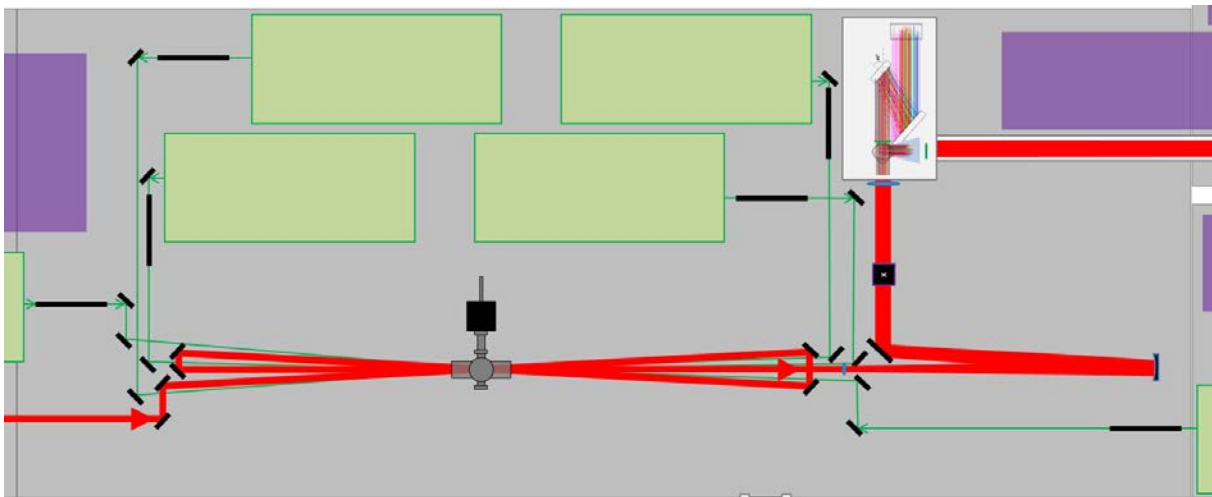


Figure 2.26: Representation of the third-stage amplifier layout at the IFAST lab. At the time of writing, four PRO350 systems (represented by the green boxes in the top-middle) were available.

In addition to the pulse energy, the spatial profile of the pumping lasers was also a key design concern, as malformed beams can lead to optical damage and attosecond pulse source irregularities.

Relay imaging is one common method for resizing the beam while preserving the original spatial profile emerging from the laser head. This is usually accomplished using a single lens, which results in a focus in the vicinity of the amplifier. While a vacuum tube can be used at such a focus to prevent ionization-induced loss of the beam's energy and spatial quality, the close proximity of *six* such foci would leave no room for the vacuum tubes or even the seed pulse. Therefore, single-lens relay imaging could not be implemented in this case.

To fit the spatial constraints of the lab environment while maintaining the benefits of relay imaging, a two-lens system was simulated (Fig. 2.27(a)) and then implemented (Fig. 2.27(b)). Although atypical, this relay imaging system still preserved the output laser's spatial profile while positioning the focus-enclosing vacuum tubes near the laser head rather than near the crystal (as represented by the vertically- or horizontally-oriented black lines near the output of each PRO350 system in Fig. 2.26). This allowed space for three relay-imaged beams to combine on each side of the crystal without disturbing one another or the multiple passes of the seed beam.

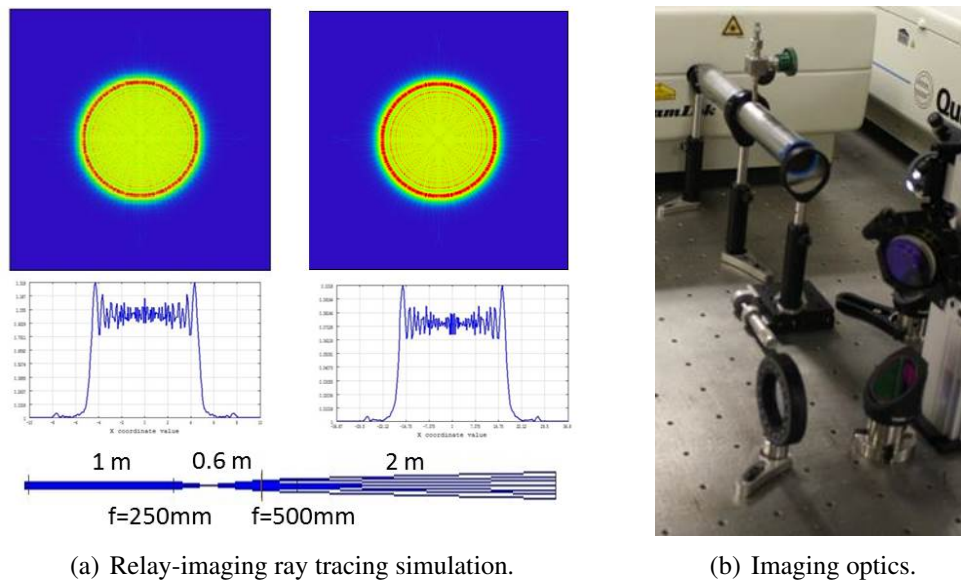


Figure 2.27: Relay imaging preserves the smooth pump profile output from the laser head.

For the amplification test shown in the previous section (Fig. 2.25), three relay-imaged beams were combined to the crystal. The arrival time of each pulse was controlled individually using a delay generator – an important capability that can help avoid the onset of parasitic oscillations. The profiles of the pump beams are shown in Fig. 2.28 (left) along with the amplified pulse profile (right). While small, ring-like structures were present in any single pump profile, the spatial averaging from overlapping several beams was sufficient to wash out any fine modulations, and the amplified profile was smooth due to the even total energy distribution in each pump beam.

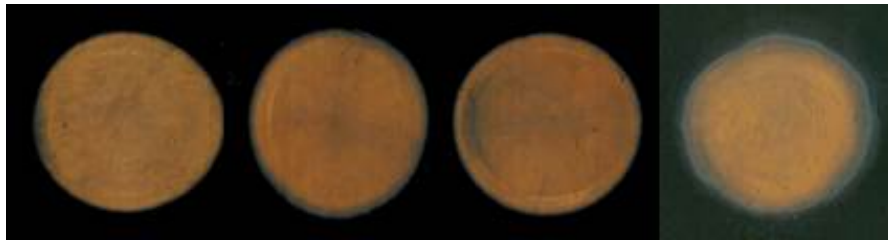


Figure 2.28: Beam profiles of three pump beams (left) and amplified beam (right).

To account for the non-negligible space, electricity, and cooling requirements for these laser systems, the IFAST laboratory was renovated to create two new utility closets. These closets were designed specifically to suit the operating needs of the pump lasers and included: twelve total 220VAC outlets (30A), eight total 110VAC outlets, and multiple access ports into the laboratory and between the two closets themselves. A new closed-loop chilled-water system was also installed, and five pairs of supply and return ports were placed in each closet that could each provide 18°C water flowing at 3 gal/min. A heavy-duty shelf was built in each closet in order to make enough space for all required power supplies. A separate air conditioning control loop was installed to handle the residual heat generated by the electronics. The results of the renovation can be seen in Fig. 2.29.



Figure 2.29: Utility closets constructed to house power supplies of the pump lasers for the IFAST 200 TW system.

2.3.1.3 Index Matching

As stated in Sec. 2.1.3, gain in high-energy, large-aperture amplifiers can be squandered by laser oscillations occurring in the transverse dimension of the crystal. In the IFAST 200 TW laser system, the output of the second stage amplifier when using an *untreated* crystal was limited by the onset of parasitic lasing, capping the seed energy into the third stage amplifier at <700 mJ. If this energy could be increased, it would relax the requirement on the total gain of the third stage amplifier, where parasitic lasing is an even bigger threat due to the larger beam diameter and higher pump fluence.

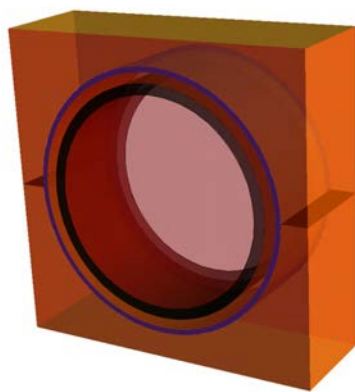
One common technique used to forestall the beginning of parasitic lasing is index matching. Under this method, the outside edge of the crystal is put into optical contact with an absorber-doped material with an index of refraction similar to the crystal itself. This diminishes the amount of Fresnel reflection occurring at the boundary. Therefore, edge-incident photons are transmitted into the cladding medium and then absorbed rather than creating a parasitic, transverse laser cavity.

Many index-matching materials for Ti:sapphire are thermoplastics that can be heated and applied to the crystal directly [142]; others are liquids that can also be circulated around the crystal to provide a cooling effect [157]. However, for cryogenically-cooled amplifiers such as the third stage of the IFAST 200 TW laser, the low-temperature, low-vacuum environment precludes the use of these standard index-matching materials. Even if a hardy material could be found, many index-matching materials are also poor thermal conductors, which could lower the effectiveness of the cooling unit and limit the repetition rate of the laser.

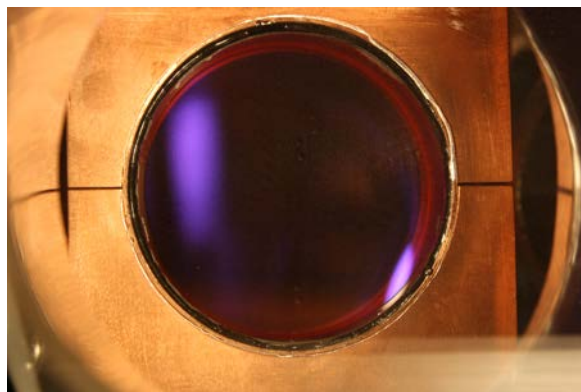
To solve this problem, a mixture of cryogenic-safe epoxies – Stycast 1266 and Stycast 2850 – was identified that could maintain optical contact with the ground edge of a Ti:sapphire crystal while preserving its mechanical properties in a low-vacuum environment. Because the two epoxies had

largely different refractive indices, mixing them with a predetermined ratio (in this case, near 1:1) resulted in an aggregate compound whose refractive index suitably matched that of sapphire. Furthermore, the epoxy's pre-hardened matrix could accept graphite and graphene, which could serve to increase the optical absorption and the thermal conduction of the final product as needed.

In applying this technique to the second-stage and third-stage amplifiers of the IFAST 200 TW laser, the thickness of the epoxy layer itself was kept around 1 mm to avoid possible cracking caused by a mismatch between the thermal coefficients of the composite epoxy and the sapphire. This was accomplished by using a copper ring as a cavity mold, choosing an inner diameter that was ~ 2 mm larger than the diameter of the crystal. Once the epoxy had been poured and given time to harden, the copper ring with its cladding-coated crystal was aligned and mounted in thermal contact with a water-cooled copper block (as with the second amplifier) or the cold finger of a pulse tube cryorefrigerator (as with the third amplifier). As a result of this application, the energy output of the second-stage Ti:sapphire amplifier could be increased from <700 mJ to beyond the joule-level. It is anticipated that this anti-parasitic-lasing effect will be of even greater importance to the third-stage amplifier once all of its intended pump energy is available.



(a) Cladding (black), cavity mold (copper), indium foil (gray).



(b) Third-stage Ti:sapphire crystal with visible cladding, cavity mold, and indium foil.

Figure 2.30: Index-matched, ASE-absorbing cladding for suppressing parasitic lasing.

2.3.2 200 TW Pulse Compression

2.3.2.1 Grating Compressor

Because of the higher power and the additional dispersion from the third-stage amplifier, a new compression scheme was implemented to achieve 15 fs pulse durations. As in the IFAST 10 TW system, the pulse compressor was housed in a vacuum chamber, which is depicted in Fig. 2.31(a). This chamber was designed to allow measurements of important beam parameters such as the pulse energy, duration, wavefront, CEP, and focusing. The compressor itself adopted the double-pass design with two reflective diffraction gratings featuring groove densities of 1480 l/mm.

To keep the fluence on the gratings at safe levels ($<100 \text{ mJ/cm}^2$), the input beam was expanded to 75 mm in diameter, thus requiring gratings with large dimensions in order to fit both passes through the pair. Grating 1 (175 mm \times 135 mm; left) and Grating 2 (165 mm \times 220 mm; bottom-right) are both visible with the roof mirror (top-right) in Fig. 2.31(b). The large beam size also constrained the angles (52° incidence, 28° deviation) and separation (21.7 cm) of the gratings, as the compressor arrangement could not clip the beam at any location (Fig. 2.31(c)).

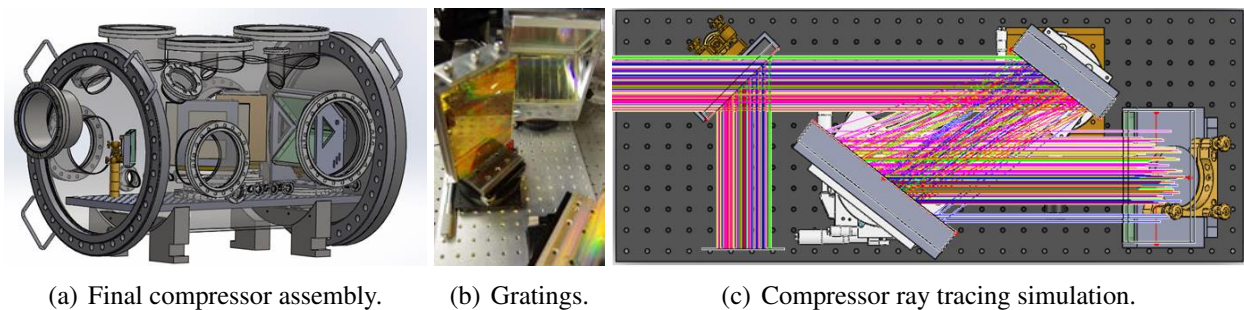


Figure 2.31: The grating compressor was designed to output 3 J, 15 fs pulses.

In addition to their spatial properties, the selected gratings were also selected for their high diffraction efficiency ($>90\%$) across nearly the full 700 nm – 900 nm laser bandwidth, leading to an overall measured throughput of $>60\%$. This was also accomplished without any serious reshaping of the spectral profile, as demonstrated by Fig. 2.32, which shows the spectral response of the Offner stretcher, the 4-f zero-dispersion pulse shaper (discussed in Sec. 2.3.2.3), and the grating compressor.

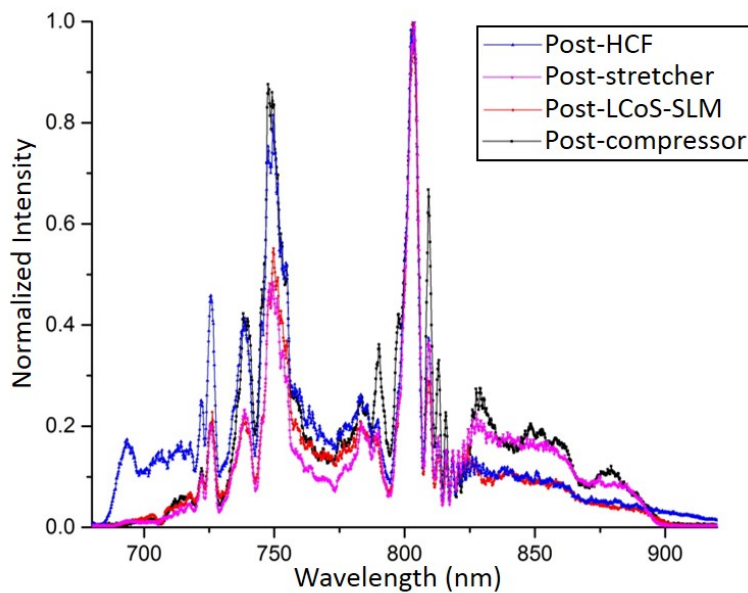


Figure 2.32: Pulse spectrum after various stages of the IFAST 200 TW system.

2.3.2.2 Plasma Cleaning

One common problem with high-power pulse compressors is the deposition of carbon on optical surfaces, which arises from the laser-induced breakdown of organic molecules persistent in the residual vacuum. This process can detrimentally affect the beam quality and permanently damage the optical elements. While several methods have been conceived to address the issue, many of them are time-consuming, inconvenient, expensive, or even all of the above.

In the IFAST 10 TW compressor chamber, this problem was solved by using an RF plasma cleaning technique. This method, like other plasma cleaning schemes, harnessed the reactivity of species in the plasma to bond with the carbon contaminants, resulting in gas molecules that could be pumped from the chamber. The difference was that traditional plasma cleaners are very expensive and operate at a single, fixed frequency (e.g. 13.56 MHz); the IFAST method used off-the-shelf amateur radio parts, and the operating frequency could be tuned to match the length of a home-made antenna. This freedom allowed the online recovery of contaminated optics, as the antenna could be installed inside the chamber in a position appropriate for cleaning. Figure 2.33 shows an example of the effectiveness of this cleaning method in completely removing two carbon spots from the surface of a birefringent element used in GDOG. The compressor chamber for the IFAST 200 TW compressor was designed to accommodate several radio antennae for online plasma cleaning.

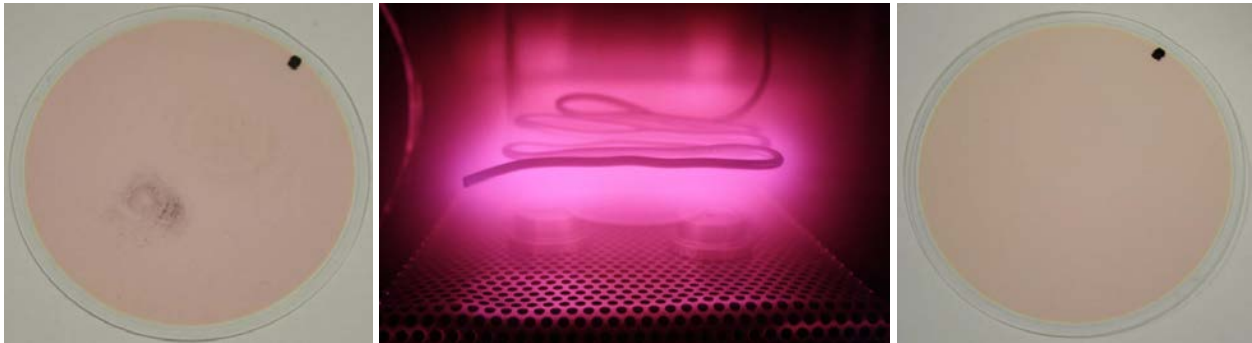


Figure 2.33: Recovery of a carbon-contaminated quartz plate before (left), during (center), and after (right) RF plasma cleaning.

2.3.2.3 Spectral Shaping

Of course, even an optimally-tuned grating compressor may be incapable of achieving transform-limited pulse durations due to high-order phase errors that can develop from material dispersion, non-flat-phase mirror coatings, and the like. For this reason, many short-pulse laser systems in-

clude a spectral phase modulator – such as those mentioned in Sec. 2.1.2.4 – that can correct these phase errors and improve the pulse duration.

In the IFAST 10 TW laser system, a deformable mirror was placed at the Fourier plane of a high-throughput, 4f-zero-dispersion stretcher (see Sec. 2.2.2). The voltages of the actuators attached to the gold reflective surface could be tuned to shift the phase of different spectral components relative to each other. Unfortunately, this particular deformable mirror only featured 20 channels for the 700 nm to 900 nm bandwidth, resulting in a lack of fine control. Additionally, the continuous reflective membrane prevented rapidly-varying correction such as phase jumps. Both of these limitations impeded the IFAST 10 TW laser from outputting pulses even closer to the Fourier limit.

In order to improve on these short-comings, the deformable mirror was replaced with a liquid-crystal-on-silicon (LCoS) spatial-light modulator (SLM) – a tool that was used for phase shaping at the terawatt level for the first time in the IFAST lab. When placed at the Fourier plane of a 4-f, zero-dispersion stretcher, such a device works as follows: a collimated, spectrally-dispersed pulse transmits through a transparent, grounded electrode and propagates through a liquid crystal cell before retro-reflecting off a high-reflective broadband dielectric stack and exiting the way it came. Beneath the mirror surface are individually-addressable electrodes, which can change the index of refraction of the liquid crystal region directly on the other side of the dielectric stack. As different electrodes apply different voltages, the relative phases between the different wavelength components of the spectrally-dispersed pulse can be adjusted. A schematic and picture of the LCoS-SLM are shown in Fig. 2.34.

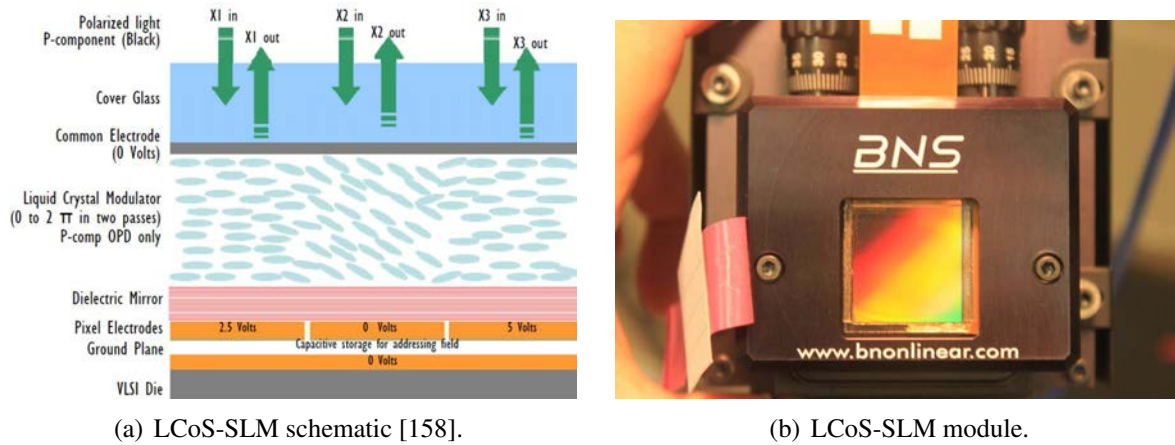


Figure 2.34: A LCoS-SLM corrects phase errors to help with pulse compression. (Courtesy of Boulder Nonlinear Systems.)

A LCoS-SLM possesses several advantages over its deformable mirror counterpart:

- Because the electrodes can be very small, the number of LCoS-SLM pixels can be much larger than the number of deformable mirror actuators – in this case 12,288 compared to 20!
- The increased number of pixels can allow a more individualized control over the incident wavelengths (in this case, $\Delta\lambda/\text{actuator} = 200 \text{ nm}/20 \text{ actuators} = \mathbf{10 \text{ nm/actuator}}$ for the deformable mirror compared to $\Delta\lambda/\text{pixel} = 200 \text{ nm}/12,288 \text{ pixels} = \mathbf{0.016 \text{ nm/pixel}}$ for the LCoS-SLM) to the point that the addressability may be limited by the spectral resolution of the zero-dispersion stretcher rather than by the pixel density of the pulse shaper.
- Since the pixel resolution can be so fine with respect to the wavelength spread, the LCoS-SLM can theoretically be used for *amplitude* shaping in addition to phase shaping, as adjacent pixels can be patterned to add a phase correction *and* create grating-like structures that partially diffract away incident light. While this function can be used simply to smooth out modulations in the spectrum, it can also mitigate the effects of gain narrowing by adding

spectral loss near the peak of the gain profile. This can flatten the overall gain across the entire spectrum.

- In a LCoS-SLM, neighboring pixels are no longer coupled together with a membrane, meaning that drastically-differing corrections can be applied even from pixel to pixel. This also means that the applied corrections can wrap the phase by containing a phase jump from one pixel to the next, if so desired.

To use the LCoS-SLM for phase shaping, the same approach was used that was described in Sec. 2.2.2 with the deformable mirror: a home-built single-shot SHG FROG was used to initially tune the grating compressor and then to provide feedback for an evolutionary algorithm, which optimized the voltages of the LCoS-SLM pixels. Due to the sheer number of pixels, it would be too computationally taxing to allow several thousand pixels to participate in the optimization process; therefore, it was found to be sufficient to use 56 equally-spaced pixels with the intermediary pixels determined by a smoothing function. Using this method, low-energy laser pulses were compressed to 13.4 fs in duration, as shown by the FROG retrieval in Fig. 2.35.

Assuming that a similar compression can be achieved when allowing the grating compressor to experience the full pulse energy of the third amplifier (Sec. 2.3.1.1), and conservatively estimating a compressor throughput of 60% (Sec. 2.3.2), it is expected that the peak power of the IFAST laser system would reach 150 TW even without further amplification:

$$3.3 \text{ J} \times 60\% \text{ efficiency} / 13.4 \text{ fs} = 150 \text{ TW}$$

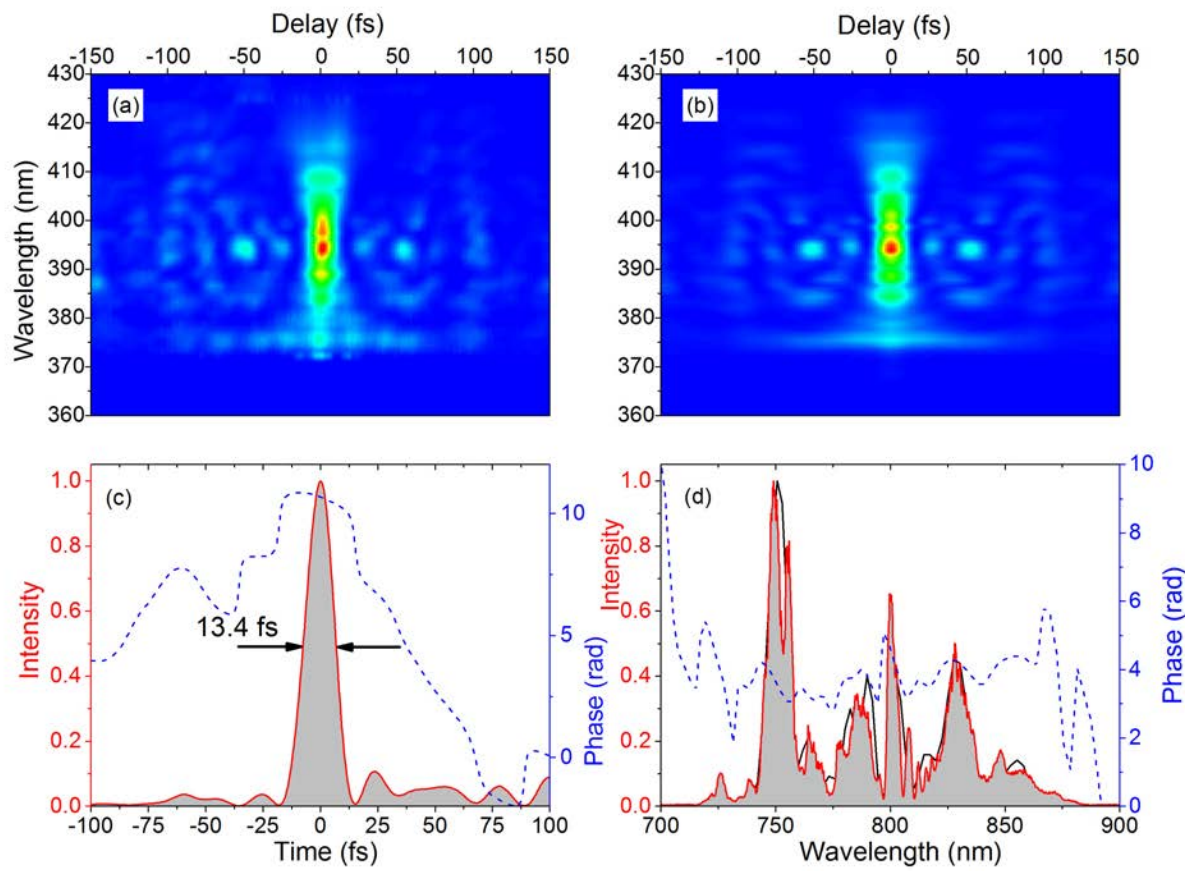


Figure 2.35: FROG measurement of pulses compressed by the IFAST 200 TW compressor and LCoS-SLM.

CHAPTER 3: CARRIER-ENVELOPE PHASE CONTROL AT 10 Hz

The carrier-envelope phase (CEP) of a laser pulse plays a critical role in attosecond pulse generation, making it an important parameter to control when producing pulses for all-attosecond pump-probe experiments. Unfortunately, traditional methods do not allow for the CEP stabilization of chirped pulse amplification (CPA) systems operating at repetition rates much lower than 1 kHz. This chapter outlines a new technique for enabling CEP control in sub-1 kHz repetition-rate CPA systems such as the IFAST 200 TW laser.

3.1 Introduction to Carrier-Envelope Phase

In the field of high-intensity ultrafast laser science, there are certain processes such as high-harmonic generation and isolated attosecond pulse production that do not rely on the time-averaged intensity of the femtosecond driving pulse, but rather on the instantaneous amplitude of the underlying electric field oscillations themselves. In order to describe this sub-cycle dependence adequately, the concept of carrier-envelope phase must be introduced.

3.1.1 *Fundamental Concept*

The carrier-envelope phase ϕ_{CE} of a laser pulse is defined as the phase difference between the temporal peak of the pulse's Gaussian envelope and the maximum instantaneous value of its underlying carrier electric field. For example, a pulse with $\phi_{\text{CE}} = 0$ is one in which the maximum of the Gaussian envelope and the maximum value of the electric field coincide in time (i.e. the carrier wave looks like a cosine function); alternatively, a pulse with $\phi_{\text{CE}} = -\pi/2$ is one in which the electric field is zero at the time when the Gaussian envelope is maximum (i.e. the carrier wave looks

like a sine function). This distinction is shown graphically in Fig. 3.1. Mathematically, the time-dependent instantaneous electric field can be expressed as $E(t) = \exp[-(t/\tau_p)^2] \cos[\omega t + \phi_{\text{CE}}]$, where τ_p is the temporal duration of the Gaussian envelope, ω is the carrier frequency of the laser pulse, and ϕ_{CE} is the carrier-envelope phase.

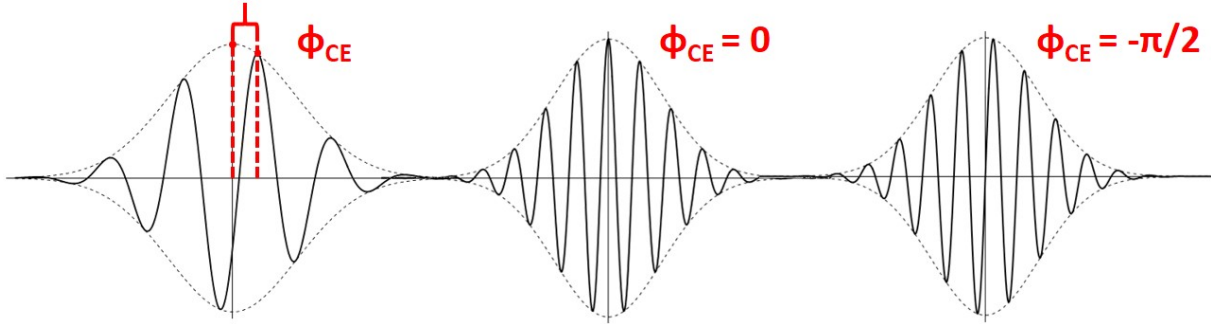


Figure 3.1: The CEP describes the position of the electric field beneath the pulse envelope.

3.1.2 Influence on Physical Phenomena

The CEP of a laser pulse has been shown to influence many physical processes such as pulse propagation through polar molecules [159], cross-phase modulation [160], ponderomotive surface-plasmon electron acceleration [161], above-threshold ionization [162, 163], photoemission from metallic surfaces [164, 165], and terahertz emission from the laser breakdown of air [166]. The process of high-harmonic generation is also highly-dependent on the CEP [167–172], meaning that attosecond pulse generation [173–175] and its gating schemes [176–180] are fundamentally affected as well.

Of greatest concern to the 200 TW IFAST project is the dependence of attosecond pulse flux on the CEP. When using generalized double optical gating (GDOG), the width of the polarization gate can be constrained to be smaller than an optical cycle: in this case, only one attosecond pulse

is generated, no matter the value of the CEP [181]. However, the CEP value *does* determine the *efficiency* of this pulse-production process. This means that a driving pulse with unstabilized CEP may indeed be manipulated such that only one attosecond pulse is produced per shot, but the flux of that single pulse relies closely on the CEP (depicted in Fig. 3.2). This variation is undesirable for usage in all-attosecond pump-probe measurements or nonlinear XUV experiments. Therefore, it becomes essential to monitor and, when possible, stabilize the CEP in order to regulate the attosecond generation process.

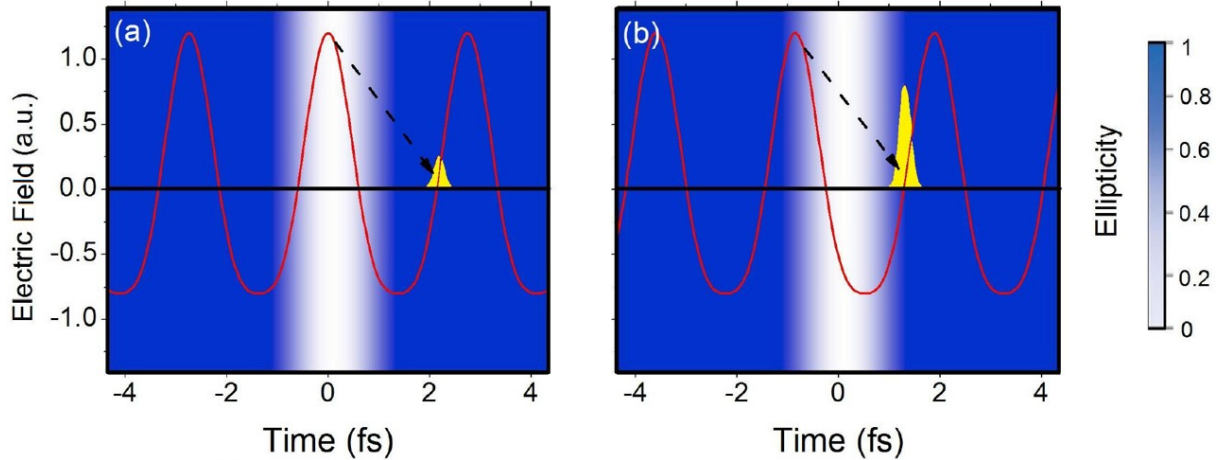


Figure 3.2: Attosecond flux from a two-color sub-cycle gate with (a) $\phi_{CE} = 0$ and (b) $\phi_{CE} = \pi/2$. Reprinted with permission from [181]. Copyright 2010 by the American Physical Society.

3.2 Standard CEP Measurement and Stabilization Techniques

In a typical Ti:sapphire oscillator and CPA, nothing naturally constrains the pulses to have consistent CEP values from shot to shot. In fact, pump energy fluctuations, thermal variations, pointing instabilities, air currents, and mechanical vibrations (especially in the diffraction gratings of the CPA stretcher and compressor [182]) can all cause the CEP to change over time. Numerous ways of stabilizing these CEP fluctuations in both the oscillator and the CPA have been devised over the

past decade using feedback or feed-forward control loops. Such stabilization techniques rely on 1) measuring the latest CEP of a pulse (or average CEP of a group of pulses), 2) comparing the value to a set point (or, in a feed-forward configuration, inserting the value into the mathematical model), and 3) providing corrective action to reduce the CEP drift.

Many methods have been proposed for measuring the CEP, typically by way of one or more nonlinear processes. One of the most common – the f-to-2f interferometer – uses second harmonic generation. Other physical indicators used to extract a pulse's CEP include: above-threshold ionization [162, 163, 183–185], photo-ionized electron angular and spatial distributions [186, 187], SHG-THG or 2f-3f interferences [188, 189], DFG-SHG interferences [190], one- and two-photon absorption interferences [191], half-cycle HHG cutoff positions [172], self-DFG or 0-f interferences [192, 193], and other interferences involving multiple nonlinear processes [194].

These phase measurements can be used to direct feedback or feed-forward control loops for locking the CEP. As the CEP is sensitive to many parameters, corrective action can be applied in many ways. Such feedback mechanisms include: tuning wedges inside the oscillator [195–197], adjusting cavity mirrors inside the oscillator [191, 196, 198], varying pump power to the oscillator or amplifier using an acousto-optic modulator [179, 196, 199–202] or electro-optic modulator (EOM) [190, 197, 203], changing the grating or prism separation in stretchers and compressors [182, 204, 205], or even modifying the phase directly using an AOPDF [206], acousto-optics frequency shifter (AOFS) [207], or EOM [208].

Going into more detail, the f-to-2f interferometer is often used to measure the CEP of both high-repetition rate oscillator pulses and low-repetition rate amplified pulses. As functionality in each case differs slightly, the following two sections individually describe the measurement the CEP in the IFAST oscillator and kHz amplifier. (Note that oftentimes both types of locking are performed simultaneously to correct fast and slow CEP drifts [179, 202].)

3.2.1 Oscillator Pulses (80 MHz)

Because of the frequency comb-like nature of femtosecond oscillators, it is convenient to consider CEP using the language of frequency combs and the frequency domain. First, the carrier-envelope offset frequency f_{CEO} is measured using f-to-2f interferometry [187]. In a typical setup, a fraction of the output of the oscillator is taken using a beam splitter. The pulse sampling is first passed through a photonic crystal fiber, which broadens the spectrum of the laser such that it covers a full octave. The beam is separated into its long and short wavelength components using dichroic optics, and the long wavelengths are frequency-doubled using a nonlinear crystal. Where these two beams now overlap in the frequency domain, the individual teeth of the two different frequency combs are separated by f_{CEO} . Thus when recombined, the interference produces a beat frequency equal to f_{CEO} , which can be measured by an avalanche photodiode connected to an RF spectrum analyzer. For ease of detection, the pulse-to-pulse phase slip of the oscillator is often locked to $\pi/2$ in order to produce a beat note that is easily detectable at a frequency one-quarter of the repetition rate (i.e. far away from the DC peak).

To lock the CEP change between pulses, a fast photodiode reads the repetition rate of the oscillator and divides it by four. This signal is sent to a digital phase detector along with the measured beat frequency from the f-t-2f interferometer; as the two signals are meant to be equal, any residual difference between the two frequencies serves as an error signal. This provides feedback to a PID controller, which in turn adjusts the oscillator pump power with an acousto-optical modulator. Such a setup is shown in Fig. 3.3. This locks the CEP change of the oscillator pulses such that every fourth pulse possesses the same CEP, which is not a problem for femtosecond amplifiers since the repetition-rate-reducing pulse-picker can be triggered appropriately to choose pulses with consistent CEP values.

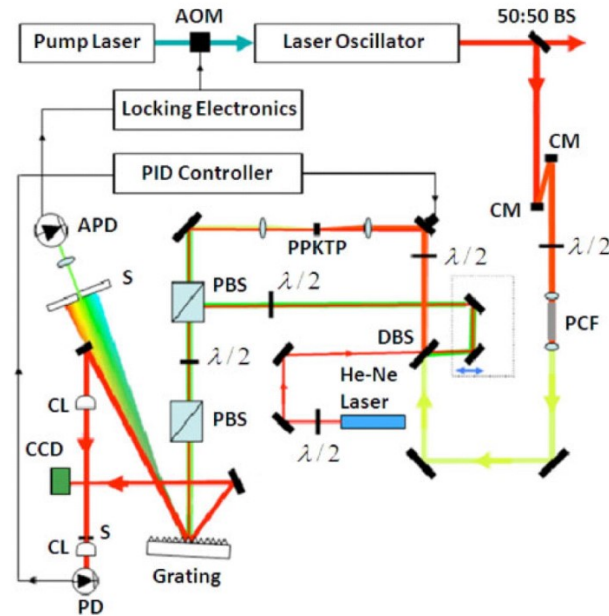


Figure 3.3: F-to-2f interferometry with oscillator pulses. Copyright 2010 Wiley. Used with permission from [205].

3.2.2 Amplified Pulses (1 kHz)

Amplified pulses differ from the oscillator pulses in that the repetition rate is much lower, so the beat frequency between the f and $2f$ components would no longer be in the RF domain. In this case, a different-yet-related technique is used called Fourier transform spectral interferometry (FTSI) [209].

As before, the first step is to broaden the spectrum of the laser pulse to cover an octave. Because higher energies are available after amplification, this can be performed easily using white light generation in bulk material (fused silica, undoped YAG, sapphire, etc.). The dispersion in the plate causes a fixed delay in time τ_g between the short and long wavelength components. A nonlinear crystal is then used to double the frequency of the long wavelengths such that the resulting second harmonic overlaps in frequency with (but remains separated in time from) the short wavelengths.

When this overlap region is detected by a spectrometer, an interference pattern is observed from which the CEP can be extracted using FTSI. This process is sketched in Fig. 3.4.

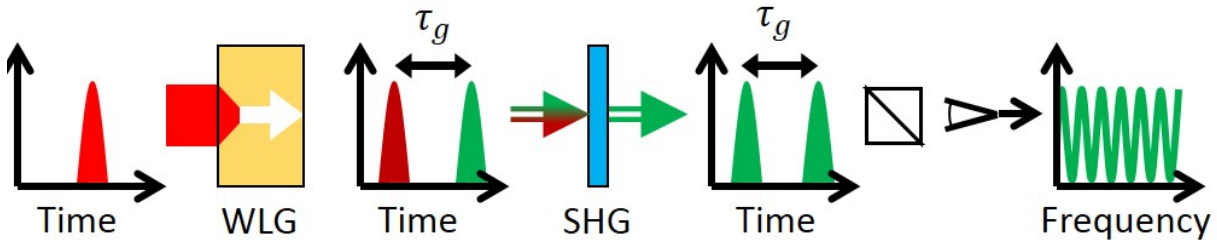


Figure 3.4: F-to-2f interferometry with amplified pulses.

The inverse Fourier transform is first applied to the spectrum, which reveals a DC term at $t = 0$ and an interference term at $t = \pm\tau_g$. The Fourier transform is taken of the positive delay term only, and the resulting total phase of the transform includes information about the CEP. If it is assumed that the spectral phase and the delay τ_g remain nearly constant between two consecutive pulses, then the shot-to-shot difference between the extracted total phases is equal to the shot-to-shot difference between the two pulses' CEP values. When locking the CEP, this value serves as the error signal that is input to the PID controller. Feedback in this case is provided to a piezoelectric actuator controlling the position of the grating in the stretcher or compressor. A block diagram of such a setup is shown in Fig. 3.5.

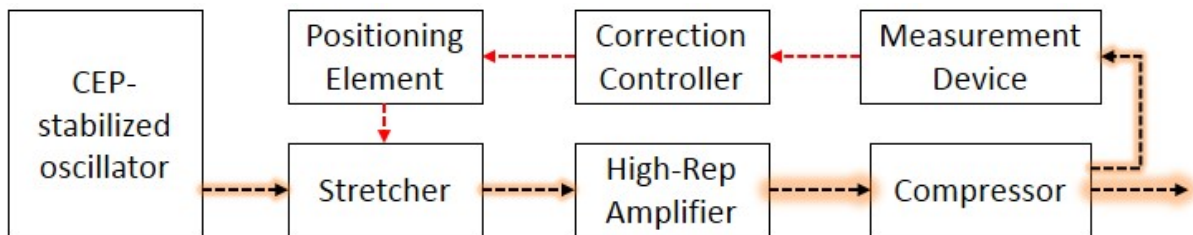


Figure 3.5: Scheme for locking the CEP of the IFAST 1 kHz system.

3.3 Stabilization of the CEP at 10 Hz

3.3.1 *Difficulty of Sub-kHz CEP Control*

Besides the use of different detectors, another crucial distinction between the oscillator (80 MHz) and CPA (1 kHz) CEP locking schemes is the limit on compensable noise frequencies (or, rather, on the fastest possible feedback response). Because of the high repetition rate of the oscillator, pulses arrive at the detector so quickly that the latency of the electronics limits the timeliness of CEP-corrective action. In the case of a CPA, however, CEP adjustments can be applied *only as often as a new pulse arrives with the latest CEP error information*. This means that any CEP jitter occurring at frequencies near to or higher than half the laser's repetition rate (in accordance with the Nyquist sampling criterion) cannot be compensated.

Considering the problem in the time domain: a single-shot f-to-2f interferometer of a *1 kHz* CPA can track and correct changes to the CEP every *1 ms*. If no large disruptions take place on the sub-millisecond time scale, then corrective feedback still carries relevance by the time the next pulse arrives 1 ms later. This is typically true at 1 kHz: corrective action successfully stabilizes the jitter of the upcoming pulse since the CEP values of consecutive pulses are still correlated.

A single-shot f-to-2f interferometer of a *10 Hz* CPA, however, can only track and correct changes to the CEP every *100 ms*. This means that any type of disturbance – mechanical vibrations, air currents, thermal fluctuations, etc. – occurring within tens of milliseconds is completely invisible to the CEP measurement. Even if a feedback loop executes an adjustment based on the phase retrieved by the f-to-2f interferometer, the action becomes outdated and irrelevant well before the next pulse arrives to make use of the correction. In other words, the CEP values of pulses separated by 100 ms are not naturally well-correlated with each other.

3.3.2 The “CEP Probe” Technique

Since a low repetition-rate CPA cannot be locked because new feedback information arrives too infrequently, a high repetition-rate “CEP probe” can be procured in order to increase the sampling rate for the CEP feedback system.

In general: for a low repetition-rate amplifier seeded directly by a high repetition-rate amplifier, the beam is sampled directly after the high repetition-rate amplifier rather than after the compressor (as performed in Sec. 3.2.2). This high-repetition-rate beam bypasses the low repetition-rate amplifier – permissible because most CEP drift arises from mechanical vibrations in the stretcher and compressor, not in the amplifier – and then passes through the same compressor used by the low repetition-rate amplified pulses. By doing so, all additional CEP errors arising from mechanical vibrations in the compressor are encoded in the probe beam. Thus when the CEP of the probe beam is measured and the control loop signal is established, the feedback is made using information describing nearly the same set of conditions encountered by the low repetition-rate laser. This effectively locks the high repetition-rate pulse’s CEP along with the low repetition-rate pulse’s CEP. A schematic of such a setup is shown in Fig. 3.6.

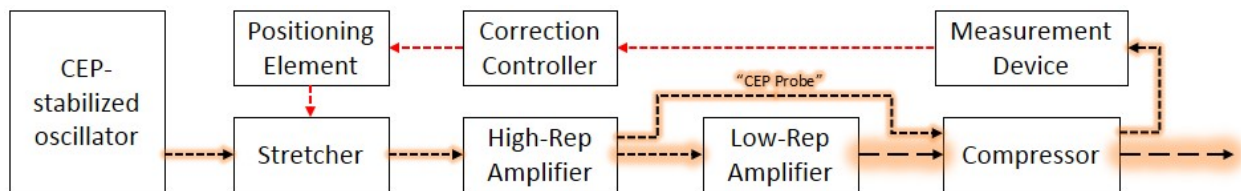


Figure 3.6: The CEP probe provides phase information relevant to both beams.

3.4 CEP Control of the IFAST 10 TW Laser

Because of the potential impact of successfully locking the CEP of a low repetition-rate CPA, early testing of the CEP probe technique was carried out on the IFAST 10 TW laser system.

3.4.1 Application of the CEP Probe Technique

The block diagram in Fig. 3.7 depicts how the CEP probe technique can be applied to a double CPA laser in which the high- and low-repetition amplifiers are in separate CPA systems. This scheme is relevant to the 1 kHz-front-end, 10 Hz-back-end double CPA scheme used in the IFAST lab, as described in Sec. 2.2.2.

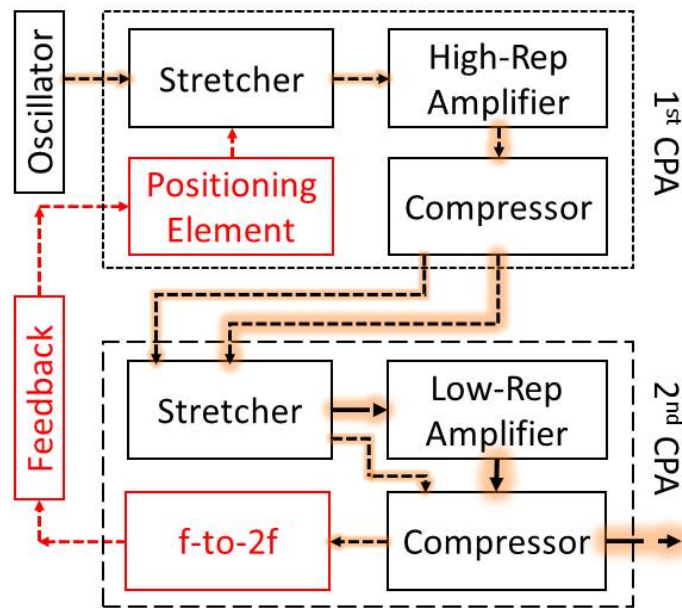


Figure 3.7: Scheme for locking the CEP of the IFAST 10 Hz system.

First, the CEP-stabilized pulses from a femtosecond oscillator were stretched, amplified, and compressed at a repetition rate of 1 kHz. After the compressor, a sampling of the beam was taken to

serve as the CEP probe, which always maintained the same 1 kHz repetition rate.

Before the two beams passed through the second CPA's pulse stretcher, the fluence of the 1 kHz main beam was reduced in order to prevent damage to the diffraction grating. For this purpose, a phase-locked optical chopper was used to block most of the incoming pulses, leaving only the pulses destined to be amplified in the 10 Hz CPA. In practice, a few neighboring pulses were also transmitted, but these pulses could be ignored as they did not see any gain in the 10 Hz amplifiers and therefore became negligible compared to the amplified pulses. In total, the chopper was able to reduce the power incident on the stretcher grating by $\sim 90\%$. (This chopper wheel was no longer necessary after the system was changed to accept a larger beam in the stretcher, as discussed in Sec. 2.3.)

Next, the laterally-separated seed beam (now at 10 Hz) and the probe beam (still at 1 kHz) were chirped in the pulse stretcher, and then the seed beam was sent to be amplified. The probe beam, however, bypassed the 10 Hz amplifiers – mainly done to prevent losses to the probe beam signal due to absorption inside the amplifier that would otherwise attenuate the probe beam below the threshold needed for white-light generation in the f -to- $2f$ interferometer. As the mechanism for CEP jitter is not as sensitive in the amplifier as in the stretcher and compressor, avoiding the amplifier with the probe beam was nonideal but still permissible for achieving CEP control.

By skipping all the passes through the gain medium, however, a probe beam experienced less dispersion as compared to the 10 Hz amplified pulse. This dispersion needed to be compensated so that the probe could be compressed by the same grating configuration used for the 10 Hz amplified pulse; otherwise, the probe would become negatively dispersed, and its peak intensity would become too weak for white-light generation in the f -to- $2f$ interferometer. Therefore, the probe pulse propagated through several bulk glass rods prior to entering the compressor in order to match the material dispersion experienced by the 10 Hz pulses in the Ti:sapphire amplifiers.

Finally, the equally-chirped seed beam (now amplified at 10 Hz) and the vertically-displaced probe beam (still at 1 kHz) traversed the pulse compressor. While the amplified, compressed 10 Hz beam was directed towards the experimental setup, the compressed 1 kHz probe beam was injected into the f-to-2f interferometer. The residual CEP error of the pulse – accumulated over the course of both CPA systems – was measured and recorded, and a feedback signal was sent to a piezoelectric actuator in the stretcher of the first CPA. This corrected for the cumulative CEP error of the entire system.

The singular occurrence of this process was not responsible for locking the CEP of the 10 Hz laser. Rather, the crucial point is that *this process was repeated **even in the absence** of the 10 Hz beam* every 1 ms by the 1 kHz CEP probe beam. These intermediate measurements and adjustments were essential to ensuring that the physical system was also locked every 100 ms when the next 10 Hz pulse was generated. Considering the application of the CEP probe technique in the frequency domain: by sampling the CEP at the 1 kHz repetition rate, the feedback loop was able to compensate for CEP jitter caused by prominent acoustic noise frequencies in the tens to few hundreds of Hz range which would have been otherwise missed by sampling at 10 Hz.

3.4.2 *Effect of CEP on Gated HHG*

To test the efficacy of the CEP probe method, the influence of the CEP on the gated HHG spectrum in argon was measured with the IFAST 10 TW laser (see Sec. 2.2.2). For this experiment, the system provided 350 mJ, 14 fs pulses which propagated through the birefringent GDOG optics in order to create an electric field appropriate for isolated attosecond pulse production. After loosely focusing to a 100 mm-long gas cell backed by 4 Torr of argon, the XUV pulse was generated and then separated from the residual NIR pulse. The isolated XUV spectrum was then measured with a flat-field soft x-ray spectrometer and a charge-coupled device (CCD) detector. As the CEP of the driving laser pulse was scanned linearly from 0 to 6π , the harmonic spectra varied with a 2π periodicity, which is consistent with the periodicity of a two-color driving field. This spectrum is shown in Fig. 3.8.

3.4.3 *Difficulty of f-to-2f with 10 Hz Beam*

Perhaps the most straightforward evaluation of the viability of the CEP probe method would be a direct observation of the 10 Hz pulse's CEP itself. In such a setup, a second "out-loop" f-to-2f interferometer would measure the CEP of the 10 Hz amplified pulse, which could then be compared to the CEP value of the 1 kHz probe pulse captured by the first "in-loop" f-to-2f interferometer. Assessing the level of correlation between the two measurements would be informative about how accurately and effectively the 10 Hz pulse's CEP can be represented by the 1 kHz probe's CEP.

Unfortunately, f-to-2f measurements themselves are prone to error due to, among other influences, the fluctuations of the incident pulse parameters [210–212]. This can be explained in part by the dependence of the white-light generation process on pulse energy: for a pulse with a higher pulse energy, the self-focusing effect is stronger in the sapphire plate, leading to a longer filament than

for lower pulse energies. This difference changes the phase accrued before and after the filament, thus defying the previous assumption that such phases remain constant shot-to-shot [212].

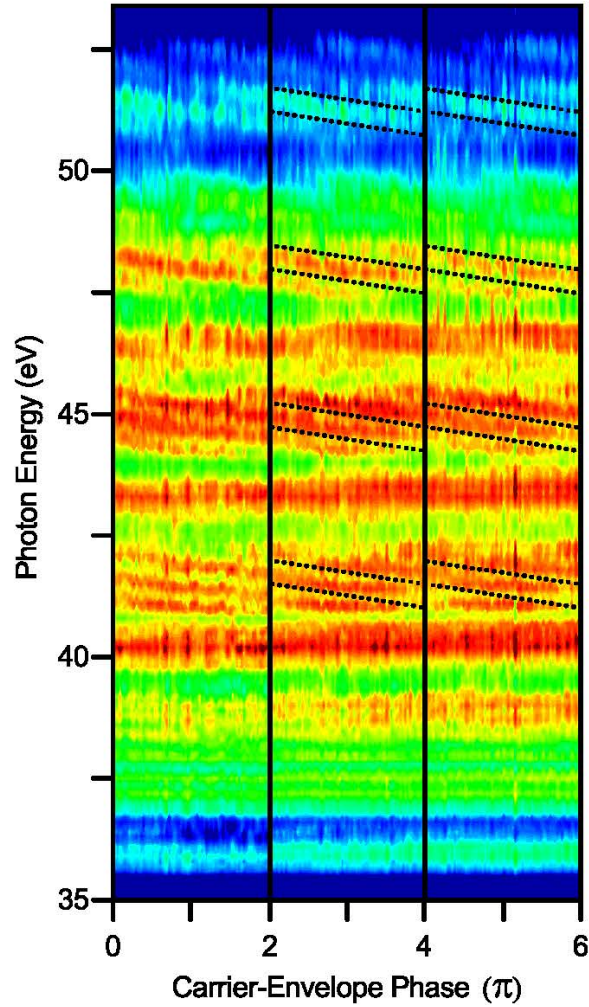


Figure 3.8: Repeating structures in a 6π CEP scan of the gated HHG spectrum in argon.

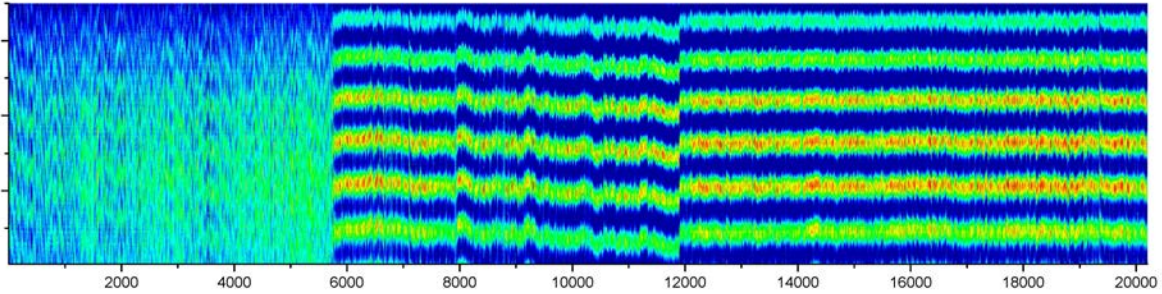
Traditionally, this has not been a major concern, as all CEP-relevant laser systems operate at 1 kHz repetition rates or higher. In these systems, the pulse energy is either responsive to power-locking techniques [213] or already relatively stable (due in part to the availability of highly-consistent diode-pumped pump lasers in this low-energy regime). However, this is not the case with low-

repetition rate laser systems, in which power locking is not available and energy instabilities tend to be large (due in part to the necessity of using relatively-inconsistent flash lamp-pumped pump lasers to access this high-energy regime).

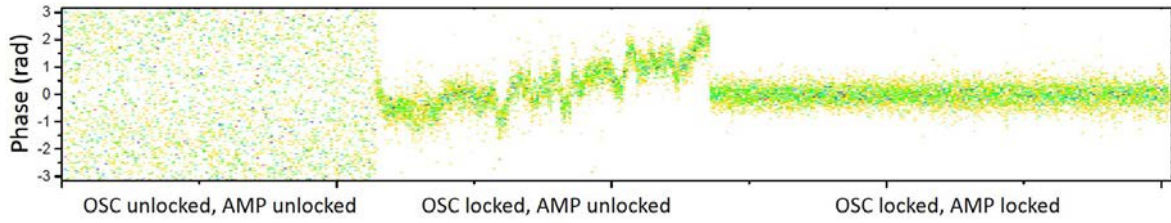
3.5 CEP Control of the IFAST 200 TW Laser

In the case of the IFAST 10 TW laser, the “in-loop” measurement was taken with the 1 kHz probe beam using f-to-2f interferometry, and the “out-loop” measurement was taken with the 10 Hz amplified beam by observing the CEP dependence of the structures in an XUV continuum. Prior to the completion of the HHG end-station for the IFAST 200 TW laser, the in-loop measurement of the 1 kHz probe beam was taken to test the performance of the CEP probe technique using the new grating compressor. Figure 3.9 shows the results of the in-loop f-to-2f measurement and phase retrieval for the situations where the oscillator was unlocked (left), the oscillator was locked but the amplifier was unlocked (center), and both the oscillator and the amplifier were locked (right). The CEP stability when both locking servos were enabled was <300 mrad at 20 ms integration for the measurement pictured.

Because long-term CEP stability is also crucial for time-consuming experiments and applications, the CEP stability was also measured over a nine-hour period to demonstrate stabilization capabilities that can cover a full working day. This is shown in Fig. 3.10. Notice that the calmer region of phase stability near the center of the plot corresponds to lunch time, when disturbances inside the lab were minimal.



(a) Raw f-to-2f fringes (wavelength vs. shot number) with different locking servos enabled.



(b) Phase retrieved from the f-to-2f fringes plotted above.

Figure 3.9: In-loop measurement of the 1 kHz probe beam through the 200 TW system.

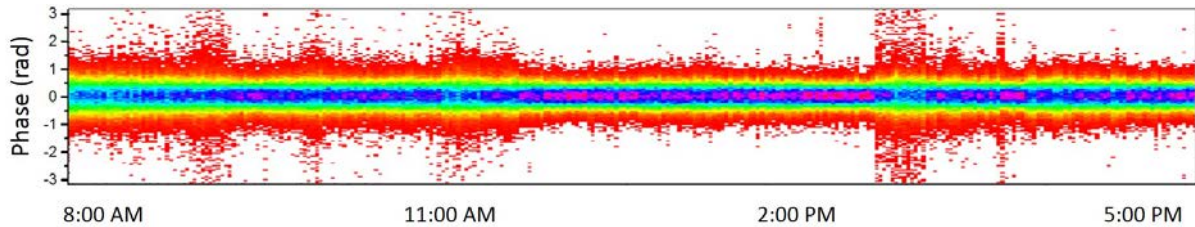


Figure 3.10: Demonstration of the CEP locking of the probe beam through the IFAST 200 TW compressor over a full work day. Notice the relative stability in the lab during the lunch hour.

CHAPTER 4: OPTICAL GATING WITH ASYMMETRIC FIELDS

Besides scaling the power of the input pulse energy, it is possible that the attosecond flux might also be enhanced by increasing the efficiency of the gated HHG process. This has been shown in the past, as double optical gating and generalized double optical gating both improved upon the performance of polarization gating by limiting pre-ionization of the XUV pulse-generating gas target. In this chapter, an asymmetric gating is introduced that offers an additional method for curbing target pre-ionization. This technique may help increase attosecond flux by improving phase matching, while also opening the possibility of isolated attosecond pulse production with longer, more common driving laser pulse durations.

4.1 Common Types of Optical Gating

Extreme ultraviolet (XUV) isolated attosecond pulses are generated using a variety of methods. In general, each method prevents high-harmonic generation (and, thus, attosecond pulse production) by exploiting one of the steps in the famed “three-step model” for high-harmonic generation [167].

Ionization Under **ionization gating**, a single field maximum of the driving laser pulse is responsible for ionizing a substantial portion of the atoms in the interaction region. While these electrons can be accelerated and recombined to generate an attosecond pulse, there are either 1) no more electrons for the ensuing driving laser cycles to ionize because the target has been depleted or 2) no longer appropriate phase-matching conditions because of the plasma created by the pulse. This effectively results in the production of a single attosecond pulse.

Acceleration Under **amplitude gating**, the strongest field maximum of the driving laser pulse accelerates the photoionized electrons the hardest, leading to the generation of the highest-

energy photons out of all the laser cycles. By filtering out the spectral components below the cutoff generated by the next strongest field maximum, it is ensured that the remaining spectrum all originated from the same attosecond burst. This effectively results in the production of a single attosecond pulse.

Recombination Under **polarization gating**, the ellipticity of the laser field is caused to vary with time such that a single linearly-polarized field maximum is surrounded on both sides by field maxima with increasing ellipticity. Because these elliptically-polarized fields lead their associated electrons on trajectories *away* from the parent ions, only the electrons accelerated by the single linearly-polarized field maximum experience recombination and yield high-energy photons. This effectively results in the production of a single attosecond pulse.

Both ionization gating and amplitude gating work almost exclusively with few-cycle pulses, as the pulse envelope must change appreciably over the scale of one wavelength in order to achieve an appreciable contrast between the largest two extrema of the carrier wave. Polarization gating, on the other hand, does not require as short of pulse durations, making it a more favorable option for many laser systems. Moreover, several refinements to polarization gating have been made to improve performance of the gating and relax constraints on the driving laser. This section explores polarization gating and a few of its useful variations.

4.1.1 Polarization Gating (PG)

Under polarization gating (PG) [176–178, 214, 215], a linearly-polarized infrared pulse is transformed into a pair of counter-rotating circularly-polarized pulses. The delay between the peaks of the two pulses can be carefully tailored to create an overlap region in which a single near-linear half-cycle of the laser is surrounded on both sides by regions of quickly-increasing ellipticity. Because high-harmonic generation – responsible for producing the attosecond pulse-supporting XUV

bandwidth – is ellipticity-dependent, attosecond pulse generation is suppressed in the peripheral laser cycles, while a single isolated attosecond pulse can be produced by the near-linear half-cycle.

Physically, this polarization gating is accomplished using two phase retarders: a multi-cycle delay plate and a zero-order quarter-wave plate (shown in Fig. 4.1). The delay plate is positioned such that its axes are rotated 45° from the input linear polarization direction. This splits the pulse into two orthogonally-polarized pulses of equal amplitude, where the separation between the peaks of the two pulses is determined by the delay plate's thickness and refractive indices. The zero-order quarter-wave plate, with its fast axis rotated 45° from the axis of first phase retarder, converts the two linear pulses into circularly-polarized pulses with opposite handedness. The overlap of these two pulses yields a “polarization gate”: a single half-cycle region in which the total field ellipticity is below the threshold ellipticity for high-harmonic generation.

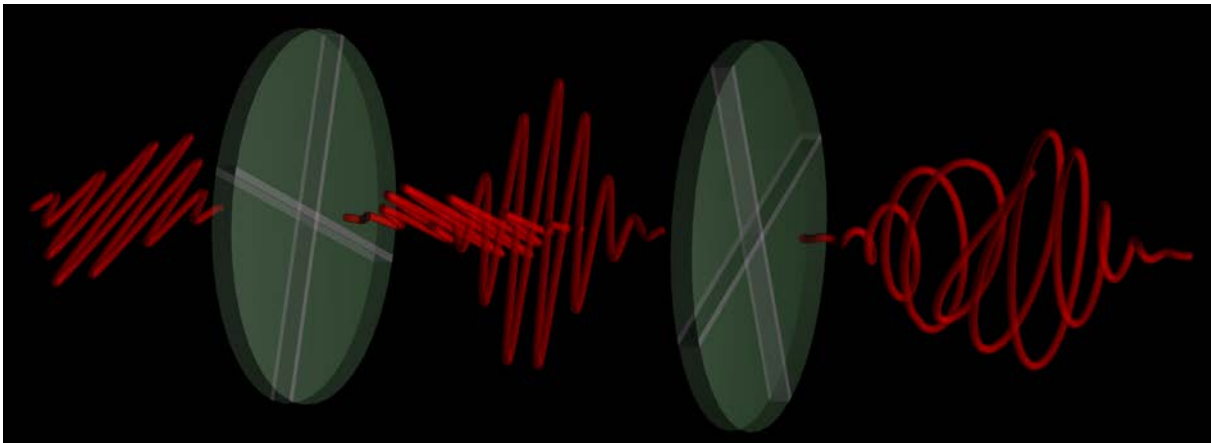


Figure 4.1: Birefringent optics for polarization gating (PG): one multi-order full-wave plate and one zero-order half-wave plate.

While no other half-cycle contributes to the generation of high-harmonics, the laser cycles on the leading edge of the pulse cause unwanted ionization of the gas target before the arrival of the linear half-cycle. This pre-ionization places a limit on 1) the maximum driving laser intensity at which phase matching conditions can be achieved, 2) the longest driving laser pulse duration

still capable of generating isolated attosecond pulses, and 3) the highest driving laser intensity attainable without depleting the gas target.

Two methods have proven successful at limiting the amount of gas target ionization before the generation of an isolated attosecond pulse within a polarization gate: 1) the addition of a second harmonic field to the polarization-gated field and 2) the utilization of elliptically-polarized counter-rotating pulses (as opposed to circularly-polarized pulses).

4.1.2 Double Optical Gating (DOG)

When a linearly-polarized pulse generates high-order harmonics in the spectral domain, this corresponds to a train of attosecond pulses in the time domain, where the spacing between the attosecond bursts is equal to one-half of the cycle of the driving field. If a weak second harmonic field is added to the fundamental field, the amplitude of every other half-cycle of the combined field is comparatively enhanced, while the half-cycles in between are diminished. Because the HHG process is highly nonlinear, even this minor adjustment to the electric field can be enough to prevent the weakened half-cycles from producing attosecond pulses. This technique, depicted graphically in Fig. 4.2, is known by itself as two-color gating [216–218].

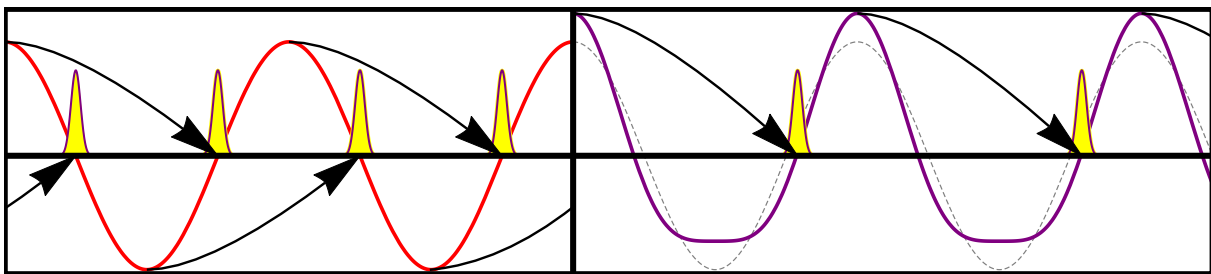


Figure 4.2: Attosecond pulse spacing is only half as much when produced (a) with a fundamental field versus (b) with a fundamental field augmented by its second harmonic.

If two-color gating is combined with polarization gating, the addition of the second harmonic field to the polarization-gated field relaxes the constraint on the polarization gate width from half-cycle to full-cycle. This decreases the required separation between the peaks of the two counter-rotating pulses, meaning that fewer photoionizing laser cycles precede the arrival of the polarization gate. This technique is called double optical gating (DOG) [219,220], and it is physically accomplished by making two changes to the PG setup. First, the initial phase retarder is changed to decrease the delay between the two counter-rotating pulses. Second, the zero-order quarter-wave plate is replaced with the combination of a positive-uniaxial phase plate and a negative-uniaxial frequency-doubling crystal. By choosing the thicknesses properly, these form a zero-order quarter-wave plate while also generating a second harmonic field. This is shown in Fig. 4.3.

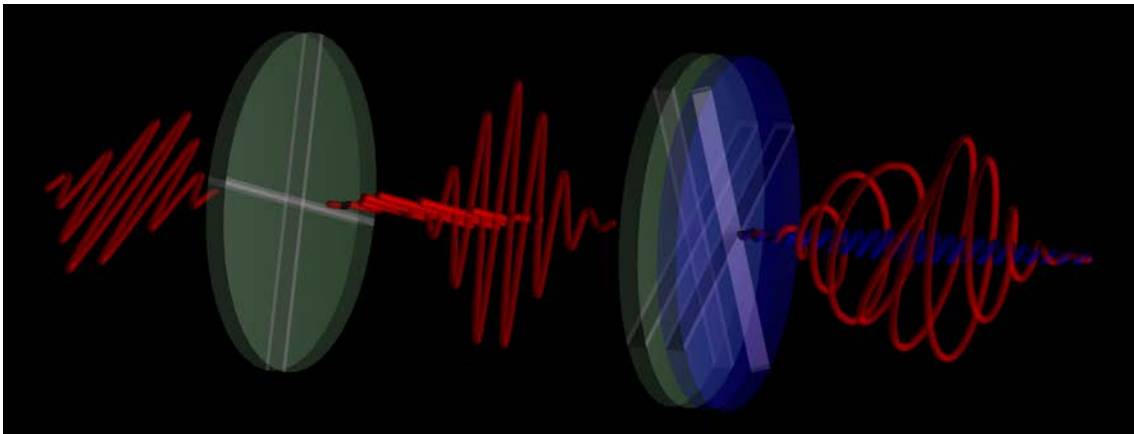


Figure 4.3: Birefringent optics for double optical gating (DOG): one multi-order full-wave plate and one zero-order half-wave plate comprised of a multi-order full-wave plate and a multi-order quarter-wave second-harmonic crystal.

4.1.3 Generalized Double Optical Gating (GDOG)

When elliptically-polarized counter-rotating pulses are utilized instead of the circularly-polarized pulses employed under PG, the amplitude of the laser cycles preceding the polarization gate decreases, thus leading to a reduction in leading-edge ionization. More importantly, the polarization gate can also become sharper by specifically decreasing the driving laser component responsible for the pulse's linear center-most cycle. This allows the spacing between the two counter-rotating pulses to be decreased, which (as stated earlier) reduces leading-edge ionization by minimizing the number of laser cycles preceding the polarization gate.

When this technique is combined with the two-color method described above, both effects simultaneously contribute to the reduction of leading-edge ionization. Such a gating scheme is called generalized double optical gating (GDOG) [150, 181], and it represents one of the most effective methods to-date for limiting pre-ionization of a gas target. Physically, this is achieved in the DOG setup by attenuating the polarization component 45° from the axis of the first phase retarder (typically performed using a Brewster window, as illustrated in Fig. 4.4).

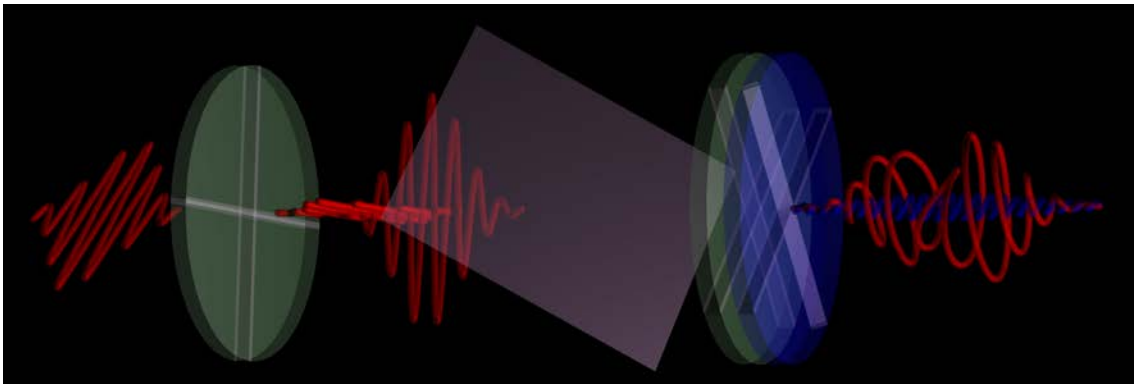


Figure 4.4: Birefringent optics for generalized double optical gating (GDOG): one multi-order full-wave plate, one Brewster window, and one zero-order half-wave plate comprised of a multi-order full-wave plate and a multi-order quarter-wave second-harmonic crystal.

4.2 Asymmetric Gating

In addition to the two approaches described above, a third method is proposed that is capable of limiting the amount of pre-ionization of the gas target. This new technique alters the ratio between the amplitudes of the two counter-rotating circularly- or elliptically-polarized pulses, making the leading pulse smaller than the trailing pulse. This diminishes the field strength prior to the linearly-polarized gate cycle and shortens the time between the polarization gate and the leading edge of the pulse, as suggested by Fig. 4.5. The result is a decrease in the pre-ionization of the gas target used for generating isolated attosecond pulses. This technique can be applied to any of the gating methods mentioned above, yielding asymmetric versions that further reduce ionization: asymmetric PG (APG), asymmetric DOG (ADOG), asymmetric GDOG (AGDOG), etc.

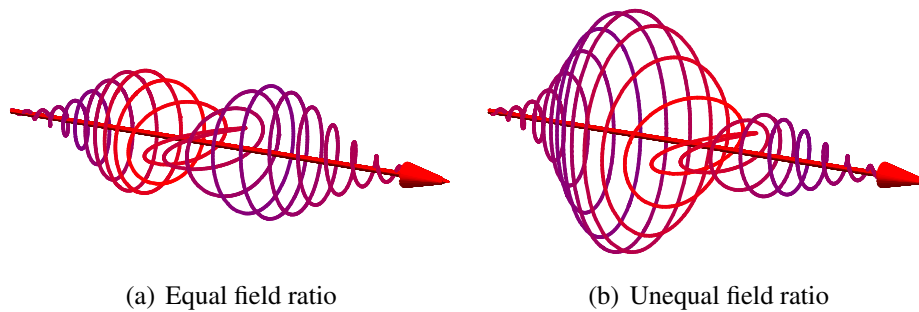


Figure 4.5: Examples of symmetric and asymmetric gating fields [221]. (© 2015 IEEE)

This field asymmetry is achieved by changing the angle between the input pulse polarization and the fast axis of the first phase retarder. Instead of using a 45° angle where the field amplitude projects equally onto both optic axes, the angle is changed such that more field is projected onto the slow axis and less field is projected onto the fast axis. This effectively decreases the size of the first pulse (transmitted along the fast axis) relative to the second pulse (transmitted along the slow axis). The delay between the $e-$ and $o-$ waves remains unchanged, as the neither the thickness nor

the refractive indices of the phase retarder were adjusted. After the first phase retarder, the rest of the gating setup is identical: the field is still attenuated 45° from the axis of the first phase retarder, and the (true or effective) zero-order quarter-wave plate is still oriented 45° from the axis of the first phase retarder.

As for the apparatus, the configuration described above can be achieved by 1) adding a zero-order half-wave plate before the first phase retarder to rotate the relative input polarization or 2) rotating all gating optics around the axis given by the propagation direction.

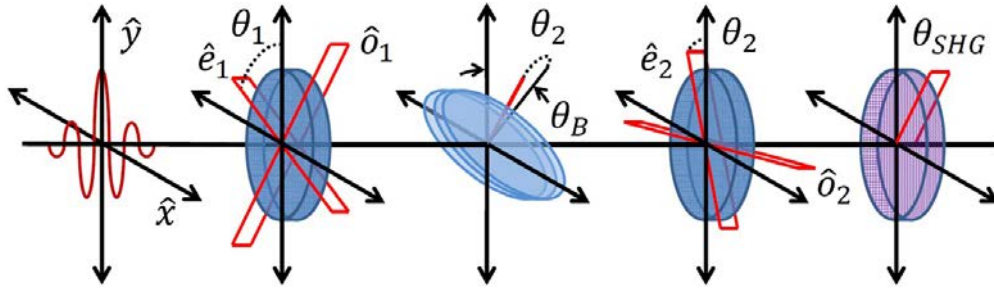


Figure 4.6: Birefringent optics for asymmetric generalized double optical gating [221]. (© 2015 IEEE)

4.2.1 Physical Apparatus and Gating Parameters

Like the GDOG setup described in Sec. 4.1.3, an AGDOG field can be generated using a full-wave phase retarder, Brewster windows, a second phase retarder, and a second harmonic crystal, as depicted in Fig. 4.6. The linearly-polarized field incident to this setup can be written as

$$\vec{E}_{\text{input}} = E_0 \exp \left[-2 \ln 2 \left(\frac{t}{\tau_p} \right)^2 \right] \cos \omega t \hat{y} \quad (4.1)$$

where τ_p is the pulse duration and ω is the carrier frequency.

The first phase retarder, whose e -axis forms an angle θ_1 with the y -axis in the x - y plane, splits the field into two orthogonally-polarized pulses separated in time by T_d :

$$\begin{aligned}
\vec{E}_{QP1} &= E_0 \cos \omega t \{ \exp [\mathcal{T}_-] \cos \theta_1 \hat{e}_1 + \exp [\mathcal{T}_+] \sin \theta_1 \hat{o}_1 \} \\
&= E_0 \cos \omega t \{ \sin \theta_1 \cos \theta_1 (\exp [\mathcal{T}_+] - \exp [\mathcal{T}_-]) \hat{x} \\
&\quad + (\sin^2 \theta_1 \exp [\mathcal{T}_+] + \cos^2 \theta_1 \exp [\mathcal{T}_-]) \hat{y} \} \\
&= E_0 \cos \omega t \{ (\sin \theta_1 \sin (\theta_1 - \theta_2) \exp [\mathcal{T}_+] \\
&\quad + \cos \theta_1 \cos (\theta_1 - \theta_2) \exp [\mathcal{T}_-]) \hat{e}_2 \\
&\quad + (\sin \theta_1 \cos (\theta_1 - \theta_2) \exp [\mathcal{T}_+] \\
&\quad - \cos \theta_1 \sin (\theta_1 - \theta_2) \exp [\mathcal{T}_-]) \hat{o}_2 \}
\end{aligned} \tag{4.2}$$

where $\mathcal{T}_\pm \equiv -2 \ln 2 ((t \pm T_d/2)/\tau_p)^2$ for convenience. Equation 4.2 has also been re-written in Eq. 4.3 using the new basis shared by the Brewster windows and the second phase retarder, whose e -axis forms an angle θ_2 with the y -axis in the x - y plane. Because θ_2 is fixed to be $\theta_1 - 45^\circ$ (just as in the case for PG, DOG, and GDOG), Equation 4.3 can be simplified at the same time the effect of the Brewster windows is considered:

$$\begin{aligned}
\vec{E}_{BW} &= \frac{E_0}{\sqrt{2}} \cos \omega t \{ \epsilon (\sin \theta_1 \exp [\mathcal{T}_+] + \cos \theta_1 \exp [\mathcal{T}_-]) \hat{e}_2 \\
&\quad + (\sin \theta_1 \exp [\mathcal{T}_+] - \cos \theta_1 \exp [\mathcal{T}_-]) \hat{o}_2 \}
\end{aligned} \tag{4.4}$$

where ϵ refers to the ellipticity at the leading and trailing edges of the final pulse, as dictated by the attenuation of the Brewster windows.

The \hat{e}_2 and \hat{o}_2 terms in Eq. 4.4 can be identified as the driving and gating fields, respectively. Taking into account the zero-order quarter wave plate (second phase retarder and frequency doubling crystal combination), the field can be broken down as follows:

$$E_{drive} = \epsilon \frac{E_0}{\sqrt{2}} (\sin \theta_1 \exp [\mathcal{T}_+] + \cos \theta_1 \exp [\mathcal{T}_-]) \quad (4.5)$$

$$E_{gate} = \frac{E_0}{\sqrt{2}} (\sin \theta_1 \exp [\mathcal{T}_+] - \cos \theta_1 \exp [\mathcal{T}_-]) \quad (4.6)$$

$$E_{tot} = \sqrt{|E_{drive} \cos(\omega t)|^2 + |E_{gate} \cos(\omega t + \pi/2)|^2} \quad (4.7)$$

where E_{drive} and E_{gate} are the envelopes of the driving and gating fields, respectively, and E_{tot} is the magnitude of the total field (i.e. including carrier wave).

It is evident that while still enforcing the condition that $\theta_2 = \theta_1 - 45^\circ$, the tuning of θ_1 adjusts the field ratio between the front and back pulse. When $\theta_1 = 45^\circ$, the $\exp [\mathcal{T}_-]$ and $\exp [\mathcal{T}_+]$ pulses have equal magnitude, and Eqs. 4.5 and 4.6 reduce to the standard expressions for GDOG fields. When $\theta_1 \neq 45^\circ$, the electric field is *not* projected onto the slow and fast axes of the first phase retarder in equal proportion, and the size of the first pulse (transmitted along the fast axis) is effectively changed relative to the second pulse (transmitted along the slow axis). As stated earlier, the angle θ_1 can be tuned while maintaining the fixed 45° angle between θ_1 and θ_2 by either 1) adding a zero-order half-wave plate before the first phase retarder or 2) rotating all gating optics around the axis given by the propagation direction.

4.2.2 Effect on Polarization Gate Position t_c

When the ratio between the amplitudes of the two counter-rotating pulses changes, the location of the polarization gate moves closer to the smaller side of the pulse. To determine how the gate position in time changes with θ_1 , the time must be found for which the gating field E_{gate} in Eq. 4.6 becomes zero. This time corresponding to the center of the polarization gate, referred to as t_c , can be expressed as

$$t_c = \frac{\tau_p^2}{T_d} \frac{\ln(\tan \theta_1)}{4 \ln 2} \quad (4.8)$$

When $\theta_1 = 45^\circ$, this expression reduces to $t_c = 0$, as expected in the cases of PG, DOG, and GDOG. When $\theta_1 \neq 45^\circ$, the polarization gate position t_c becomes nonzero.

The reliance of the polarization gate position on the field asymmetry is illustrated in Fig. 4.7. The top, middle, and bottom rows show the cases of $\cot^{-1}(2) = 26.6^\circ$, $\cot^{-1}(1) = 45^\circ$, and $\cot^{-1}(1/2) = 63.4^\circ$, respectively. These angles correspondingly produce field ratios of 2:1, 1:1, and 1:2. In the left column, the total field (red), gating field (blue), driving field (green), and polarization gate (magenta) are plotted as a function of time for all three field ratios. In the right column, the absolute field magnitude $||\vec{E}_{PG}||$ (red) and ellipticity (blue) are plotted as a function of time for all three field ratios. Notice here that the width of the polarization gate remains constant while the position of the polarization gate changes.

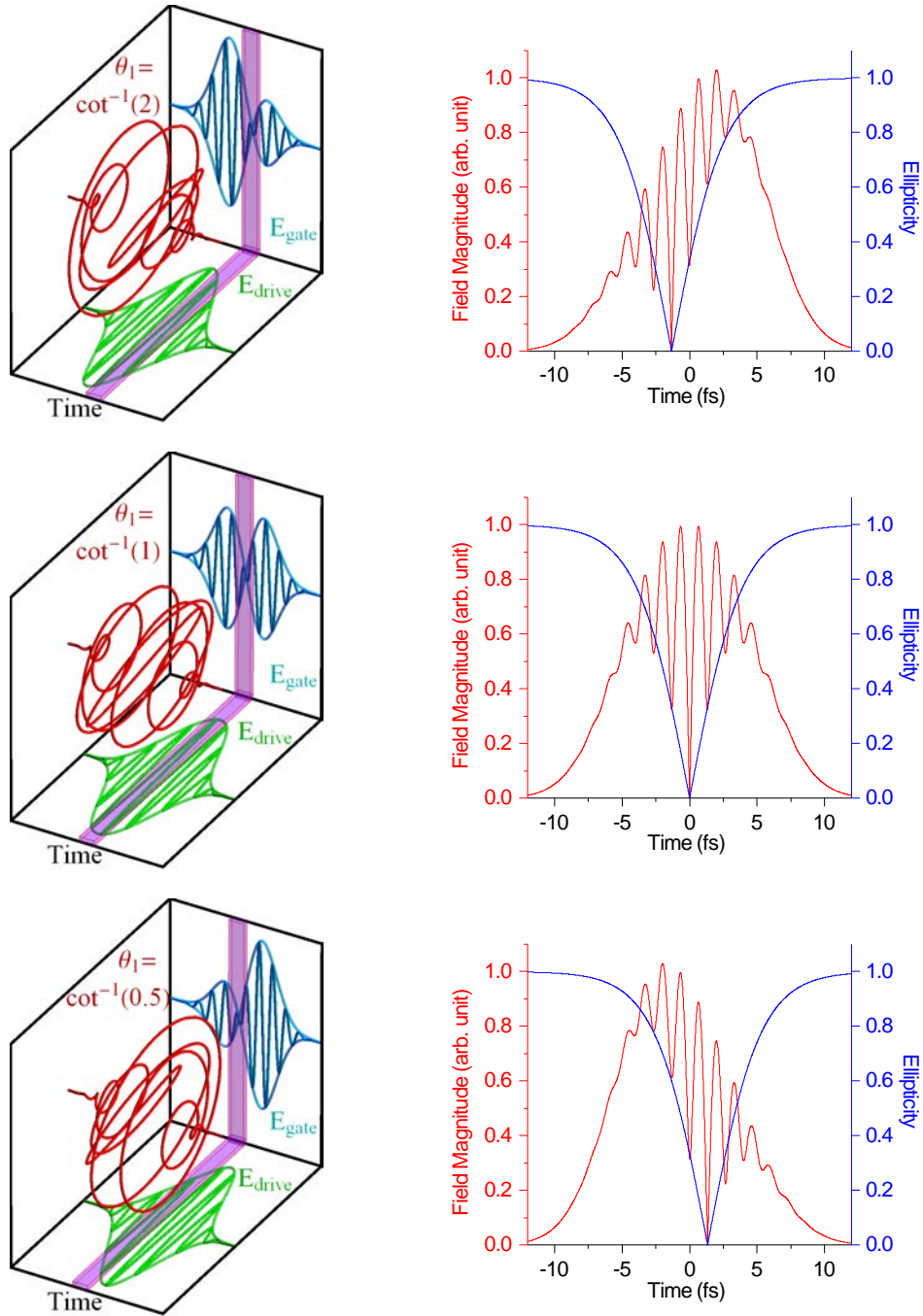


Figure 4.7: An example of polarization-gated few-cycle pulses, demonstrating the cases of $\theta_1 = \cot^{-1}(1/2)$ (top row, 2:1 ratio), $\theta_1 = \cot^{-1}(1)$ (middle row, 1:1 ratio), and $\theta_1 = \cot^{-1}(1/2)$ (bottom row, 1:2 ratio) and their effect on the electric field, polarization gate, and ellipticity.

4.2.3 Effect on Pulse Separation T_d

In order to isolate a single attosecond pulse, the time-dependent field ellipticity $\xi(t)$ at either side of the polarization gate must reach a threshold ellipticity ξ_{th} above which the electron recombination in HHG is strongly suppressed [173]. Mathematically, this requirement is expressed as

$$\xi \left(t = t_c \pm \frac{\delta t_G}{2} \right) = \xi_{th} \quad (4.9)$$

where t_c is the position in time of the center of the polarization gate, and the width of the polarization gate δt_G is either half of an optical cycle (when using a single-color driving field, as in PG) or a full optical cycle (when using a two-color driving field, as in DOG and GDOG).

Because the gating field E_{gate} is always bigger than the driving field E_{drive} in the vicinity of the polarization gate, the time-dependent ellipticity $\xi(t)$ itself can be defined as

$$\begin{aligned} \xi(t) \equiv \frac{E_{gate}}{E_{drive}} &= \frac{\frac{E_0}{\sqrt{2}} (\sin \theta_1 \exp [\mathcal{T}_+] - \cos \theta_1 \exp [\mathcal{T}_-])}{\epsilon \frac{E_0}{\sqrt{2}} (\sin \theta_1 \exp [\mathcal{T}_+] + \cos \theta_1 \exp [\mathcal{T}_-])} \\ &= \frac{1 (\tan \theta_1 - \exp [\mathcal{T}_- - \mathcal{T}_+])}{\epsilon (\tan \theta_1 + \exp [\mathcal{T}_- - \mathcal{T}_+])} \end{aligned} \quad (4.10)$$

Applying the condition given in Eq. 4.9 to Eq. 4.10, an expression can be derived for the pulse separation T_d necessary for achieving a suitable polarization gate:

$$\begin{aligned} \xi_{th} &= \frac{1 \left(\tan \theta_1 - \exp \left[4 \ln 2 \frac{T_d}{\tau_p^2} (t_c \pm \delta t_G / 2) \right] \right)}{\epsilon \left(\tan \theta_1 + \exp \left[4 \ln 2 \frac{T_d}{\tau_p^2} (t_c \pm \delta t_G / 2) \right] \right)} \\ \Rightarrow 4 \ln 2 \frac{T_d}{\tau_p^2} \left(t_c \pm \frac{\delta t_G}{2} \right) &= \ln \left(\tan \theta_1 \frac{1 - \epsilon \xi_{th}}{1 + \epsilon \xi_{th}} \right) \end{aligned} \quad (4.11)$$

Inserting the expression for t_c given in Eq. 4.8 leads to

$$\begin{aligned} \pm 2 \ln 2 \frac{T_d \delta t_G}{\tau_p^2} + \ln(\tan \theta_1) &= \ln(\tan \theta_1) + \ln\left(\frac{1 - \epsilon \xi_{th}}{1 + \epsilon \xi_{th}}\right) \\ \Rightarrow T_d &= \pm \frac{1}{2 \ln 2} \frac{\tau_p^2}{\delta t_G} \ln\left(\frac{1 - \epsilon \xi_{th}}{1 + \epsilon \xi_{th}}\right) \end{aligned} \quad (4.12)$$

where the plus/minus simply indicates that the same ellipticity is achieved regardless of which pulse comes first. Notice that Eq. 4.12, independent of θ_1 , is identical to the formula used to calculate the requisite pulse separation for symmetric PG-type fields [215].

It is also interesting to note that by inserting Eq. 4.12 into Eq. 4.8, it is seen that the position of the polarization gate t_c is *not* a function of the pulse duration τ_p :

$$t_c = \frac{\tau_p^2}{T_d} \frac{\ln(\tan \theta_1)}{4 \ln 2} = \pm \frac{\delta t_G}{2} \frac{\ln(\tan \theta_1)}{\ln\left(\frac{1 + \epsilon \xi_{th}}{1 - \epsilon \xi_{th}}\right)} \quad (4.13)$$

4.2.4 Effect on HHG-Producing Field Amplitude $E_{drive}(t = t_c)$

The intensity of the laser inside the polarization gate is also affected by the ratio between the two counter-rotating pulses. In order to scale this intensity to a specific value for appropriately comparing different gating schemes, the electric field amplitude E_0 must be expressed as a function of the driving field strength at $t = t_c$. From Eq. 4.5, it follows that

$$E_0 = \frac{E_{drive}(t_c)}{\epsilon \sqrt{\sin 2\theta_1}} \exp\left[2 \ln 2 \left(\frac{t_c^2 + \frac{T_d^2}{4}}{\tau_p^2}\right)\right] \quad (4.14)$$

In order to isolate the effect of the field asymmetry, the ratio is taken between the two instances of Eq. 4.14 where $\theta_1 \neq 45^\circ$ (asymmetric field) and $\theta_1 = 45^\circ$ (symmetric field):

$$\frac{E_0(\theta_1 \neq 45^\circ)}{E_0(\theta_1 = 45^\circ)} = \frac{1}{\sqrt{\sin 2\theta_1}} (\tan \theta_1)^{\frac{1}{8 \ln 2} \frac{\tau_d^2}{\tau_p^2} \ln(\tan \theta_1)} \quad (4.15)$$

Figure 4.8 plots Eq. 4.15 using parameters that simulate an 800 nm driving laser gated by one of three different methods: APG ($\tau_p = 7$ fs), ADOG ($\tau_p = 20$ fs), and AGDOG ($\epsilon = 0.5$, $\tau_p = 28$ fs). The resulting coefficients are plotted in red, green, and blue, respectively. Because pulse energy is proportional to the modulus squared of the electric field, a scaling factor of $\sqrt{2}$ means that the original pulse energy needs to be twice as large to keep the same driving field intensity at $t = t_c$.

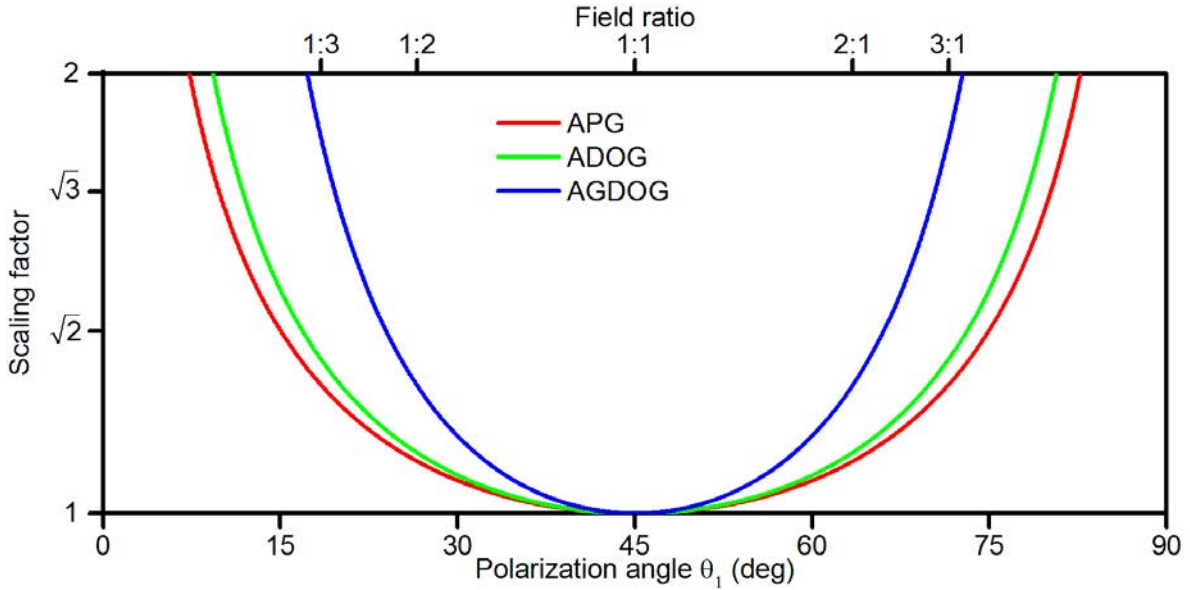


Figure 4.8: Scaling factors required to maintain a constant driving field intensity inside the polarization gate as the field asymmetry is changed [221]. (© 2015 IEEE)

Figure 4.8 depicts the “cost” of field asymmetry variation – the amount of additional pulse energy needed to scale the polarization gate intensity when θ_1 changes. This is compared to the “cost” of varying the field ellipticity ϵ , which can be expressed by taking the ratio between the two instances of Eq. 4.14 where the ellipticity ϵ is variable (elliptically-polarized case) and $\epsilon = 1$ (circularly-polarized case). Figure 4.9 plots this ratio using the same pulse durations and gating methods as in Fig. 4.8, except this time the ellipticity is varied and the field ratio is symmetric ($\theta_1 = 45^\circ$): generalized PG or GPG ($\tau_p = 7$ fs, in red), GDOG ($\tau_p = 20$ fs, in green), and GDOG ($\tau_p = 28$ fs, in blue). From this analysis, it is evident that the “cost” of using field asymmetry is low compared to that of using field ellipticity.

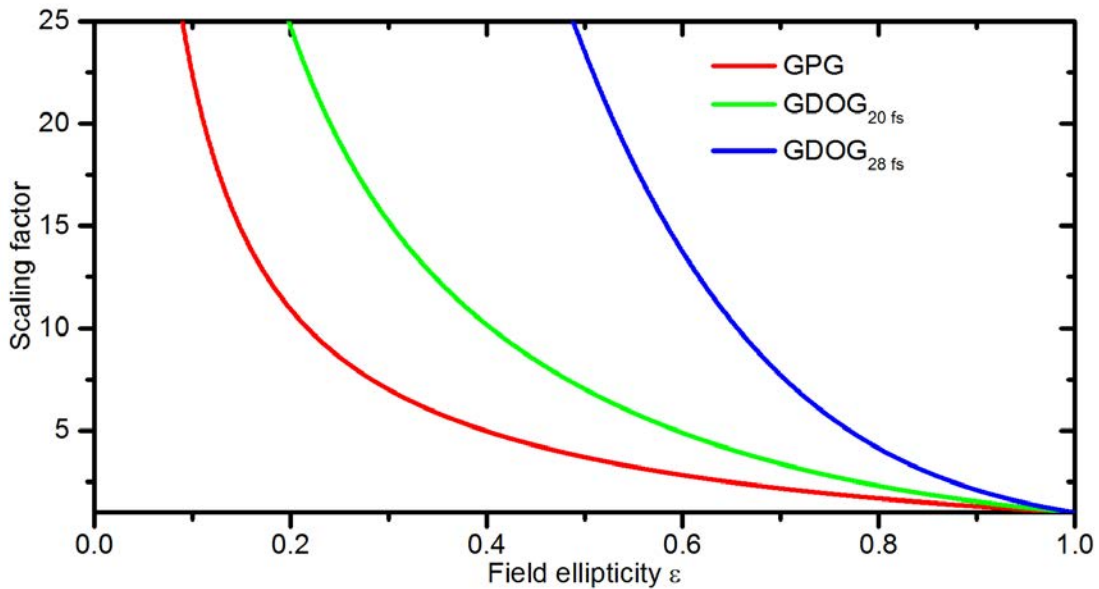


Figure 4.9: Scaling factors required to maintain a constant driving field intensity inside the polarization gate as the field ellipticity is changed [221]. (© 2015 IEEE)

4.2.5 Ionization Simulations

To examine how field asymmetry influences the fundamental physical limit of the field intensity on pre-ionization in the single-atom picture, several simulations were performed using the ADK ionization rate [222], which is given by

$$w_{ADK} = |C_{n^*l^*}|^2 G_{lm} I_p \left(\frac{2F_0}{E_{tot}} \right)^\Xi \exp \left(-\frac{2}{3} \frac{F_0}{E_{tot}} \right) \quad (4.16)$$

where $\Xi = 2n^* - |m| - 1$, E_{tot} is given by Eq. 4.7, and the parameters $|C_{n^*l^*}|^2$, G_{lm} , I_p , F_0 , n^* , l^* , l , and m are constants unique to the chosen target element [223]. From Eq. 4.16, the ionization probability of a targeted atom at time t is calculated by integrating:

$$P(t) = 1 - \exp \left[\int_{-\infty}^t w_{ADK}(t') dt' \right] \quad (4.17)$$

In order to make a fair comparison between the pre-ionization associated with different gating schemes, the intensity inside the polarization gate was kept constant for all simulations using Eq. 4.14. Note, however, that this expression only insures that the *envelope* of the driving field E_{drive} remains the same for different values of θ_1 . Thus for simulation purposes, it was further necessary to specify the phase of the carrier wave to guarantee that the full driving field $E_{drive} \cos(\omega t + \phi_{CE})$ was always maximum at the center of the gate. This was achieved by adjusting the value of the carrier-envelope phase ϕ_{CE} as a function of the gate center t_c :

$$\begin{aligned} \cos(\omega t_c + \phi_{CE}) &= 1 \\ \Rightarrow \phi_{CE} &= -\omega t_c = -\omega \frac{\tau_p^2}{T_d} \frac{\ln(\tan \theta_1)}{4 \ln 2} \end{aligned} \quad (4.18)$$

Figure 4.10 shows an example of an ADK simulation comparing GDOG and AGDOG (3:1 ratio, expressed hereafter using subscripts). Here, the field ionized argon with a polarization gate intensity of $2.19 \times 10^{14} \text{ W/cm}^2$, corresponding to a theoretical XUV photon cut-off of 57 eV (matching the spectral edge in the reflection curve for a Brewster-angled silicon XUV-IR beam splitter). In both cases, an 800 nm, 20 fs driving laser pulse was assumed, and the ellipticity ϵ was 0.5.

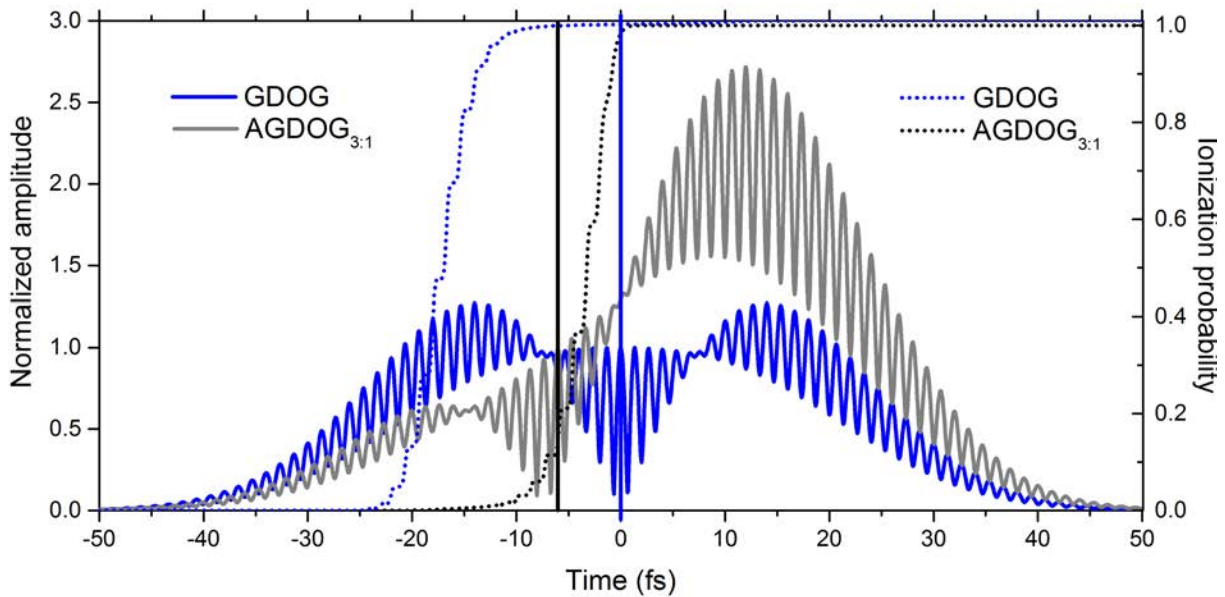


Figure 4.10: Predicted ionization rates in argon with GDOG and AGDOG_{3:1} fields ($\lambda = 800 \text{ nm}$, $\tau_p = 20 \text{ fs}$, $\epsilon = 0.5$, $I_{gate} = 2.19 \times 10^{14} \text{ W/cm}^2$) [221]. (© 2015 IEEE)

In the case of GDOG (blue), the ionizing field saturated the target more than 10 fs before the arrival of the polarization gate (blue vertical line), meaning that no neutral atoms remained to generate an isolated attosecond pulse. Alternatively, the asymmetric ionizing field (gray) was smaller leading up to the polarization gate (black vertical line), which itself arrived ~ 6 fs earlier than in the GDOG case. As a result, the ionization probability at the polarization gate (black) was less than 10% – a dramatic improvement in the limitation of target pre-ionization as compared to the symmetric field.

In general, this suppression of pre-ionization leads to three potential benefits: 1) production of isolated attosecond pulses with longer driving pulse durations, 2) phase matching at higher photon energies, and 3) extension of the theoretical cut-off of the XUV continuum.

4.2.5.1 Longer Driving Pulse Duration

To provide an example of the effectiveness of field asymmetry in limiting ionization, a set of simulations was carried out calculating the expected ionization probability at the polarization gate as a function of the driving pulse duration when using PG, DOG, GDOG, and AGDOG_{3:1}. In the case plotted in Fig. 4.11, the polarization gate intensity of the 800 nm pulses was held constant at $2.8 \times 10^{14} \text{ W/cm}^2$, which corresponds to a theoretical XUV photon cut-off in argon up to the edge of the transmission window of aluminum near 70 eV. According to the simulation, AGDOG remained serviceable for much longer pulse durations than any of the other studied gating strategies.

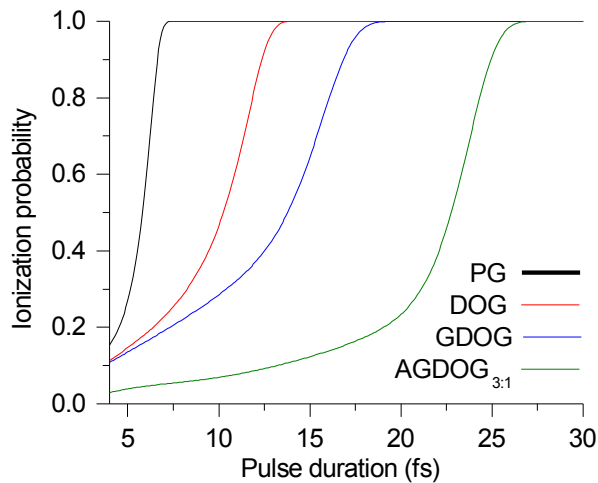


Figure 4.11: Predicted ionization rates in argon with different gating schemes as a function of pulse duration ($\epsilon = 1$ (PG, DOG) or $\epsilon = 0.5$ (GDOG, AGDOG), $\lambda = 800 \text{ nm}$, $I_{gate} = 2.8 \times 10^{14} \text{ W/cm}^2$) [221]. (© 2015 IEEE)

4.2.5.2 Improved Phase Matching

In noble gas atoms, phase matching can usually occur when only a few percent of the target atoms are ionized [224]. To operate in such a regime, the laser pulse must be relatively weak, which consequently limits the highest intensity achievable inside the polarization gate. This in turn determines the maximum HHG photon energy that can be phase-matched.

To compare the phase matching cut-off allowable by different gating schemes, the ionization rate was simulated using the ADK model, and a gate intensity was found which ionizes the correct percentage of the generation gas necessary for phase matching. The theoretical HHG photon energy cut-off for such an intensity was then calculated using $E_{max} = I_p + 3.17U_p$, where I_p is the ionization potential and U_p is the ponderomotive potential [225]. Figure 4.12 compares the phase matching cut-off of PG, DOG, GDOG, and AGDOG_{3:1} in argon gas ($P_{PM} = 3.8\%$, $I_p = 11.6$ eV) as a function of pulse duration. For these parameters, the AGDOG field allowed for an increase in the phase matching cut-off of ~ 10 eV.

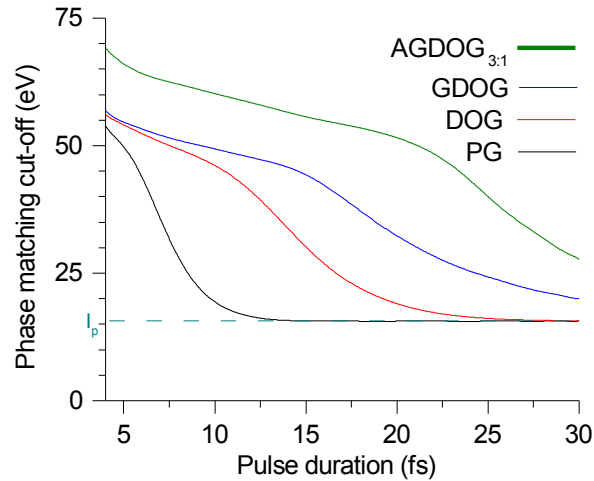


Figure 4.12: The XUV cut-off energy associated with the highest polarization gate intensity that did not result in ionization surpassing the criteria for phase matching ($\epsilon = 1$ (PG, DOG) or $\epsilon = 0.5$ (GDOG, AGDOG), $\lambda = 800$ nm) [221]. (© 2015 IEEE)

4.2.5.3 Higher Saturation Intensity

In noble gas atoms, the target is “saturated” when 97% of the atoms become ionized. This determines the strongest possible laser field usable before isolated attosecond pulse generation is frustrated inside the polarization gate by an insufficient number of neutral atoms remaining in the target. This in turn leads to the maximum XUV photon energy achievable by the gated laser field.

To compare the uppermost cut-off allowable by different gating schemes, the ionization rate was simulated using the ADK model, and a gate intensity was found which ionizes the target up to the point of saturation. The theoretical HHG photon energy cut-off for such an intensity was then calculated again using $E_{max} = I_p + 3.17U_p$. Figure 4.13 compares the saturation cut-off of PG, DOG, GDOG, and AGDOG_{3:1} in argon gas as a function of pulse duration. For these parameters, the AGDOG field allowed for an increase in the saturation cut-off from ~ 10 eV for long pulse durations to over ~ 50 eV for short pulse durations.

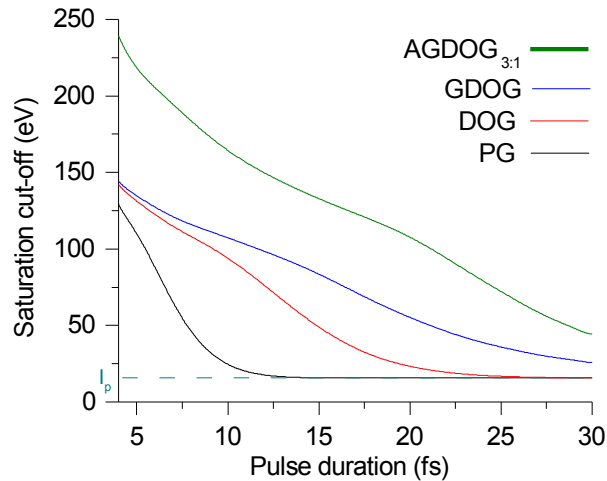


Figure 4.13: The XUV cut-off energy associated with the highest polarization gate intensity that did not result in ionization surpassing the criteria for saturation ($\epsilon = 1$ (PG, DOG) or $\epsilon = 0.5$ (GDOG, AGDOG), $\lambda = 800$ nm) [221]. (© 2015 IEEE)

4.3 Simulating HHG from Asymmetric Fields in the Low-Ionization Regime

While the simulations of Sec. 4.2 examined the effect of field asymmetry on leading-edge ionization, further calculation was necessary to provide insight into the effect of field asymmetry on the spectral and temporal structure of the high-harmonic attosecond bursts themselves. To investigate the viability of asymmetric fields in forming a sufficiently-discriminative polarization gate for isolating individual attosecond pulses, HHG driven by symmetric and asymmetric gating fields was simulated in the low-intensity regime where ionization itself does not play a differentiating role.

For this study, the single-atom response to the polarization-gated field was calculated using the strong-field approximation, meaning that the three-step model of high-harmonic generation was treated under the following assumptions: 1) the electron ionizes directly from the ground state into the continuum without transitioning to any intermediate states, 2) the influence of the atom's electric field is ignored while the electron is accelerated in free space by the intense laser field, and 3) the high-harmonic signal originates from the oscillating dipole comprised of the unmoving ion and the laser-driven electron [168]. After calculating this single-atom response to the PG field, a three-dimensional wave propagation equation was solved to simulate the macroscopic field of the attosecond pulse [226]. Once the harmonic field was obtained at the exit face, the HHG spectrum at the macroscopic level was obtained by integration over the transverse direction [227].

In this exercise, near-infrared 800 nm input pulses were simulated using with a pulse duration of $\tau_p = 5.33$ fs and a pulse separation of $T_d = 5.33$ fs. The angle θ_1 between the pulse's initial polarization and the slow axis of the first phase retarder was varied between the values $\theta_1 = \cot^{-1}(2)$, $\cot^{-1}(1)$, and $\cot^{-1}(1/2)$, corresponding to field ratios of 2:1, 1:1, and 1:2, respectively. In order to make a direct comparison of the behavior of the polarization gating with different field ratios, the envelope of the driving field at the center of the polarization gate was normalized in each case to $E_{drive}(t_c) = 0.14$ a.u. = 7.2×10^8 V/cm, which was chosen to limit the role of the

ionization level of the helium target to <10% depletion inside the polarization gate for all field ratios. Due to the change in position of the polarization gate with varying θ_1 , the carrier-envelope phase was also changed according to

$$\phi_{CE} = \frac{\pi}{2} - \omega \frac{\tau_p^2}{T_d} \frac{\ln(\tan \theta_1)}{4 \ln 2} \quad (4.19)$$

to insure that the positions of the closest two carrier-wave extrema straddled the polarization gate in the same way for all three cases. For the 3D wave propagation, the simulation employed a 1 mm-long helium gas cell, which was centered 1.5 mm after the laser focus. The assumed focal spot size was $w_0 = 25 \mu\text{m}$, which corresponded to a Rayleigh range of $z_R = 2.6 \text{ mm}$. Plasma effects were ignored in this simulation, which was a valid assumption given the low ionization probability; the density of the helium target itself was taken to be held at a constant value of $1.3 \times 10^{18} \text{ cm}^{-3}$.

4.3.1 Simulation Results – Frequency Domain

The simulated single-atom and macroscopic harmonic signals for the pulse parameters described above are plotted in Fig. 4.14. Even though the pulse envelope at the center of the polarization gate was normalized, two differences between the three field ratios are apparent: 1) the relative intensity and 2) the harmonic cut-off. Both of these effects can be explained by the relative character of the driving field near the polarization gate in all three cases, as displayed in Fig. 4.15. In the case of $\theta_1 = \cot^{-1}(2)$, the leading pulse is small while the trailing pulse is large; therefore, the first field extremum is *smaller* and the second field extremum is *larger* than $E_{drive}(t_c)$. Conversely, in the case of $\theta_1 = \cot^{-1}(1/2)$, the leading pulse is large while the trailing pulse is small; therefore, the first field extremum is *larger* and the second field extremum is *smaller* than $E_{drive}(t_c)$. In the symmetric case of $\theta_1 = \cot^{-1}(1)$, the leading pulse and the trailing pulse are equal in magnitude; therefore, the first and second field extrema are both nearly the same as $E_{drive}(t_c)$.

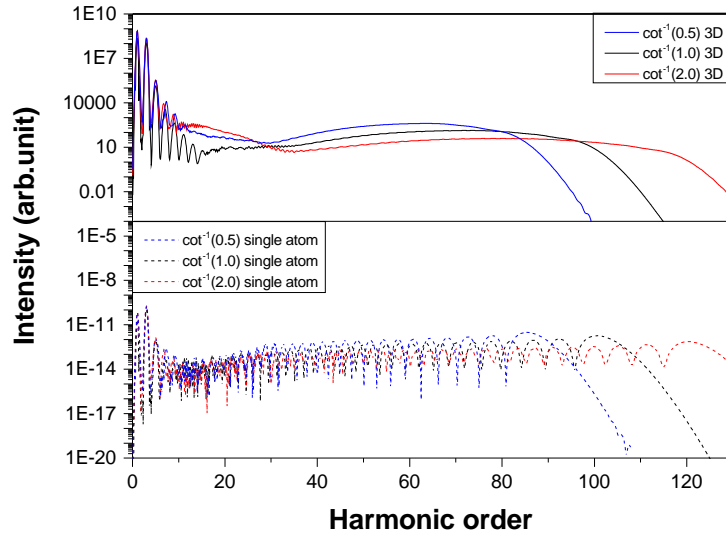


Figure 4.14: Single-atom (bottom) and 3D macroscopic (top) harmonic spectra generated by polarization gating fields with different field ratios.

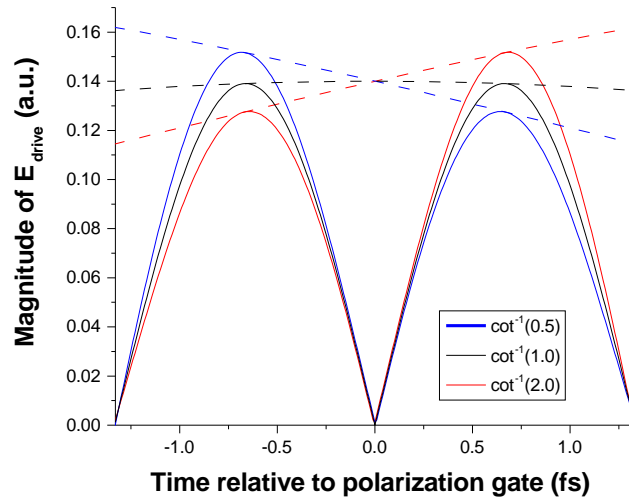


Figure 4.15: Driving field extrema surrounding the polarization gate for different field ratios. While the envelope of all three fields (dotted lines) were normalized at the center of the polarization gate, the fields themselves (solid lines) differed in magnitude because of the field asymmetry.

These differences can alter the character of the high-harmonic generation process. In the first stage of the three-step model, the intense field is responsible for electron *ionization*; with all other parameters equal, a stronger *ionization-inducing* field therefore results in more freed electrons, which lead to more recombination events and higher harmonic yield. In the second stage of the three-step model, the intense field, now with opposite direction, is responsible for electron *acceleration*; with all other parameters equal, a stronger *accelerating* field therefore results in higher electron kinetic energies, which lead to higher harmonic cut-offs. This is why the case of $\theta_1 = \cot^{-1}(1/2)$ featured the highest yield and the lowest cut-off, while the case of $\theta_1 = \cot^{-1}(2)$ featured the lowest yield and the highest cut-off. It is worthwhile to note that a similar trade-off has been observed previously in a simulation of high harmonics generated by two-color driving fields: as the phase difference between the fundamental and second harmonic beams was scanned, the harmonic yield and the harmonic cut-off monotonically trended in opposite directions [216].

4.3.2 Simulation Results – Time Domain

Figure 4.16 shows the macroscopic spectra from Fig. 4.14 transformed into the time domain. Compared to the symmetric case of $\theta_1 = \cot^{-1}(1)$ that yielded a pulse duration of 158 as (44 as transform limit), the case of $\theta_1 = \cot^{-1}(1/2)$ expectedly featured a higher yield and longer pulse duration (169 as; 56 as transform limit), and the case of $\theta_1 = \cot^{-1}(2)$ unsurprisingly featured a lower yield and shorter pulse duration (151 as; 30 as transform limit). The temporal displacement between the three attosecond pulses merely reflects the difference in the position of the polarization gates in each scenario.

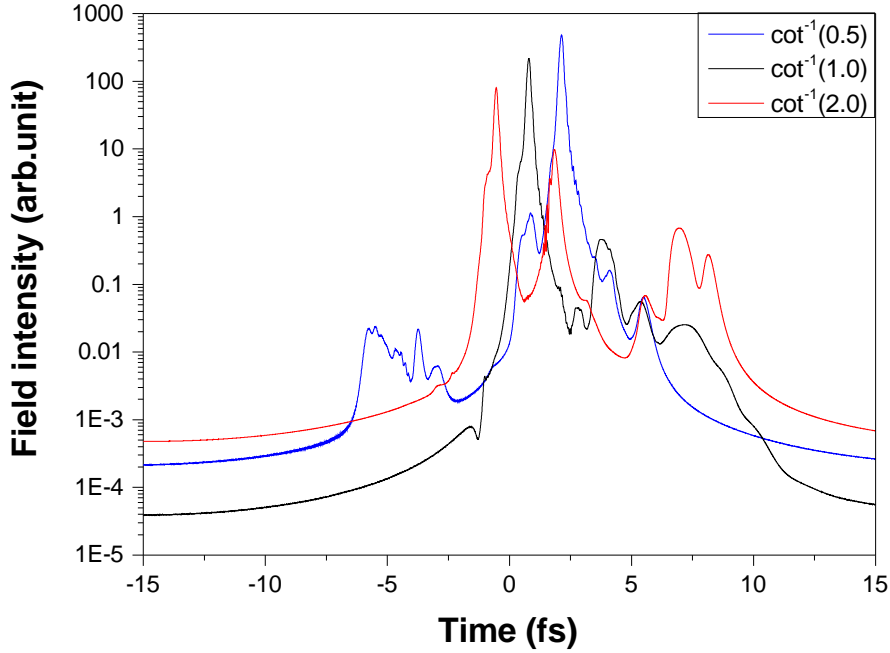


Figure 4.16: The temporal profile of the isolated attosecond pulses corresponding to the macroscopic HHG spectra plotted in the top panel in Fig. 4.14.

It is important to note that while the size of the main pulse was more than two orders of magnitude larger than the size of the largest satellite pulse for both the case of $\theta_1 = \cot^{-1}(1)$ and $\theta_1 = \cot^{-1}(1/2)$, this ratio was instead closer to 10% for the case of $\theta_1 = \cot^{-1}(2)$. It could be suspected that even though the width of the polarization gate remain unchanged, the use of field asymmetry may increase the likelihood of electron recombination in regions of relatively-high ellipticity due to the significantly-stronger electric fields on the trailing (for $\theta_1 = \cot^{-1}(2)$) or leading ($\theta_1 = \cot^{-1}(1/2)$) edges of the polarization gate.

First it is pointed out that this was *not* true for the case of $\theta_1 = \cot^{-1}(1/2)$: the stronger laser cycles were on the *leading* edge of the polarization gate, so only the *long*-trajectory electrons from the immediately-neighboring ionizing field had the rapidly-*increasing* opportunity to recombine

near the polarization gate. Because 1) photoemission from long-trajectory electrons is typically suppressed in the macroscopic signal due to phase matching [228] and 2) *long*-trajectory electrons spend a relatively *long* time experiencing the high ellipticity of the laser field, no strong satellite pulse was apparent for the case of $\theta_1 = \cot^{-1}(1/2)$ in Fig. 4.16.

In the case of $\theta_1 = \cot^{-1}(2)$, however, the stronger laser cycles were on the *trailing* edge of the polarization gate, so instead it was the *short*-trajectory electrons from the immediately-neighboring ionizing field that had the rapidly-*decreasing* opportunity to recombine near the polarization gate. Because 1) photoemission from short-trajectory electrons typically comprises the macroscopic signal and 2) *short*-trajectory electrons spend a relatively *short* time experiencing the high ellipticity of the laser field, a strong satellite pulse *was* apparent for the case of $\theta_1 = \cot^{-1}(2)$ in Fig. 4.16.

In short, satellite pulse production was not equivalent in the cases of $\theta_1 = \cot^{-1}(2)$ and $\theta_1 = \cot^{-1}(1/2)$ because the differences between short-trajectory and long-trajectory photoemission broke the symmetry of the process.

While the sharpness of the polarization gate discriminated between short-trajectory and long-trajectory photoemission, it also played a role in determining the spectral makeup of the satellite pulse itself. Typically, recombination events carry an intrinsic atto-chirp [228]: for short-trajectory electrons, the lowest-order harmonics are generated first and the cut-off harmonics are generated last; for long-trajectory electrons, the cut-off harmonics are generated first and the lowest-order harmonics are generated last. Referring to the case of $\theta_1 = \cot^{-1}(2)$: because the ellipticity was still rapidly increasing in the region far from the center of the polarization gate where the satellite pulse was produced, the atto-chirp dictated that the generation of cut-off harmonics in this region was far less efficient than the lowest-order harmonics which were generated closer to (albeit still far removed from) the polarization gate. Figure 4.17, plotting the temporal profile of twenty harmonic-wide segments of the spectrum for the case of $\theta_1 = \cot^{-1}(2)$, confirms that only

the shortest short-trajectory electrons with the lowest-order harmonic photoemission contributed to satellite pulse production.

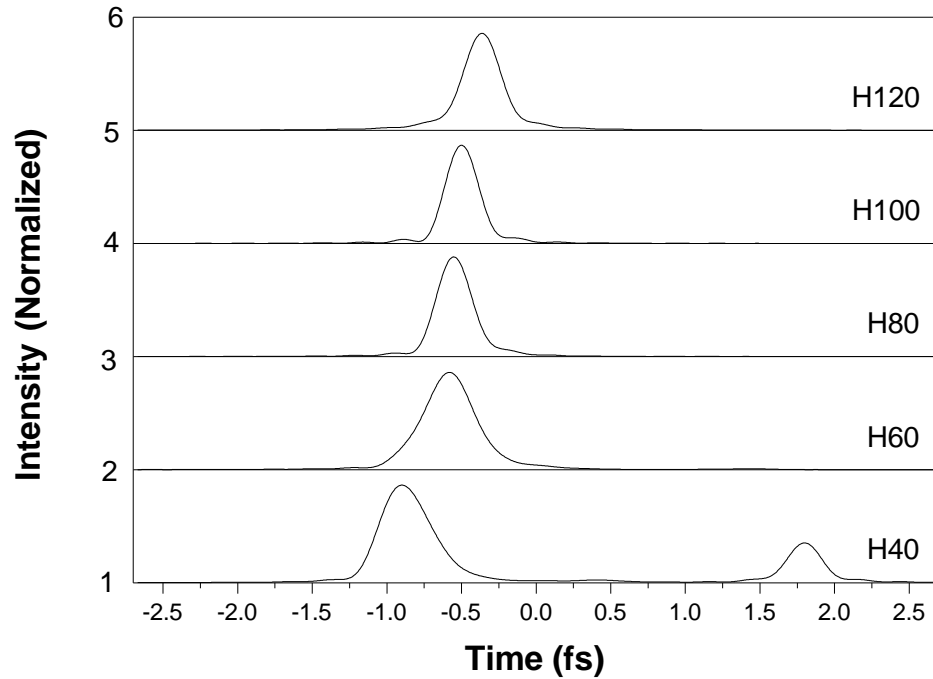


Figure 4.17: The temporal profile of twenty harmonic-wide ranges of the macroscopic spectrum in the top panel of Fig. 4.14 corresponding to $\theta_1 = \cot^{-1}(2)$ (red curve). Each range was centered at the harmonic order specified at the right of each panel (H40, ... , H120). The satellite pulse was only apparent when selecting the lowest-order harmonic region.

This analysis suggests that removing the lower-energy portion of the harmonic spectrum may improve the ratio between the amplitudes of the primary and satellite attosecond pulses. In a laboratory setting, this filtering can be accomplished using thin metal filters, which are already added to many HHG setups in order to remove the residual energy from the near-infrared driving laser. For this simulation, a zirconium filter was used because of its spectral cut-off near 70 eV, which is close to the 45th harmonic of the 800 nm driving laser. Using the case of $\theta_1 = \cot^{-1}(2)$, Figure 4.18 plots the macroscopic spectrum from Fig. 4.14 in gray, the filtered macroscopic spectrum in red, and the transmission curve of the zirconium filter in blue.

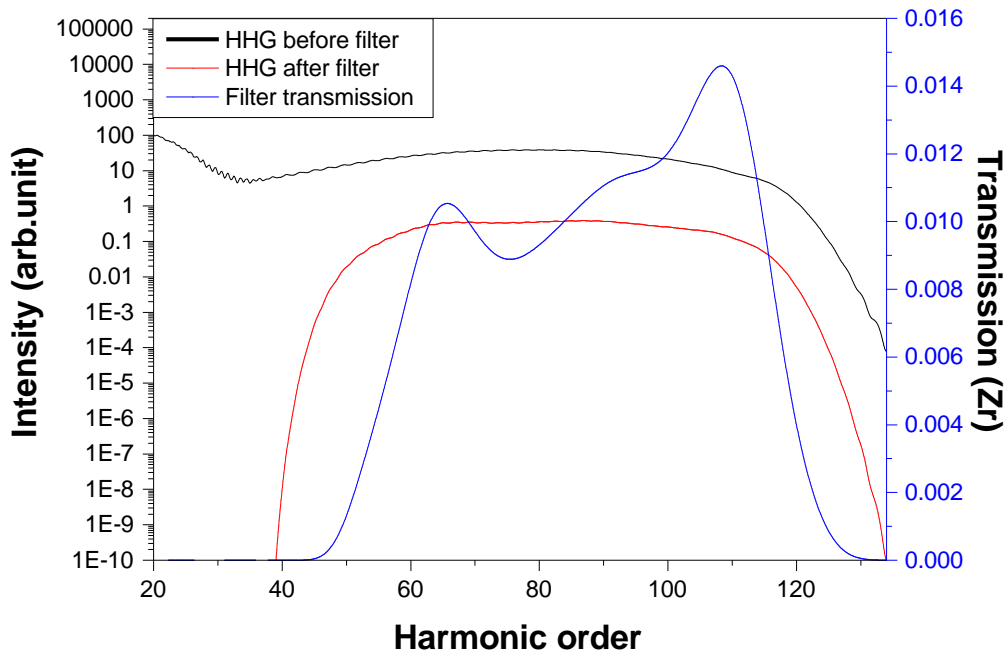


Figure 4.18: The effect of a 1400 nm-thick zirconium filter on the macroscopic spectrum in the top panel of Fig. 4.14 for the case of $\theta_1 = \cot^{-1}(2)$ (red curve).

The thickness of the zirconium filter was chosen to be 1400 nm. This thickness was specifically selected to provide an amount of material dispersion that matched the intrinsic phase of the high-harmonic generation as closely as possible. In this way, the pulse contrast could be improved while simultaneously compressing the attosecond pulse to much shorter temporal durations [229]. Figure 4.19 demonstrates the effect of the 1400 nm zirconium filter on the macroscopic spectrum when using $\theta_1 = \cot^{-1}(2)$: the pulse contrast improved by over three orders of magnitude, while the pulse duration was compressed from 151 as to 59 as.

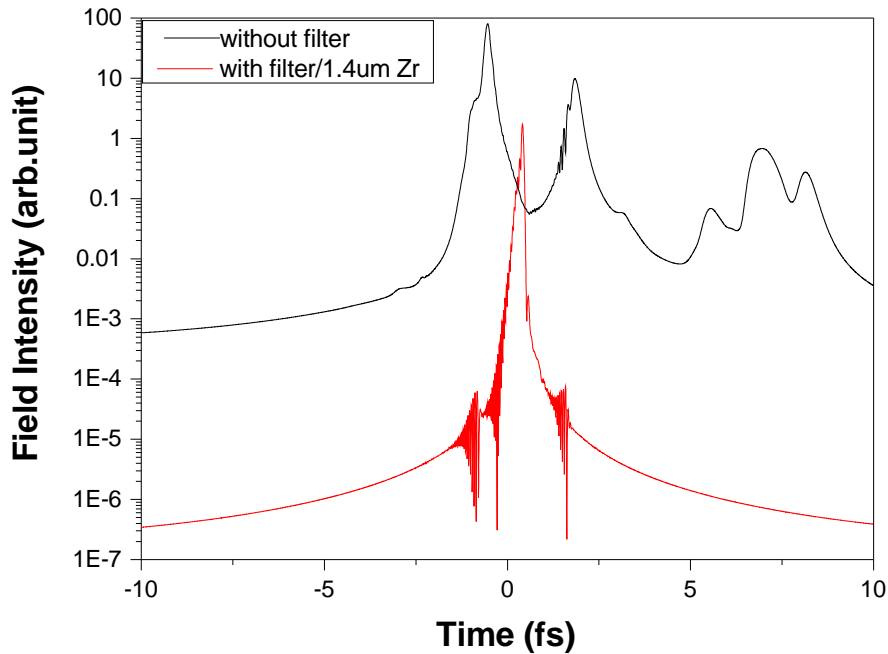


Figure 4.19: The temporal profiles of the attosecond pulses corresponding to the HHG spectra shown in Fig. 4.18.

CHAPTER 5: OUTLOOK

To conclude this dissertation, plans for future work on the IFAST 200 TW system are discussed.

5.1 Improve Pulse Energy and Stability Using a 4 J, Diode-Pumped Pump Laser

In early iterations of the IFAST 200 TW laser architecture, six frequency-doubled Nd:YAG Quanta Ray PRO350 laser systems were used to pump the second stage 10 Hz amplifier (two PRO350s) and the third stage 10 Hz amplifier (four PRO350s). With each system providing close to 2 J/pulse, this configuration allowed the second stage amplifier to reach pulse energies close to the joule level, while the output of the third stage amplifier surpassed 3 J. Because the efficiency of the grating compressor is close to 60%, however, the output of the third stage amplifier must be close to 5 J in order to achieve a peak power of 200 TW.

To this end, more pumping power must be added. This will be accomplished by moving the two PRO350s from the second stage to the third stage and by adding a new pump laser to pump both the first and second stages. This new system, the Gigashot-HE developed by Cutting Edge Optronics, is a 10 Hz, frequency-doubled Nd:YLF system outputting 4 J/pulse, thus making it fit to pump the first two amplifiers. The remarkable characteristic of the Gigashot-HE is its pulse stability: because the internal amplifiers use diode bars rather than flash lamps to pump the Nd:YLF rods, the power output is much more stable.

The improvement of power stability on the first two stages of the IFAST 200 TW laser system is crucial for several reasons: 1) improving the stability of the third stage output to regularize the isolated attosecond pulse generation process, 2) limiting the impact of phase-energy coupling to potentially perform meaningful, direct f-to-2f measurements of the 10 Hz CEP, and 3) providing

a higher-quality seed and pump source for a pre-OPA system that will seed the FOPA system described in Sec. 5.3.

5.2 Attosecond Pulse Generation

The general layout of the post-compressor beamline is depicted in Fig. 5.1. The ultimate goal is to generate 1 μJ , 100 as pulses centered at 50 eV.

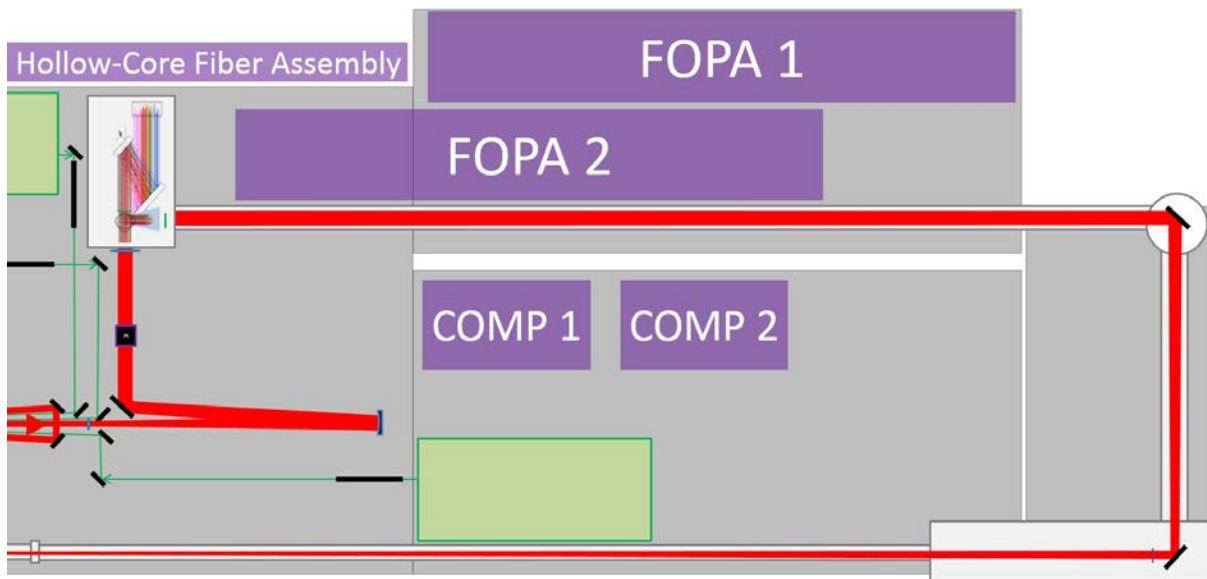


Figure 5.1: Proposed scheme for beam propagation after the pulse compressor.

After the third amplifier, the beam is re-sized in a reflective telescope to 75 mm (middle-left). Before the compressor chamber (top-left), a long-focal-length lens ($f > 20$ m) begins to focus the beam. This is done for the following reasons: 1) by using the lens *before* instead of *after* the compressor, no significant B-integral is accrued, 2) the large beam size makes it difficult to use an on-axis focusing mirror, so the lens is more convenient, and 3) since the focal length of the lens is desired to be as long as possible, placing the optic before the compressor allows the longest

possible propagation distance before reaching the focus.

Because of B-integral issues, the gating optics should be placed as close to the compressor as possible where the beam size is still relatively large. However, this means that there are several 45° mirrors between the first birefringent plate and the gas target. This is generally avoided in other attosecond pulse generation setups because the differences of the mirror's phase and reflectivity response between the orthogonally-polarized driving and gating field components can disrupt the structure of the polarization gate. To minimize these effects, it was chosen to allow the driving field component to be p-polarized, thereby experiencing a narrower reflection bandwidth than the s-polarized gating field. This is because the sharpness of the polarization gate depends on the gating field, whereas the driving field is long in duration; therefore, it is more important to protect the gating field's pulse duration by using the s-polarized reflection.

To put this into practice, the first wave plate is chosen to be full-order (rather than half-order), thus choosing the original polarization direction (gratings use p-polarization) as the driving field direction. This is done after the last diffraction grating but before the first 45° mirror in order to allow the gating field to experience the s-polarized reflection. After this turning mirror, the Brewster window and the second wave plate are added, but not the second harmonic crystal. This is because the second harmonic would not be reflected by the two remaining 45° mirrors, so it must be mounted after the final mirror. To account for the undesired phase shift between the driving and gating fields as a result of the different responses of the mirror, the pedestal holding the second birefringent plate is itself mounted to a stage that can rotate in the plane of the table. This allows for corrective tuning of the relative phase shift between the driving and gating fields.

In spite of the choice of lens, the intensity of the gated pulse at the focus is still predicted to be $\sim 10^{16}$ W/cm², so the gas cell must be placed an additional meter or more downstream in order to prevent saturation of the gas target. (The cell must not be placed too far after the focus, however,

as the intensity must still be high enough to generate a cut-off above 50 eV). The exact position of the beam waist can be finely controlled by changing the reflective telescope before the pulse compressor. Because of the large beam size, the hole in the gas cell wall is large, so the gas line feeding the HHG cell is pulsed using a gas jet in order to maintain appropriate levels of vacuum.

After the high harmonics are generated, the residual near-infrared field is removed by using silicon plates or dielectric beam splitters set at Brewster's angle. Afterwards, thin metal filters are used to prevent any infrared light from making it into the end station, which is designed and constructed by project collaborators at the University of California, Berkeley. This apparatus, which includes focusing mirrors, an experimental chamber, and beam diagnostics, will be used to perform experiments such as all-attosecond pump-probe measurements in gas and condensed matter targets, XUV two-photon absorption, and ion time-of-flight auto-correlation. A depiction of the entire setup of the completed IFAST 200 TW system is shown in Fig. 5.2.

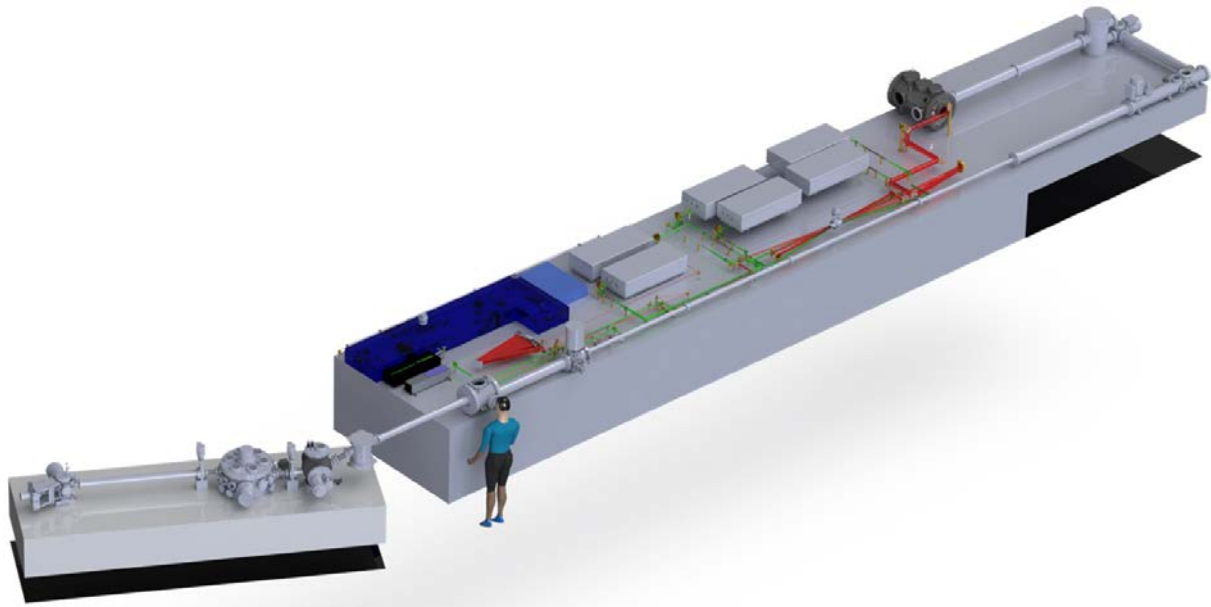


Figure 5.2: The IFAST 200 TW amplifier (center), compressor (top), focusing beamline (front edge), and end station (left).

5.3 Frequency-Domain Optical Parametric Amplification (FOPA)

In addition to generating high-flux attosecond pulses, the IFAST 200 TW system will be used to pump a 1.8 μm , 100 mJ, 10 fs (10 TW) laser constructed by project collaborators at the Institut National de la Recherche Scientifique (INRS) in Canada. The block diagram for this system is depicted in Fig. 5.3.

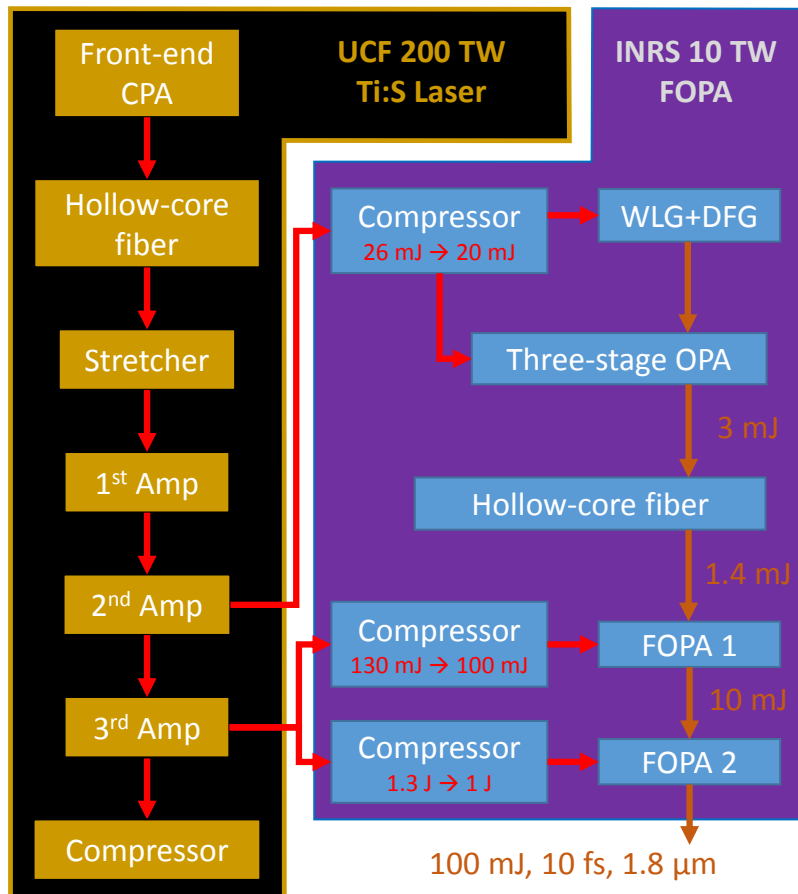


Figure 5.3: Block diagram of the proposed scheme for the FOPA laser system.

The seed for the INRS 10 TW system is produced using a 26 mJ sampling (less 5%) taken from the second amplifier of the IFAST 200 TW laser system. This pulse is compressed to 15 fs and then

divided four ways: the first part is used for white-light generation (WLG) and difference-frequency generation (DFG) to produce a broadband, mid-IR seed pulse, and the other three parts are used for pumping a three-stage optical parametric amplifier (OPA) which amplifies the broadband seed pulse to 3 mJ. The spectrum of this pulse is further broadened in a hollow-core fiber, the throughput of which is close to 50%. This output seeds two additional broadband amplification stages based on frequency-domain optical parametric amplification, or FOPA [230].

The operating principle of the FOPA is as follows: a broadband seed pulse is injected into a 4-f, zero-dispersion stretcher, as shown in Fig. 5.4. At the stretcher's Fourier plane, the individual components of the pulse spectrum are spatially addressable. By placing several nonlinear crystals at this location, the phase matching for each part of the spectrum can be optimized by using crystals with different cuts, and the shape of the output spectrum can be tuned by judiciously adjusting the pumping of the different crystals. This allows for ultrabroadband amplification capable of supporting single-cycle pulse durations. Another major benefit of this technique is the suppression of superfluorescence, which is diffracted away by the final grating of the 4-f setup.

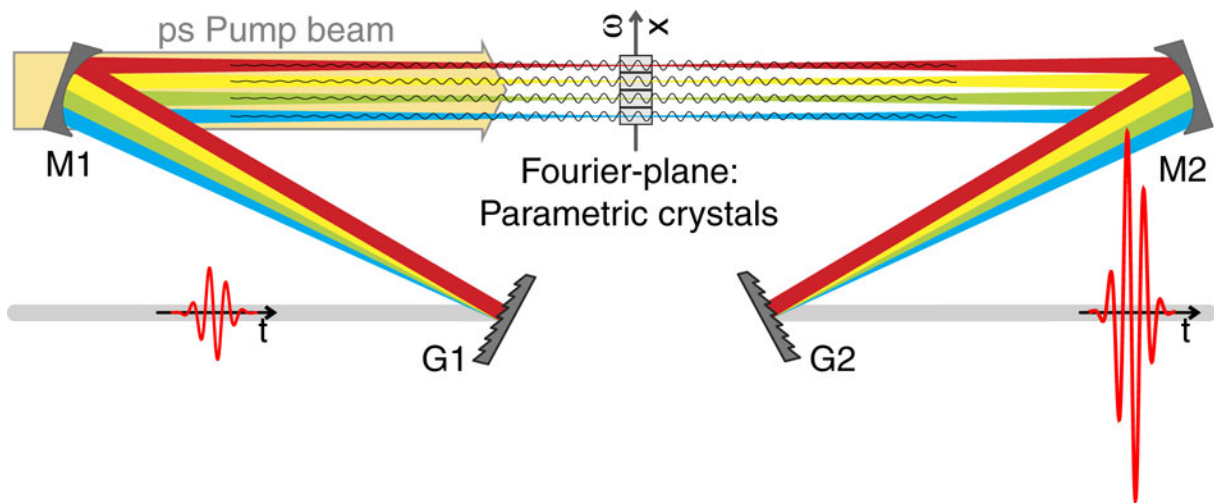


Figure 5.4: The principle of frequency-domain optical parametric amplification [230].

For the INRS 10 TW system at the IFAST lab, the pump pulses for the two FOPA stages are taken from the output of the third amplifier of the IFAST 200 TW laser system. The first pump pulse (130 mJ) is compressed to several picoseconds and directed to the first FOPA, which amplifies the broadband fiber output to 10 mJ. The second pump pulse (1.3 J) is also compressed to several picoseconds before propagating to the second FOPA, which outputs 100 mJ, 10 fs pulses centered at 1.8 μm . The goal of this system is to generate 10 nJ, sub-100 as pulses centered at 540 eV at the same time as the 800 nm-driven 1 μJ , 100 as pulses centered at 50 eV. These pulses will be used to perform attosecond pump–attosecond probe experiments.

**APPENDIX A: NON-TIME-AVERAGED OPTICS FOR SUB-CYCLE
INTERESTS**

Simulations of sub-envelope behavior of optical pulses are often performed using standard definitions of physical quantities that are time-averaged in nature. This is inappropriate for investigations of sub-cycle dynamics such as ionization or polarization gating. This appendix serves as a reminder of how to correctly calculate 1) the “instantaneous” intensity and 2) the “instantaneous” ellipticity and polarization for sub-envelope studies.

Instantaneous Intensity

Using the approach of [231], the Poynting vector is defined as

$$\vec{\mathbf{S}} = \vec{\mathbf{E}} \times \vec{\mathbf{H}} = \Re \left\{ \sum_j \vec{E}_j e^{i\phi_j} \right\} \times \frac{1}{\mu_0} \Re \left\{ \sum_j \frac{\vec{k} \times \vec{E}_j}{\omega_j} e^{i\phi_j} \right\} \quad (\text{A.1})$$

where

$$\vec{\mathbf{E}} = \Re \left\{ \sum_j \vec{E}_j e^{i\phi_j} \right\} \quad (\text{A.2})$$

and

$$\vec{\mathbf{H}} = \frac{1}{\mu_0} \Re \left\{ \sum_j \frac{\vec{k} \times \vec{E}_j}{\omega_j} e^{i\phi_j} \right\} \quad (\text{A.3})$$

with $\phi_j = \vec{k}_j \cdot \vec{r} - \omega t$.

Assuming k_m is real, simplify using the BAC-CAB identity:

$$\vec{\mathbf{S}} = \sum_{j,m} \frac{1}{\omega_m \mu_0} \left[\vec{k}_m \left(\Re \left\{ \vec{E}_j e^{i\phi_j} \right\} \cdot \Re \left\{ \vec{E}_m e^{i\phi_m} \right\} \right) - \Re \left\{ \vec{E}_m e^{i\phi_m} \right\} \left(\Re \left\{ \vec{E}_j e^{i\phi_j} \right\} \cdot \vec{k}_m \right) \right] \quad (\text{A.4})$$

Since \vec{k} and $\vec{\mathbf{E}}$ are essentially parallel for a laser in an isotropic medium, the dot product in the second term evaluates to zero.

It can be shown that

$$\Re \left\{ \vec{\zeta}_1 \right\} \cdot \Re \left\{ \vec{\zeta}_2 \right\} = \frac{1}{2} \left[\Re \left\{ \vec{\zeta}_1 \cdot \vec{\zeta}_2 \right\} + \Re \left\{ \vec{\zeta}_1^* \cdot \vec{\zeta}_2 \right\} \right] \quad (\text{A.5})$$

Therefore,

$$\vec{\mathbf{S}} = \sum_{j,m} \frac{1}{\omega_m \mu_0} \frac{\vec{k}_m}{2} \left[\Re \left\{ \vec{E}_j e^{i\phi_j} \cdot \vec{E}_m e^{i\phi_m} \right\} + \Re \left\{ \vec{E}_j^* e^{-i\phi_j} \cdot \vec{E}_m e^{i\phi_m} \right\} \right] \quad (\text{A.6})$$

If the index of refraction is approximately uniform such that $\frac{k_m}{\omega_m \mu_0} \approx n c \epsilon_0$, then

$$\|\vec{\mathbf{S}}\| = \frac{n c \epsilon_0}{2} \left[\Re \left\{ \sum_j \vec{E}_j e^{i\phi_j} \cdot \sum_m \vec{E}_m e^{i\phi_m} \right\} + \Re \left\{ \sum_j \vec{E}_j^* e^{-i\phi_j} \cdot \sum_m \vec{E}_m e^{i\phi_m} \right\} \right] \quad (\text{A.7})$$

$$\Rightarrow \|\vec{\mathbf{S}}\| = \frac{n c \epsilon_0}{2} \left[\Re \left\{ \vec{\mathbf{E}} \cdot \vec{\mathbf{E}} \right\} + \Re \left\{ \vec{\mathbf{E}}^* \cdot \vec{\mathbf{E}} \right\} \right] = \frac{n c \epsilon_0}{2} \left[\Re \left\{ \vec{\mathbf{E}} \cdot \vec{\mathbf{E}} \right\} + |\vec{\mathbf{E}}|^2 \right] \quad (\text{A.8})$$

Typically ‘intensity’ is defined as the time average of the Poynting vector. When performing this operation, the rapidly-oscillating first term $\Re \left\{ \vec{\mathbf{E}} \cdot \vec{\mathbf{E}} \right\}$ drops out, leaving the familiar expression for intensity $I = \langle \|\vec{\mathbf{S}}\| \rangle_t = \frac{n c \epsilon_0}{2} |\vec{\mathbf{E}}|^2$. However, in pursuits such as ADK calculations where carrier wave dynamics are of interest, the first term $\Re \left\{ \vec{\mathbf{E}} \cdot \vec{\mathbf{E}} \right\}$ must be allowed to remain since it holds the information about the fast oscillations.

For a pulse of the form

$$\vec{\mathbf{E}} = (|E_{0x}| e^{i\delta_x} \hat{x} + |E_{0y}| e^{i\delta_y} \hat{y}) e^{\phi_{\Re} + i\phi_{\Im}} \quad (\text{A.9})$$

the instantaneous intensity can be calculated as

$$\begin{aligned}
\|\vec{\mathbf{S}}\| &= \frac{nC\epsilon_0}{2} \left[\Re \left\{ \vec{\mathbf{E}} \cdot \vec{\mathbf{E}} \right\} + |\vec{\mathbf{E}}|^2 \right] \\
&= \frac{nC\epsilon_0}{2} \left[\Re \left\{ (|E_{0x}|^2 e^{2i\delta_x} + |E_{0y}|^2 e^{2i\delta_y}) e^{2\phi_{\Im} + 2i\phi_{\Im}} \right\} \right. \\
&\quad \left. + (|E_{0x}|^2 + |E_{0y}|^2) e^{2\phi_{\Re}} \right] \\
&= \frac{nC\epsilon_0}{2} e^{2\phi_{\Re}} \left[|E_{0x}|^2 (1 + \cos(2(\phi_{\Im} + \delta_x))) \right. \\
&\quad \left. + |E_{0y}|^2 (1 + \cos(2(\phi_{\Im} + \delta_y))) \right] \tag{A.10}
\end{aligned}$$

For linear polarization, $|E_{0x}| = |E_0|$, $|E_{0y}| = 0$, and $\delta_x = \delta_y = 0$:

$$\|\vec{\mathbf{S}}\| = \frac{nC\epsilon_0}{2} e^{2\phi_{\Re}} |E_0|^2 (1 + \cos(2\phi_{\Im})) \tag{A.11}$$

For circular polarization, $|E_{0x}| = |E_0|/\sqrt{2}$, $|E_{0y}| = |E_0|/\sqrt{2}$, $\delta_x = 0$, and $\delta_y = \pi/2$:

$$\begin{aligned}
\|\vec{\mathbf{S}}\| &= \frac{nC\epsilon_0}{2} e^{2\phi_{\Re}} \left[\frac{1}{2} |E_0|^2 (1 + \cos(2\phi_{\Im})) + \frac{1}{2} |E_0|^2 \left(1 + \cos \left(2 \left(\phi_{\Im} + \frac{\pi}{2} \right) \right) \right) \right] \\
&= \frac{nC\epsilon_0}{2} e^{2\phi_{\Re}} \left[\frac{1}{2} |E_0|^2 (1 + \cos(2\phi_{\Im})) + \frac{1}{2} |E_0|^2 (1 - \cos(2\phi_{\Im})) \right] \\
&= \frac{nC\epsilon_0}{2} e^{2\phi_{\Re}} |E_0|^2 \tag{A.12}
\end{aligned}$$

For the special case of elliptical polarization where $|E_{0x}| = |E_0|/\sqrt{2}$, $|E_{0y}| = \epsilon|E_0|/\sqrt{2}$, $\delta_x = 0$, and $\delta_y = \pi/2$ (note that the field strength is no longer normalized, but rather $|E_{0y}|$ is reduced using

loss from a Brewster window (for example)):

$$\begin{aligned}
\|\vec{\mathbf{S}}\| &= \frac{n c \epsilon_0}{2} e^{2\phi_{\Re}} \left[\frac{1}{2} |E_0|^2 (1 + \cos(2\phi_{\Im})) + \frac{1}{2} \epsilon^2 |E_0|^2 \left(1 + \cos\left(2\left(\phi_{\Im} + \frac{\pi}{2}\right)\right) \right) \right] \\
&= \frac{n c \epsilon_0}{2} e^{2\phi_{\Re}} \left[\frac{1}{2} |E_0|^2 (1 + \cos(2\phi_{\Im})) + \frac{1}{2} \epsilon^2 |E_0|^2 (1 - \cos(2\phi_{\Im})) \right] \\
&= \frac{n c \epsilon_0}{2} e^{2\phi_{\Re}} |E_0|^2 \left[\frac{1 + \epsilon^2}{2} + \frac{1 - \epsilon^2}{2} \cos(2\phi_{\Im}) \right] \tag{A.13}
\end{aligned}$$

Instantaneous Polarization and Ellipticity

Many sources introducing the concept of polarization make reference to the shape drawn out by the time-evolving tip of the electric field vector at some point in space. This definition works well for determining the polarization of a continuous-wave beam whose ellipticity does not change with time. However, this illustration works poorly when the polarization is time-dependent, as is the case with polarized-based gatings (e.g. symmetric and asymmetric PG, DOG, GDOG).

Typically a polarization-gated field is broken down into two components, the driving field E_{drive} and the gating field E_{gate} , and it is tempting to calculate the time-dependent field ellipticity $\xi(t)$ by directly using the ratio between the *envelopes* of these two fields. Indeed, this works well when using the common assumption that the difference in phase between the *carrier waves* of E_{drive} and E_{gate} is exactly $\pm\pi/2$. However, if this is not the case due to the inclusion of dispersion in the calculation or due to the use of an imperfect quarter-wave plate, then it is necessary to use a mathematically-rigorous definition of polarization that can be adapted to PG for calculating the ellipticity. Following the definitions as set forth in [232]: first express the total field as having the form

$$\vec{E}(t) = |E_{dr}(t)| \exp[i\phi_{dr}(t)] \hat{e}_{dr} + |E_{ga}(t)| \exp[i\phi_{ga}(t)] \hat{e}_{ga} \tag{A.14}$$

where $|E_{dr}|$ and $|E_{ga}|$ hold the information about the driving and gating field envelopes, and ϕ_{dr} and ϕ_{ga} hold the information about the driving and gating field carrier waves. Next, introduce the following definitions:

$$\begin{aligned} A &\equiv \frac{|E_{dr}|}{\sqrt{|E_{dr}|^2 + |E_{ga}|^2}} \\ B &\equiv \frac{|E_{ga}|}{\sqrt{|E_{dr}|^2 + |E_{ga}|^2}} \\ E_{eff} &\equiv \sqrt{|E_{dr}|^2 + |E_{ga}|^2} \exp[i\phi_{dr}] \end{aligned} \quad (\text{A.15})$$

such that Eq. A.14 can be re-written with the form

$$\vec{E}(t) = E_{eff}(A\hat{e}_{dr} + B \exp[i\delta]\hat{e}_{ga}) \quad (\text{A.16})$$

where $\delta = \phi_{ga} - \phi_{dr}$.

When $\delta = \pm\pi/2$, the semi-major and semi-minor axes of the ‘‘instantaneous’’ polarization ellipse are in the same directions as \hat{e}_{dr} and \hat{e}_{ga} . However, when $\delta \neq \pm\pi/2$, the angles of the semi-major and semi-minor axes are given by

$$\alpha = \frac{1}{2} \tan^{-1} \left(\frac{2AB \cos \delta}{A^2 - B^2} \right) \quad (\text{A.17})$$

and $\alpha \pm \pi/2$. Rewriting Eq. A.16 in terms of the orthogonal basis set defined by α yields field components

$$E_{\alpha} = |E_{eff}| \sqrt{A^2 \cos^2 \alpha + B^2 \sin^2 \alpha + AB \cos \delta \sin 2\alpha} \quad (\text{A.18})$$

and

$$E_{\alpha \pm \pi/2} = |E_{eff}| \sqrt{A^2 \sin^2 \alpha + B^2 \cos^2 \alpha - AB \cos \delta \sin 2\alpha} \quad (\text{A.19})$$

It is *these* fields that must be used to calculate the time-dependent ellipticity:

$$\xi(t) \equiv \text{Min} \left[\frac{E_\alpha}{E_{\alpha \pm \pi/2}}, \frac{E_{\alpha \pm \pi/2}}{E_\alpha} \right] \quad (\text{A.20})$$

APPENDIX B: GENERAL GATING FIELDS

For a general AGDOG field, the linearly-polarized incident field is expressed as

$$\vec{E}_{\text{input}}(t) = E_0 \exp \left[-2 \ln 2 \left(\frac{t}{\tau_p} \right)^2 \right] \exp[-i\omega_0 t] \hat{y} \quad (\text{B.1})$$

where τ_p is the pulse duration and ω_0 is the carrier frequency.

The Fourier transform of this field ($\vec{E}(t) \Leftrightarrow \vec{\tilde{E}}(\omega)$) is

$$\vec{\tilde{E}}_{\text{input}}(\omega) = \tau_p \frac{E_0}{2\sqrt{\ln 2}} \exp \left[-\frac{\tau_p^2 (\omega - \omega_0)^2}{8 \ln 2} \right] \hat{y} \quad (\text{B.2})$$

After propagating through the first phase retarder, which splits the field into two orthogonally-polarized pulses, the field looks like this:

$$\begin{aligned} \vec{\tilde{E}}_{\text{QP1}} &= \frac{\tau_p E_0}{2\sqrt{\ln 2}} \exp \left[-\frac{\tau_p^2 (\omega - \omega_0)^2}{8 \ln 2} \right] \{ \exp [i(kz)_{QP1e}] \cos \theta_1 \hat{e}_1 + \exp [i(kz)_{QP1o}] \sin \theta_1 \hat{o}_1 \} \\ &= \mathcal{C} \times \{ \sin \theta_1 \cos \theta_1 (\exp [i(kz)_{QP1o}] - \exp [i(kz)_{QP1e}]) \hat{x} \\ &\quad + (\sin^2 \theta_1 \exp [i(kz)_{QP1o}] + \cos^2 \theta_1 \exp [i(kz)_{QP1e}]) \hat{y} \} \end{aligned} \quad (\text{B.3})$$

$$\begin{aligned} &= \mathcal{C} \times \{ (\sin \theta_1 \sin (\theta_1 - \theta_2) \exp [i(kz)_{QP1o}] + \cos \theta_1 \cos (\theta_1 - \theta_2) \exp [i(kz)_{QP1e}]) \hat{e}_2 \\ &\quad + (\sin \theta_1 \cos (\theta_1 - \theta_2) \exp [i(kz)_{QP1o}] - \cos \theta_1 \sin (\theta_1 - \theta_2) \exp [i(kz)_{QP1e}]) \hat{o}_2 \} \end{aligned} \quad (\text{B.4})$$

where $\mathcal{C} \equiv \frac{\tau_p E_0}{2\sqrt{\ln 2}} \exp \left[-\frac{\tau_p^2 (\omega - \omega_0)^2}{8 \ln 2} \right]$ for convenience. Equation B.4 is simply Eq. B.3 rewritten in the basis common to the Brewster windows and the second phase retarder. In the case of PG, DOG, and GDOG, θ_2 is fixed to be $\theta_1 - 45^\circ$, and Equation B.4 can be simplified at the same time the effect of the Brewster windows is accounted for (but this assumption is set aside for the

time being):

$$\begin{aligned}
\vec{E}_{\text{QWP}} = \mathcal{C} \times \{ & \epsilon (\sin \theta_1 \sin (\theta_1 - \theta_2) \exp [i(kz)_{QP1o}] \\
& + \cos \theta_1 \cos (\theta_1 - \theta_2) \exp [i(kz)_{QP1e}] \exp [i(kz)_{QWPe}] \hat{e}_2 \\
& + (\sin \theta_1 \cos (\theta_1 - \theta_2) \exp [i(kz)_{QP1o}] \\
& - \cos \theta_1 \sin (\theta_1 - \theta_2) \exp [i(kz)_{QP1e}] \exp [i(kz)_{QWPe}] \hat{o}_2 \} \quad (\text{B.5})
\end{aligned}$$

where ϵ refers to the ellipticity induced by the attenuation of the Brewster windows.

It should be noted that in the case of DOG and GDOG, the second phase retarder is actually a combination of two phase retarders, the second of which providing the second harmonic of the fundamental field for achieving the two-color effect. In this case,

$$(kz)_{\text{QWP}} = (kz)_{\text{QP2}} + (kz)_{\text{SHG}} \quad (\text{B.6})$$

where we have incorporated the requirement that the principal axes of the two phase retarders must be aligned.

Equation B.5 describes four pulses, each one seeing a unique set of dispersion parameters:

$$\begin{aligned}
\vec{E}_{\text{QWP}} = \mathcal{C} \times \{ & \epsilon (\sin \theta_1 \sin (\theta_1 - \theta_2) \exp [i(kz)_1] + \cos \theta_1 \cos (\theta_1 - \theta_2) \exp [i(kz)_2]) \hat{e}_2 \\
& + (\sin \theta_1 \cos (\theta_1 - \theta_2) \exp [i(kz)_3] - \cos \theta_1 \sin (\theta_1 - \theta_2) \exp [i(kz)_4]) \hat{o}_2 \} \quad (\text{B.7})
\end{aligned}$$

where

$$\begin{aligned}
(kz)_1 &= k_{QP1o}z_{QP1} + k_{QWP e}z_{QWP} \\
(kz)_2 &= k_{QP1e}z_{QP1} + k_{QWP e}z_{QWP} \\
(kz)_3 &= k_{QP1o}z_{QP1} + k_{QWP o}z_{QWP} \\
(kz)_4 &= k_{QP1e}z_{QP1} + k_{QWP o}z_{QWP}
\end{aligned} \tag{B.8}$$

To continue back to the time domain, two different approaches can be taken: 1) find an analytical solution of the fields valid up to second-order dispersion (useful for obtaining closed-form expressions that can be readily manipulated to obtain expressions for things like ellipticity, gate position, required pulse separation, etc.) or 2) numerically calculate the inverse Fourier transform back to the time domain (accounts for higher-order dispersion terms, but does not lend itself well to calculations of important gating parameters). The remainder of this appendix pursues an analytical solution using the form of the solution found in [233].

Examining first of the four pulses from Eq. B.7 and momentarily ignoring the ω -independent factor of $\epsilon \sin \theta_1 \sin (\theta_1 - \theta_2)$, the Fourier integral takes the form of

$$\vec{E}_1(t) = \frac{1}{\sqrt{2\pi}} \int_{-\infty}^{+\infty} \frac{\tau_p E_0}{2\sqrt{\ln 2}} \exp \left[-\frac{\tau_p^2 (\omega - \omega_0)^2}{8 \ln 2} \right] \exp [i(kz)_1] \exp [-i\omega t] d\omega \tag{B.9}$$

Here we have also re-introduced \mathcal{C} explicitly to account for its dependence on ω .

In general, the term (kz) can be expanded by Taylor series as

$$k(\omega)z \approx k(\omega_0)z + \left. \frac{\partial k}{\partial \omega} \right|_{\omega_0} (\omega - \omega_0)z + \frac{1}{2} \left. \frac{\partial^2 k}{\partial \omega^2} \right|_{\omega_0} (\omega - \omega_0)^2 z + \dots \tag{B.10}$$

Defining the terms

$$(k_0 z) \equiv k(\omega_0) z = n(\omega_0) \frac{\omega_0}{c} z \quad (\text{B.11})$$

$$(v_g^{-1} z) \equiv \left. \frac{\partial k}{\partial \omega} \right|_{\omega_0} z = n'(\omega_0) \frac{\omega_0}{c} z + \frac{n(\omega_0)}{c} z \quad (\text{B.12})$$

$$(\alpha z) \equiv \left. \frac{1}{2} \frac{\partial^2 k}{\partial \omega^2} \right|_{\omega_0} z = n''(\omega_0) \frac{\omega_0}{2c} z + \frac{n'(\omega_0)}{c} z \quad (\text{B.13})$$

Equation B.9 then becomes

$$E_1(t) = \frac{\tau_p E_0}{2\sqrt{2\pi \ln 2}} \exp [i((k_0 z)_1 - \omega_0 t)] \times \int_{-\infty}^{+\infty} \exp \left[- \left(\frac{\tau_p^2}{8 \ln 2} - i(\alpha z)_1 \right) \omega'^2 - i(t - (v_g^{-1} z)_1) \omega' \right] d\omega' \quad (\text{B.14})$$

where we have performed a change of variables $\omega' \equiv \omega - \omega_0$.

This integral evaluates to

$$E_1(t) = \frac{\tau_p E_0}{2\sqrt{2\pi \ln 2}} \exp [i((k_0 z)_1 - \omega_0 t)] \sqrt{\frac{\pi}{\left(\frac{\tau_p^2}{8 \ln 2} - i(\alpha z)_1 \right)}} \exp \left[- \frac{(t - (v_g^{-1} z)_1)^2}{4 \left(\frac{\tau_p^2}{8 \ln 2} - i(\alpha z)_1 \right)} \right] \quad (\text{B.15})$$

After introducing $\Phi \equiv \frac{8 \ln 2}{\tau_p^2} (\alpha z)$ and $\tau'_p \equiv \tau_p \sqrt{1 + \Phi^2}$, Equation B.15 takes on the new form

$$E_1(t) = E_0 \exp [i((k_0 z)_1 - \omega_0 t)] \frac{\exp \left[\frac{i}{2} \tan^{-1} \Phi_1 \right]}{\sqrt{\tau'_{p1} / \tau_p}} \exp \left[-2 \ln 2 \left(\frac{t - (v_g^{-1} z)_1}{\tau'_{p1}} \right)^2 (1 + i\Phi_1) \right] \quad (\text{B.16})$$

This integral of all four pulses in Eq. B.7 will evaluate in the same way, the only difference coming from the values of (kz) , $(v_g^{-1} z)$, and (αz) as identified in (B.8). Explicitly written out, this looks

like

$$\begin{aligned}
\vec{E}_{out} = E_0 \exp[-i\omega_0 t] \times \\
\left\{ \epsilon \left(\frac{\sin \theta_1 \sin(\theta_1 - \theta_2)}{\sqrt{\tau'_{p1}/\tau_p}} \exp \left[-2 \ln 2 \left(\frac{t - (v_g^{-1}z)_1}{\tau'_{p1}} \right)^2 (1 + i\Phi_1) + i(k_0z)_1 + \frac{i}{2} \tan^{-1} \Phi_1 \right] \right. \right. \\
+ \frac{\cos \theta_1 \cos(\theta_1 - \theta_2)}{\sqrt{\tau'_{p2}/\tau_p}} \exp \left[-2 \ln 2 \left(\frac{t - (v_g^{-1}z)_2}{\tau'_{p2}} \right)^2 (1 + i\Phi_2) + i(k_0z)_2 + \frac{i}{2} \tan^{-1} \Phi_2 \right] \left. \right) \hat{e}_2 \\
+ \left(\frac{\sin \theta_1 \cos(\theta_1 - \theta_2)}{\sqrt{\tau'_{p3}/\tau_p}} \exp \left[-2 \ln 2 \left(\frac{t - (v_g^{-1}z)_3}{\tau'_{p3}} \right)^2 (1 + i\Phi_3) + i(k_0z)_3 + \frac{i}{2} \tan^{-1} \Phi_3 \right] \right. \\
\left. \left. - \frac{\cos \theta_1 \sin(\theta_1 - \theta_2)}{\sqrt{\tau'_{p4}/\tau_p}} \exp \left[-2 \ln 2 \left(\frac{t - (v_g^{-1}z)_4}{\tau'_{p4}} \right)^2 (1 + i\Phi_4) + i(k_0z)_4 + \frac{i}{2} \tan^{-1} \Phi_4 \right] \right) \right) \hat{o}_2 \left. \right\}
\end{aligned} \tag{B.17}$$

This equation is useful for simulating polarization-based gatings under more realistic conditions to examine the subtle chirping effects such as changes to the ellipticity due to differences in dispersion between the ordinary and extraordinary refractive indices of the wave plates. In these non-ideal cases, it is important to calculate the polarization and ellipticity correctly as outlined in the previous appendix.

APPENDIX C: COPYRIGHT PERMISSIONS

This appendix contains the following (in order):

- Permission for Fig. 1.1 adapted from Ref. [4].
- Permission for Fig. 1.2 adapted from Ref. [5].
- Permission for Fig. 1.3 adapted from Ref. [11].
- Permission for Fig. 1.4 adapted from Ref. [13].
- Permission for Fig. 1.5 adapted from Ref. [23].
- Permission for Fig. 2.1 adapted from Ref. [48].
- Permission for the following figures copyrighted by OSA:
 - Fig. 2.2(a) adapted from Ref. [73].
 - Fig. 2.4 adapted from Ref. [82].
 - Fig. 2.6 adapted from Ref. [84].
 - Fig. 2.8 adapted from Ref. [89].
 - Fig. 2.9 adapted from Ref. [92].
 - Fig. 2.10 adapted from Ref. [105].
 - Fig. 2.12(b) adapted from Ref. [108].
 - Fig. 2.13(a) adapted from Ref. [110].
 - Fig. 2.13(b) adapted from Ref. [115].
 - Fig. 2.14 adapted from Ref. [91].
 - Fig. 2.16 adapted from Ref. [135].
- Permission for Fig. 2.3 adapted from Ref. [81].

- Permission for Fig. 2.5 adapted from Ref. [83].
- Permission for Fig. 2.7 adapted from Ref. [85].
- Permission for Fig. 2.11 adapted from Ref. [106].
- Permission for Fig. 2.12(a) adapted from Ref. [107].
- Permission for Fig. 2.15 adapted from Ref. [131].
- Permission for Fig. 2.17(a), Fig. 2.17(b), Fig. 2.18, Fig. 2.19, Fig. 2.20, and Fig. 2.21 adapted from Ref. [148].
- Permission for Fig. 2.34(a) adapted from Ref. [158].
- Permission for Fig. 3.2 adapted from Ref. [181].
- Permission for Fig. 3.3 adapted from Ref. [205].
- Permission for Fig. 4.5(a), Fig. 4.5(b), Fig. 4.6, Fig. 4.8, Fig. 4.9, Fig. 4.10, Fig. 4.11, Fig. 4.12, and Fig. 4.13 adapted from Ref. [221].
- Permission for Fig. 5.4 adapted from Ref. [230].

**THE ROYAL SOCIETY LICENSE
TERMS AND CONDITIONS**

Oct 23, 2015

This Agreement between Eric Cunningham ("You") and The Royal Society ("The Royal Society") consists of your license details and the terms and conditions provided by The Royal Society and Copyright Clearance Center.

All payments must be made in full to CCC. For payment instructions, please see information listed at the bottom of this form.

License Number	3735080035168
License date	Oct 23, 2015
Licensed Content Publisher	The Royal Society
Licensed Content Publication	Proceedings A
Licensed Content Title	Flash Photolysis and Spectroscopy. A New Method for the Study of Free Radical Reactions
Licensed Content Author	G. Porter
Licensed Content Date	1950-01-06
Licensed Content Volume Number	200
Licensed Content Issue Number	1061
Volume number	200
Issue number	1061
Type of Use	Thesis/Dissertation
Requestor type	academic/educational
Format	print and electronic
Portion	figures/tables/images
Quantity	1
Will you be translating?	no
Circulation	10
Order reference number	None
Title of your thesis / dissertation	Towards High-Flux Isolated Attosecond Pulses with a 200 TW CPA
Expected completion date	Nov 2015
Estimated size (number of pages)	150
Requestor Location	Eric Cunningham University of Central Florida 4111 Libra Dr. PS-430 ORLANDO, FL 32816

United States
Attn: Eric Cunningham

Billing Type Credit Card

Credit card info Visa ending in 6338

Credit card expiration 09/2016

Total 4.20 USD

Terms and Conditions

STANDARD TERMS AND CONDITIONS FOR REPRODUCTION OF MATERIAL FROM A ROYAL SOCIETY JOURNAL

1. Use of the material is restricted to the type of use specified in your order details.
2. The publisher for this copyrighted material is the Royal Society. By clicking "accept" in connection with completing this licensing transaction, you agree that the following terms and conditions apply to this transaction (along with the Billing and Payment terms and conditions established by Copyright Clearance Center, Inc. ("CCC"), at the time that you opened your Rightslink account and that are available at any time at <http://myaccount.copyright.com>.
3. The following credit line appears wherever the material is used: author, title, journal, year, volume, issue number, pagination, by permission of the Royal Society.
4. For the reproduction of a full article from a Royal Society journal for whatever purpose, the corresponding author of the material concerned should be informed of the proposed use. Contact details for the corresponding authors of all Royal Society journals can be found alongside either the abstract or full text of the article concerned, accessible from royalsocietypublishing.org.
5. If the credit line in our publication indicates that any of the figures, images or photos was reproduced from an earlier source it will be necessary for you to clear this permission with the original publisher as well. If this permission has not been obtained, please note that this material cannot be included in your publication/photocopies.
6. Licenses may be exercised anywhere in the world.
7. While you may exercise the rights licensed immediately upon issuance of the license at the end of the licensing process for the transaction, provided that you have disclosed complete and accurate details of your proposed use, no license is finally effective unless and until full payment is received from you (either by publisher or by CCC) as provided in CCC's Billing and Payment terms and conditions. If full payment is not received on a timely basis, then any license preliminarily granted shall be deemed automatically revoked and shall be void as if never granted. Further, in the event that you breach any of these terms and conditions or any of CCC's Billing and Payment terms and conditions, the license is automatically revoked and shall be void as if never granted. Use of materials as described in a revoked license, as well as any use of the materials beyond the scope of an unrevoked license, may constitute copyright infringement and publisher reserves the right to take any and all action to protect its copyright in the materials.
8. Publisher reserves all rights not specifically granted in the combination of (i) the license details provided by you and accepted in the course of this licensing transaction, (ii) these terms and conditions and (iii) CCC's Billing and Payment terms and conditions.
9. Publisher makes no representations or warranties with respect to the licensed material.
10. You hereby indemnify and agree to hold harmless publisher and CCC, and their respective officers, directors, employees and agents, from and against any and all claims arising out of your use of the licensed material other than as specifically authorized pursuant to this license.
11. This license may not be amended except in a writing signed by both parties (or, in the

case of publisher, by CCC on publisher's behalf).

Questions? customer care@copyright.com or +1-855-239-3415 (toll free in the US) or +1-978-646-2777.

**ROYAL SOCIETY OF CHEMISTRY LICENSE
TERMS AND CONDITIONS**

Oct 23, 2015

This is a License Agreement between Eric Cunningham ("You") and Royal Society of Chemistry ("Royal Society of Chemistry") provided by Copyright Clearance Center ("CCC"). The license consists of your order details, the terms and conditions provided by Royal Society of Chemistry, and the payment terms and conditions.

All payments must be made in full to CCC. For payment instructions, please see information listed at the bottom of this form.

License Number	3735070949626
License date	Oct 23, 2015
Licensed content publisher	Royal Society of Chemistry
Licensed content publication	Discussions of the Faraday Society
Licensed content title	Studies of free radical reactivity by the methods of flash photolysis. The photochemical reaction between chlorine and oxygen
Licensed content author	George Porter, Franklin J. Wright
Licensed content date	Dec 31, 1969
Volume number	14
Issue number	0
Type of Use	Thesis/Dissertation
Requestor type	academic/educational
Portion	figures/tables/images
Number of figures/tables/images	1
Format	print and electronic
Distribution quantity	10
Will you be translating?	no
Order reference number	None
Title of the thesis/dissertation	Towards High-Flux Isolated Attosecond Pulses with a 200 TW CPA
Expected completion date	Nov 2015
Estimated size	150
Total	0.00 USD

Terms and Conditions

This License Agreement is between {Requestor Name} ("You") and The Royal Society of Chemistry ("RSC") provided by the Copyright Clearance Center ("CCC"). The license consists of your order details, the terms and conditions provided by the Royal Society of Chemistry, and the payment terms and conditions.

RSC / TERMS AND CONDITIONS

INTRODUCTION

The publisher for this copyrighted material is The Royal Society of Chemistry. By clicking “accept” in connection with completing this licensing transaction, you agree that the following terms and conditions apply to this transaction (along with the Billing and Payment terms and conditions established by CCC, at the time that you opened your RightsLink account and that are available at any time at .

LICENSE GRANTED

The RSC hereby grants you a non-exclusive license to use the aforementioned material anywhere in the world subject to the terms and conditions indicated herein. Reproduction of the material is confined to the purpose and/or media for which permission is hereby given.

RESERVATION OF RIGHTS

The RSC reserves all rights not specifically granted in the combination of (i) the license details provided by your and accepted in the course of this licensing transaction; (ii) these terms and conditions; and (iii) CCC’s Billing and Payment terms and conditions.

REVOCAATION

The RSC reserves the right to revoke this license for any reason, including, but not limited to, advertising and promotional uses of RSC content, third party usage, and incorrect source figure attribution.

THIRD-PARTY MATERIAL DISCLAIMER

If part of the material to be used (for example, a figure) has appeared in the RSC publication with credit to another source, permission must also be sought from that source. If the other source is another RSC publication these details should be included in your RightsLink request. If the other source is a third party, permission must be obtained from the third party. The RSC disclaims any responsibility for the reproduction you make of items owned by a third party.

PAYMENT OF FEE

If the permission fee for the requested material is waived in this instance, please be advised that any future requests for the reproduction of RSC materials may attract a fee.

ACKNOWLEDGEMENT

The reproduction of the licensed material must be accompanied by the following acknowledgement:

Reproduced (“Adapted” or “in part”) from {Reference Citation} (or Ref XX) with permission of The Royal Society of Chemistry.

If the licensed material is being reproduced from New Journal of Chemistry (NJC), Photochemical & Photobiological Sciences (PPS) or Physical Chemistry Chemical Physics (PCCP) you must include one of the following acknowledgements:

For figures originally published in NJC:

Reproduced (“Adapted” or “in part”) from {Reference Citation} (or Ref XX) with permission of The Royal Society of Chemistry (RSC) on behalf of the European Society for Photobiology, the European Photochemistry Association and the RSC.

For figures originally published in PPS:

Reproduced (“Adapted” or “in part”) from {Reference Citation} (or Ref XX) with permission of The Royal Society of Chemistry (RSC) on behalf of the Centre National de la Recherche Scientifique (CNRS) and the RSC.

For figures originally published in PCCP:

Reproduced (“Adapted” or “in part”) from {Reference Citation} (or Ref XX) with permission of the PCCP Owner Societies.

HYPertext LINKS

With any material which is being reproduced in electronic form, you must include a hypertext link to the original RSC article on the RSC’s website. The recommended form for the hyperlink is <http://dx.doi.org/10.1039/DOI suffix>, for example in the link

<http://dx.doi.org/10.1039/b110420a> the DOI suffix is 'b110420a'. To find the relevant DOI suffix for the RSC article in question, go to the Journals section of the website and locate the article in the list of papers for the volume and issue of your specific journal. You will find the DOI suffix quoted there.

LICENSE CONTINGENT ON PAYMENT

While you may exercise the rights licensed immediately upon issuance of the license at the end of the licensing process for the transaction, provided that you have disclosed complete and accurate details of your proposed use, no license is finally effective unless and until full payment is received from you (by CCC) as provided in CCC's Billing and Payment terms and conditions. If full payment is not received on a timely basis, then any license preliminarily granted shall be deemed automatically revoked and shall be void as if never granted. Further, in the event that you breach any of these terms and conditions or any of CCC's Billing and Payment terms and conditions, the license is automatically revoked and shall be void as if never granted. Use of materials as described in a revoked license, as well as any use of the materials beyond the scope of an unrevoked license, may constitute copyright infringement and the RSC reserves the right to take any and all action to protect its copyright in the materials.

WARRANTIES

The RSC makes no representations or warranties with respect to the licensed material.

INDEMNITY

You hereby indemnify and agree to hold harmless the RSC and the CCC, and their respective officers, directors, trustees, employees and agents, from and against any and all claims arising out of your use of the licensed material other than as specifically authorized pursuant to this licence.

NO TRANSFER OF LICENSE

This license is personal to you or your publisher and may not be sublicensed, assigned, or transferred by you to any other person without the RSC's written permission.

NO AMENDMENT EXCEPT IN WRITING

This license may not be amended except in a writing signed by both parties (or, in the case of "Other Conditions, v1.2", by CCC on the RSC's behalf).

OBJECTION TO CONTRARY TERMS

You hereby acknowledge and agree that these terms and conditions, together with CCC's Billing and Payment terms and conditions (which are incorporated herein), comprise the entire agreement between you and the RSC (and CCC) concerning this licensing transaction, to the exclusion of all other terms and conditions, written or verbal, express or implied (including any terms contained in any purchase order, acknowledgment, check endorsement or other writing prepared by you). In the event of any conflict between your obligations established by these terms and conditions and those established by CCC's Billing and Payment terms and conditions, these terms and conditions shall control.

JURISDICTION

This license transaction shall be governed by and construed in accordance with the laws of the District of Columbia. You hereby agree to submit to the jurisdiction of the courts located in the District of Columbia for purposes of resolving any disputes that may arise in connection with this licensing transaction.

LIMITED LICENSE

The following terms and conditions apply to specific license types:

Translation

This permission is granted for non-exclusive world English rights only unless your license was granted for translation rights. If you licensed translation rights you may only translate this content into the languages you requested. A professional translator must perform all

translations and reproduce the content word for word preserving the integrity of the article.

Intranet

If the licensed material is being posted on an Intranet, the Intranet is to be password-protected and made available only to bona fide students or employees only. All content posted to the Intranet must maintain the copyright information line on the bottom of each image. You must also fully reference the material and include a hypertext link as specified above.

Copies of Whole Articles

All copies of whole articles must maintain, if available, the copyright information line on the bottom of each page.

Other Conditions

v1.2

Gratis licenses (referencing \$0 in the Total field) are free. Please retain this printable license for your reference. No payment is required.

If you would like to pay for this license now, please remit this license along with your payment made payable to "COPYRIGHT CLEARANCE CENTER" otherwise you will be invoiced within 48 hours of the license date. Payment should be in the form of a check or money order referencing your account number and this invoice number {Invoice Number}.

Once you receive your invoice for this order, you may pay your invoice by credit card.

Please follow instructions provided at that time.

Make Payment To:

Copyright Clearance Center

Dept 001

P.O. Box 843006

Boston, MA 02284-3006

For suggestions or comments regarding this order, contact Rightslink Customer Support: customercare@copyright.com or +1-855-239-3415 (toll free in the US) or +1-978-646-2777.

Questions? customercare@copyright.com or +1-855-239-3415 (toll free in the US) or +1-978-646-2777.

American Physical Society License Details

Oct 23, 2015

This is an Agreement between Eric Cunningham ("You") and American Physical Society ("Publisher"). It consists of your order details, the terms and conditions provided by American Physical Society, and the payment instructions.

License Number	3735081079173
License date	Oct 23, 2015
Licensed content publisher	American Physical Society
Licensed content publication	Physical Review Letters
Licensed content title	Optical and Microwave-Optical Experiments in Ruby
Licensed copyright line	Copyright © 1960, American Physical Society
Licensed content author	T. H. Maiman
Licensed content date	Jun 1, 1960
Volume number	4
Type of Use	Thesis/Dissertation
Requestor type	Student
Format	Print, Electronic
Portion	image/photo
Number of images/photos requested	1
Portion description	Fig. 1
Rights for	Main product
Duration of use	Life of current edition
Creation of copies for the disabled	no
With minor editing privileges	no
For distribution to	United States
In the following language(s)	Original language of publication
With incidental promotional use	no
The lifetime unit quantity of new product	0 to 499
The requesting person/organization is:	Eric Cunningham
Order reference number	None
Title of your thesis / dissertation	Towards High-Flux Isolated Attosecond Pulses with a 200 TW CPA
Expected completion date	Nov 2015
Expected size (number of pages)	150

Total 0.00 USD

[Terms and Conditions](#)

Terms and Conditions

The American Physical Society (APS) is pleased to grant the Requestor of this license a non-exclusive, non-transferable permission, limited to [**print** and/or **electronic** format, depending on what they chose], provided all criteria outlined below are followed.

1. For electronic format permissions, Requestor agrees to provide a hyperlink from the reprinted APS material using the source material's DOI on the web page where the work appears. The hyperlink should use the standard DOI resolution URL, <http://dx.doi.org/{DOI}>. The hyperlink may be embedded in the copyright credit line.
2. For print format permissions, Requestor agrees to print the required copyright credit line on the first page where the material appears: "Reprinted (abstract/excerpt/figure) with permission from [(FULL REFERENCE CITATION) as follows: Author's Names, APS Journal Title, Volume Number, Page Number and Year of Publication.] Copyright (YEAR) by the American Physical Society."
3. Permission granted in this license is for a one-time use and does not include permission for any future editions, updates, databases, formats or other matters. Permission must be sought for any additional use.
4. Use of the material does not and must not imply any endorsement by APS.
5. Under no circumstance does APS purport or intend to grant permission to reuse materials to which it does not hold copyright. It is the requestors sole responsibility to ensure the licensed material is original to APS and does not contain the copyright of another entity, and that the copyright notice of the figure, photograph, cover or table does not indicate that it was reprinted by APS, with permission from another source.
6. The permission granted herein is personal to the Requestor for the use specified and is not transferable or assignable without express written permission of APS. This license may not be amended except in writing by APS.
7. You may not alter, edit or modify the material in any manner.
8. You may translate the materials only when translation rights have been granted.
9. You may not use the material for promotional, sales, advertising or marketing purposes.
10. The foregoing license shall not take effect unless and until APS or its agent, Copyright Clearance Center (CCC), receives payment in full in accordance with CCC Billing and Payment Terms and Conditions, which are incorporated herein by reference.
11. Should the terms of this license be violated at any time, APS or CCC may revoke the license with no refund to you and seek relief to the fullest extent of the laws of the USA. Official written notice will be made using the contact information provided with the permission request. Failure to receive such notice will not nullify revocation of the permission.
12. APS reserves all rights not specifically granted herein.
13. This document, including the CCC Billing and Payment Terms and Conditions, shall be the entire agreement between the parties relating to the subject matter hereof.

Other Terms and Conditions

Questions? customer@copyright.com or +1-855-239-3415 (toll free in the US) or +1-978-646-2777.

American Physical Society License Details

Oct 23, 2015

This is an Agreement between Eric Cunningham ("You") and American Physical Society ("Publisher"). It consists of your order details, the terms and conditions provided by American Physical Society, and the payment instructions.

License Number	3735090570440
License date	Oct 23, 2015
Licensed content publisher	American Physical Society
Licensed content publication	Physical Review (1893-1969)
Licensed content title	Stimulated Optical Emission in Fluorescent Solids. II. Spectroscopy and Stimulated Emission in Ruby
Licensed copyright line	Copyright © 1961, American Physical Society
Licensed content author	T. H. Maiman et al.
Licensed content date	Aug 15, 1961
Volume number	123
Type of Use	Thesis/Dissertation
Requestor type	Student
Format	Print, Electronic
Portion	image/photo
Number of images/photos requested	1
Portion description	Fig. 7
Rights for	Main product
Duration of use	Life of current edition
Creation of copies for the disabled	no
With minor editing privileges	no
For distribution to	United States
In the following language(s)	Original language of publication
With incidental promotional use	no
The lifetime unit quantity of new product	0 to 499
The requesting person/organization is:	Eric Cunningham
Order reference number	None
Title of your thesis / dissertation	Towards High-Flux Isolated Attosecond Pulses with a 200 TW CPA
Expected completion date	Nov 2015
Expected size (number of	150

pages)

Total 0.00 USD

[Terms and Conditions](#)

Terms and Conditions

The American Physical Society (APS) is pleased to grant the Requestor of this license a non-exclusive, non-transferable permission, limited to [**print** and/or **electronic** format, depending on what they chose], provided all criteria outlined below are followed.

1. For electronic format permissions, Requestor agrees to provide a hyperlink from the reprinted APS material using the source material's DOI on the web page where the work appears. The hyperlink should use the standard DOI resolution URL, <http://dx.doi.org/{DOI}>. The hyperlink may be embedded in the copyright credit line.
2. For print format permissions, Requestor agrees to print the required copyright credit line on the first page where the material appears: "Reprinted (abstract/excerpt/figure) with permission from [(FULL REFERENCE CITATION) as follows: Author's Names, APS Journal Title, Volume Number, Page Number and Year of Publication.] Copyright (YEAR) by the American Physical Society."
3. Permission granted in this license is for a one-time use and does not include permission for any future editions, updates, databases, formats or other matters. Permission must be sought for any additional use.
4. Use of the material does not and must not imply any endorsement by APS.
5. Under no circumstance does APS purport or intend to grant permission to reuse materials to which it does not hold copyright. It is the requestors sole responsibility to ensure the licensed material is original to APS and does not contain the copyright of another entity, and that the copyright notice of the figure, photograph, cover or table does not indicate that it was reprinted by APS, with permission from another source.
6. The permission granted herein is personal to the Requestor for the use specified and is not transferable or assignable without express written permission of APS. This license may not be amended except in writing by APS.
7. You may not alter, edit or modify the material in any manner.
8. You may translate the materials only when translation rights have been granted.
9. You may not use the material for promotional, sales, advertising or marketing purposes.
10. The foregoing license shall not take effect unless and until APS or its agent, Copyright Clearance Center (CCC), receives payment in full in accordance with CCC Billing and Payment Terms and Conditions, which are incorporated herein by reference.
11. Should the terms of this license be violated at any time, APS or CCC may revoke the license with no refund to you and seek relief to the fullest extent of the laws of the USA. Official written notice will be made using the contact information provided with the permission request. Failure to receive such notice will not nullify revocation of the permission.
12. APS reserves all rights not specifically granted herein.
13. This document, including the CCC Billing and Payment Terms and Conditions, shall be the entire agreement between the parties relating to the subject matter hereof.

Other Terms and Conditions

Questions? customer@copyright.com or +1-855-239-3415 (toll free in the US) or +1-978-646-2777.



RightsLink®

[Home](#)[Account Info](#)[Help](#)

Title: Sub-cycle Oscillations in Virtual States Brought to Light

Author: Michael Chini, Xiaowei Wang, Yan Cheng, Yi Wu, Di Zhao et al.

Publication: Scientific Reports

Publisher: Nature Publishing Group

Date: Jan 22, 2013

Logged in as:
Eric Cunningham
Account #:
3000968473

[LOGOUT](#)

Copyright © 2013, Rights Managed by Nature Publishing Group

Creative Commons

The request you have made is considered to be non-commercial/educational. As the article you have requested has been distributed under a Creative Commons license (Attribution-Noncommercial), you may reuse this material for non-commercial/educational purposes without obtaining additional permission from Nature Publishing Group, providing that the author and the original source of publication are fully acknowledged (please see the article itself for the license version number). You may reuse this material without obtaining permission from Nature Publishing Group, providing that the author and the original source of publication are fully acknowledged, as per the terms of the license. For license terms, please see <http://creativecommons.org/>

[BACK](#)[CLOSE WINDOW](#)

Copyright © 2015 [Copyright Clearance Center, Inc.](#) All Rights Reserved. [Privacy statement](#). [Terms and Conditions](#).
Comments? We would like to hear from you. E-mail us at customer@copyright.com



RightsLink®

[Account Info](#)
[Help](#)


Title: Compression of amplified chirped optical pulses
Author: Donna Strickland, Gerard Mourou
Publication: Optics Communications
Publisher: Elsevier
Date: Dec 1, 1985
 Copyright © 1985, Elsevier

Logged in as:
 Eric Cunningham
 Account #:
 3000968473

[LOGOUT](#)

Order Completed

Thank you for your order.

This Agreement between Eric Cunningham ("You") and Elsevier ("Elsevier") consists of your order details and the terms and conditions provided by Elsevier and Copyright Clearance Center.

License number	Reference confirmation email for license number
License date	Oct 23, 2015
Licensed content publisher	Elsevier
Licensed content publication	Optics Communications
Licensed content title	Compression of amplified chirped optical pulses
Licensed content author	Donna Strickland, Gerard Mourou
Licensed content date	1 December 1985
Licensed content volume number	56
Licensed content issue number	3
Number of pages	3
Type of Use	reuse in a thesis/dissertation
Portion	figures/tables/illustrations
Number of figures/tables/illustrations	1
Format	both print and electronic
Are you the author of this Elsevier article?	No
Will you be translating?	No
Original figure numbers	Fig. 1
Title of your thesis/dissertation	Towards High-Flux Isolated Attosecond Pulses with a 200 TW CPA
Expected completion date	Nov 2015
Elsevier VAT number	GB 494 6272 12
Billing Type	Invoice
Billing address	Eric Cunningham University of Central Florida 4111 Libra Dr. PS-430 ORLANDO, FL 32816 United States Attn: Eric Cunningham
Permissions price	0.00 USD
VAT/Local Sales Tax	0.00 USD / 0.00 GBP
Total	0.00 USD

[CLOSE WINDOW](#)

10/27/2015

Rightslink® by Copyright Clearance Center

Copyright © 2015 [Copyright Clearance Center, Inc.](#) All Rights Reserved. [Privacy statement.](#) [Terms and Conditions.](#)
Comments? We would like to hear from you. E-mail us at customercare@copyright.com

efc

From: pubscopyright <copyright@osa.org>
Sent: Tuesday, October 27, 2015 1:06 PM
To: efc
Subject: RE: Permission request to reuse figures in PhD dissertation

Dear Mr. Cunningham,

Thank you for contacting The Optical Society.

OSA considers your requested use of its copyrighted material to be Fair Use under United States Copyright Law. It is requested that a complete citation of the original material be included in any publication.

Let me know if you have any questions.

Kind Regards,

Susannah Lehman

Susannah Lehman
October 27, 2015
Authorized Agent, The Optical Society

From: efc [mailto:efc@knights.ucf.edu]
Sent: Saturday, October 24, 2015 10:44 AM
To: pubscopyright
Subject: Permission request to reuse figures in PhD dissertation

To whom it may concern:

I am writing a dissertation in partial fulfillment of the requirements of the Optics PhD program at the University of Central Florida. The title of this dissertation is "Towards High-Flux Isolated Attosecond Pulses with a 200 TW CPA". The intended distribution of this dissertation is <10 printed copies in addition to electronic archival by the university's ETD system.

I seek your permission to reuse in my dissertation the indicated selections of the following OSA-copyrighted publications of which I am *not* co-author:

Figure 2 from 10.1364/JOSAB.14.000661:

S. Kane and J. Squier, "Grism-pair stretcher-compressor system for simultaneous second- and third-order dispersion compensation in chirped-pulse amplification," J. Opt. Soc. Am. B14, 661-665 (1997).

Figure 1 from 10.1364/OL.17.000742:

I. P. Christov, "Amplification of femtosecond pulses in a spatially dispersive scheme," Opt. Lett. 17, 742-744 (1992).

Figure 1 from 10.1364/OL.29.000201:

C. P. Hauri, M. Bruck, W. Kornelis, J. Biegert, and U. Keller, "Generation of 14.8-fs pulses in a spatially dispersed amplifier," Opt. Lett. 29, 201-203 (2004).

Figure 1 from 10.1364/OL.10.000609:

J. P. Heritage, A. M. Weiner, and R. N. Thurston, "Picosecond pulse shaping by spectral phase and amplitude manipulation," Opt. Lett. 10, 609-611 (1985)

Figure 1 from 10.1364/OL.15.000326:

A. M. Weiner, D. E. Leaird, J. S. Patel, and J. R. Wullert, "Programmable femtosecond pulse shaping by use of a multielement liquid-crystal phase modulator," Opt. Lett. 15, 326-328 (1990)

Figure 1 from 10.1364/OL.23.000709:

C. Dorrer, F. Salin, F. Verluise, and J. P. Huignard, "Programmable phase control of femtosecond pulses by use of a nonpixelated spatial light modulator," Opt. Lett. 23, 709-711 (1998).

Figure 1b from 10.1364/OL.19.000737:

C. W. Hillegas, J. X. Tull, D. Goswami, D. Strickland, and W. S. Warren, "Femtosecond laser pulse shaping by use of microsecond radio-frequency pulses," Opt. Lett. 19, 737-739 (1994).

Figure 1 (boxed portion) from 10.1364/OL.24.000493:

Erik Zeek, Kira Maginnis, Sterling Backus, Ulrich Russek, Margaret Murnane, Gérard Mourou, Henry Kapteyn, and Gleb Vdovin, "Pulse compression by use of deformable mirrors," Opt. Lett. 24, 493-495 (1999).

Figure 1 from 10.1364/OL.35.003102:

Stefan M. Weber, Jérôme Extermann, Luigi Bonacina, Wilfried Noell, Denis Kiselev, Severin Waldis, Nico F. de Rooij, and Jean-Pierre Wolf, "Ultraviolet and near-infrared femtosecond temporal pulse shaping with a new high-aspect-ratio one-dimensional micromirror array," Opt. Lett. 35, 3102-3104 (2010).

Figure 1 from 10.1364/OL.21.000219:

C. P. J. Barty, G. Korn, F. Raksi, A.-C. Tien, K. R. Wilson, V. V. Yakovlev, C. Rose-Petrucci, J. Squier, and K. Yamakawa, "Regenerative pulse shaping and amplification of ultrabroadband optical pulses," Opt. Lett. 21, 219-221 (1996).

Figure 1 from:

L. Canova, O. Albert, R. Lopez-Martens, P. Giacomini, and P. Paul, "Ultrashort Pulses Generation with the Mazzler Active Spectral Broadening and the XPW Pulse Shortening Technique," in *Conference on Lasers and Electro-Optics/Quantum Electronics and Laser Science Conference and Photonic Applications Systems Technologies*, OSA Technical Digest (CD) (Optical Society of America, 2008), paper JTUA39.

The requested permission extends to any future revisions and editions of the dissertation, including non-exclusive world rights in all languages. These rights will in no way restrict republication of the material in any other form by you or by others authorized by you. Your signing of this letter will also confirm that you or your company owns the copyright to the above-described material.

If the indicated conditions are acceptable, please respond with your approval of the enclosed request by email to efc@knights.ucf.edu. Should you require additional information or clarification, I would be happy to comply.

Thank you for your time and attention,
~Eric Cunningham
University of Central Florida
efc@knights.ucf.edu

SPRINGER LICENSE TERMS AND CONDITIONS

Oct 24, 2015

This is a License Agreement between Eric Cunningham ("You") and Springer ("Springer") provided by Copyright Clearance Center ("CCC"). The license consists of your order details, the terms and conditions provided by Springer, and the payment terms and conditions.

All payments must be made in full to CCC. For payment instructions, please see information listed at the bottom of this form.

License Number	3735140798536
License date	Oct 24, 2015
Licensed content publisher	Springer
Licensed content publication	Applied Physics B: Lasers and Optics
Licensed content title	Ultrabroadband laser using prism-based "spatially-dispersive" resonator
Licensed content author	M. B. Danailov
Licensed content date	Jan 1, 1990
Volume number	51
Issue number	4
Type of Use	Thesis/Dissertation
Portion	Figures/tables/illustrations
Number of figures/tables/illustrations	1
Author of this Springer article	No
Order reference number	None
Original figure numbers	Fig. 1b
Title of your thesis / dissertation	Towards High-Flux Isolated Attosecond Pulses with a 200 TW CPA
Expected completion date	Nov 2015
Estimated size(pages)	150
Total	0.00 USD

Terms and Conditions

Introduction

The publisher for this copyrighted material is Springer Science + Business Media. By clicking "accept" in connection with completing this licensing transaction, you agree that the following terms and conditions apply to this transaction (along with the Billing and Payment terms and conditions established by Copyright Clearance Center, Inc. ("CCC"), at the time that you opened your Rightslink account and that are available at any time at <http://myaccount.copyright.com>).

Limited License

With reference to your request to reprint in your thesis material on which Springer Science

and Business Media control the copyright, permission is granted, free of charge, for the use indicated in your enquiry.

Licenses are for one-time use only with a maximum distribution equal to the number that you identified in the licensing process.

This License includes use in an electronic form, provided its password protected or on the university's intranet or repository, including UMI (according to the definition at the Sherpa website: <http://www.sherpa.ac.uk/romeo/>). For any other electronic use, please contact Springer at (permissions.dordrecht@springer.com or permissions.heidelberg@springer.com).

The material can only be used for the purpose of defending your thesis limited to university-use only. If the thesis is going to be published, permission needs to be re-obtained (selecting "book/textbook" as the type of use).

Although Springer holds copyright to the material and is entitled to negotiate on rights, this license is only valid, subject to a courtesy information to the author (address is given with the article/chapter) and provided it concerns original material which does not carry references to other sources (if material in question appears with credit to another source, authorization from that source is required as well).

Permission free of charge on this occasion does not prejudice any rights we might have to charge for reproduction of our copyrighted material in the future.

Altering/Modifying Material: Not Permitted

You may not alter or modify the material in any manner. Abbreviations, additions, deletions and/or any other alterations shall be made only with prior written authorization of the author(s) and/or Springer Science + Business Media. (Please contact Springer at (permissions.dordrecht@springer.com or permissions.heidelberg@springer.com))

Reservation of Rights

Springer Science + Business Media reserves all rights not specifically granted in the combination of (i) the license details provided by you and accepted in the course of this licensing transaction, (ii) these terms and conditions and (iii) CCC's Billing and Payment terms and conditions.

Copyright Notice:Disclaimer

You must include the following copyright and permission notice in connection with any reproduction of the licensed material: "Springer and the original publisher /journal title, volume, year of publication, page, chapter/article title, name(s) of author(s), figure number(s), original copyright notice) is given to the publication in which the material was originally published, by adding; with kind permission from Springer Science and Business Media"

Warranties: None

Example 1: Springer Science + Business Media makes no representations or warranties with respect to the licensed material.

Example 2: Springer Science + Business Media makes no representations or warranties with respect to the licensed material and adopts on its own behalf the limitations and disclaimers established by CCC on its behalf in its Billing and Payment terms and conditions for this licensing transaction.

Indemnity

You hereby indemnify and agree to hold harmless Springer Science + Business Media and CCC, and their respective officers, directors, employees and agents, from and against any and all claims arising out of your use of the licensed material other than as specifically authorized pursuant to this license.

No Transfer of License

This license is personal to you and may not be sublicensed, assigned, or transferred by you

to any other person without Springer Science + Business Media's written permission.

No Amendment Except in Writing

This license may not be amended except in a writing signed by both parties (or, in the case of Springer Science + Business Media, by CCC on Springer Science + Business Media's behalf).

Objection to Contrary Terms

Springer Science + Business Media hereby objects to any terms contained in any purchase order, acknowledgment, check endorsement or other writing prepared by you, which terms are inconsistent with these terms and conditions or CCC's Billing and Payment terms and conditions. These terms and conditions, together with CCC's Billing and Payment terms and conditions (which are incorporated herein), comprise the entire agreement between you and Springer Science + Business Media (and CCC) concerning this licensing transaction. In the event of any conflict between your obligations established by these terms and conditions and those established by CCC's Billing and Payment terms and conditions, these terms and conditions shall control.

Jurisdiction

All disputes that may arise in connection with this present License, or the breach thereof, shall be settled exclusively by arbitration, to be held in The Netherlands, in accordance with Dutch law, and to be conducted under the Rules of the 'Netherlands Arbitrage Instituut' (Netherlands Institute of Arbitration). **OR:**

All disputes that may arise in connection with this present License, or the breach thereof, shall be settled exclusively by arbitration, to be held in the Federal Republic of Germany, in accordance with German law.

Other terms and conditions:

v1.3

Questions? customercare@copyright.com or +1-855-239-3415 (toll free in the US) or +1-978-646-2777.



RightsLink®

[Account Info](#)
[Help](#)


Title: A spatially dispersive regenerative amplifier for ultrabroadband pulses

Author: Jérôme Faure, Jiro Itatani, Subrat Biswal, Gilles Chériaux, Leah R Bruner, Glen C Templeton, Gérard Mourou

Publication: Optics Communications

Publisher: Elsevier

Date: Jan 1, 1999

Copyright © 1999, Elsevier

Logged in as:
Eric Cunningham
Account #:
3000968473

[LOGOUT](#)

Order Completed

Thank you for your order.

This Agreement between Eric Cunningham ("You") and Elsevier ("Elsevier") consists of your order details and the terms and conditions provided by Elsevier and Copyright Clearance Center.

License number	Reference confirmation email for license number
License date	Oct 24, 2015
Licensed content publisher	Elsevier
Licensed content publication	Optics Communications
Licensed content title	A spatially dispersive regenerative amplifier for ultrabroadband pulses
Licensed content author	Jérôme Faure, Jiro Itatani, Subrat Biswal, Gilles Chériaux, Leah R Bruner, Glen C Templeton, Gérard Mourou
Licensed content date	1 January 1999
Licensed content volume number	159
Licensed content issue number	1-3
Number of pages	6
Type of Use	reuse in a thesis/dissertation
Portion	figures/tables/illustrations
Number of figures/tables/illustrations	1
Format	both print and electronic
Are you the author of this Elsevier article?	No
Will you be translating?	No
Original figure numbers	Fig. 3
Title of your thesis/dissertation	Towards High-Flux Isolated Attosecond Pulses with a 200 TW CPA
Expected completion date	Nov 2015
Elsevier VAT number	GB 494 6272 12
Billing Type	Invoice
Billing address	Eric Cunningham University of Central Florida 4111 Libra Dr. PS-430 ORLANDO, FL 32816 United States Attn: Eric Cunningham
Permissions price	0.00 USD
VAT/Local Sales Tax	0.00 USD / 0.00 GBP

10/27/2015

Rightslink® by Copyright Clearance Center

Total

0.00 USD

CLOSE WINDOW

Copyright © 2015 [Copyright Clearance Center, Inc.](#) All Rights Reserved. [Privacy statement.](#) [Terms and Conditions.](#)
Comments? We would like to hear from you. E-mail us at customercare@copyright.com

SPRINGER LICENSE TERMS AND CONDITIONS

Oct 24, 2015

This is a License Agreement between Eric Cunningham ("You") and Springer ("Springer") provided by Copyright Clearance Center ("CCC"). The license consists of your order details, the terms and conditions provided by Springer, and the payment terms and conditions.

All payments must be made in full to CCC. For payment instructions, please see information listed at the bottom of this form.

License Number	3735150877160
License date	Oct 24, 2015
Licensed content publisher	Springer
Licensed content publication	Applied Physics B: Lasers and Optics
Licensed content title	Suppression of gain narrowing in multi-TW lasers with negatively and positively chirped pulse amplification
Licensed content author	M.P. Kalashnikov
Licensed content date	Jan 1, 2005
Volume number	81
Issue number	8
Type of Use	Thesis/Dissertation
Portion	Figures/tables/illustrations
Number of figures/tables/illustrations	1
Author of this Springer article	No
Order reference number	None
Original figure numbers	Fig. 1
Title of your thesis / dissertation	Towards High-Flux Isolated Attosecond Pulses with a 200 TW CPA
Expected completion date	Nov 2015
Estimated size(pages)	150
Total	0.00 USD

Terms and Conditions

Introduction

The publisher for this copyrighted material is Springer Science + Business Media. By clicking "accept" in connection with completing this licensing transaction, you agree that the following terms and conditions apply to this transaction (along with the Billing and Payment terms and conditions established by Copyright Clearance Center, Inc. ("CCC"), at the time that you opened your Rightslink account and that are available at any time at <http://myaccount.copyright.com>).

Limited License

With reference to your request to reprint in your thesis material on which Springer Science

and Business Media control the copyright, permission is granted, free of charge, for the use indicated in your enquiry.

Licenses are for one-time use only with a maximum distribution equal to the number that you identified in the licensing process.

This License includes use in an electronic form, provided its password protected or on the university's intranet or repository, including UMI (according to the definition at the Sherpa website: <http://www.sherpa.ac.uk/romeo/>). For any other electronic use, please contact Springer at (permissions.dordrecht@springer.com or permissions.heidelberg@springer.com).

The material can only be used for the purpose of defending your thesis limited to university-use only. If the thesis is going to be published, permission needs to be re-obtained (selecting "book/textbook" as the type of use).

Although Springer holds copyright to the material and is entitled to negotiate on rights, this license is only valid, subject to a courtesy information to the author (address is given with the article/chapter) and provided it concerns original material which does not carry references to other sources (if material in question appears with credit to another source, authorization from that source is required as well).

Permission free of charge on this occasion does not prejudice any rights we might have to charge for reproduction of our copyrighted material in the future.

Altering/Modifying Material: Not Permitted

You may not alter or modify the material in any manner. Abbreviations, additions, deletions and/or any other alterations shall be made only with prior written authorization of the author(s) and/or Springer Science + Business Media. (Please contact Springer at (permissions.dordrecht@springer.com or permissions.heidelberg@springer.com))

Reservation of Rights

Springer Science + Business Media reserves all rights not specifically granted in the combination of (i) the license details provided by you and accepted in the course of this licensing transaction, (ii) these terms and conditions and (iii) CCC's Billing and Payment terms and conditions.

Copyright Notice:Disclaimer

You must include the following copyright and permission notice in connection with any reproduction of the licensed material: "Springer and the original publisher /journal title, volume, year of publication, page, chapter/article title, name(s) of author(s), figure number(s), original copyright notice) is given to the publication in which the material was originally published, by adding; with kind permission from Springer Science and Business Media"

Warranties: None

Example 1: Springer Science + Business Media makes no representations or warranties with respect to the licensed material.

Example 2: Springer Science + Business Media makes no representations or warranties with respect to the licensed material and adopts on its own behalf the limitations and disclaimers established by CCC on its behalf in its Billing and Payment terms and conditions for this licensing transaction.

Indemnity

You hereby indemnify and agree to hold harmless Springer Science + Business Media and CCC, and their respective officers, directors, employees and agents, from and against any and all claims arising out of your use of the licensed material other than as specifically authorized pursuant to this license.

No Transfer of License

This license is personal to you and may not be sublicensed, assigned, or transferred by you

to any other person without Springer Science + Business Media's written permission.

No Amendment Except in Writing

This license may not be amended except in a writing signed by both parties (or, in the case of Springer Science + Business Media, by CCC on Springer Science + Business Media's behalf).

Objection to Contrary Terms

Springer Science + Business Media hereby objects to any terms contained in any purchase order, acknowledgment, check endorsement or other writing prepared by you, which terms are inconsistent with these terms and conditions or CCC's Billing and Payment terms and conditions. These terms and conditions, together with CCC's Billing and Payment terms and conditions (which are incorporated herein), comprise the entire agreement between you and Springer Science + Business Media (and CCC) concerning this licensing transaction. In the event of any conflict between your obligations established by these terms and conditions and those established by CCC's Billing and Payment terms and conditions, these terms and conditions shall control.

Jurisdiction

All disputes that may arise in connection with this present License, or the breach thereof, shall be settled exclusively by arbitration, to be held in The Netherlands, in accordance with Dutch law, and to be conducted under the Rules of the 'Netherlands Arbitrage Instituut' (Netherlands Institute of Arbitration). **OR:**

All disputes that may arise in connection with this present License, or the breach thereof, shall be settled exclusively by arbitration, to be held in the Federal Republic of Germany, in accordance with German law.

Other terms and conditions:

v1.3

Questions? customercare@copyright.com or +1-855-239-3415 (toll free in the US) or +1-978-646-2777.



RightsLink®

[Home](#)
[Account Info](#)
[Help](#)


Title: A femtosecond pulse-shaping apparatus containing microlens arrays for use with pixellated spatial light modulators

Author: Mahoney, K.M.; Weiner, A.M.

Publication: Quantum Electronics, IEEE Journal of

Publisher: IEEE

Date: Dec 1996

Copyright © 1996, IEEE

Logged in as:
Eric Cunningham
Account #:
3000968473

[LOGOUT](#)

Thesis / Dissertation Reuse

The IEEE does not require individuals working on a thesis to obtain a formal reuse license, however, you may print out this statement to be used as a permission grant:

Requirements to be followed when using any portion (e.g., figure, graph, table, or textual material) of an IEEE copyrighted paper in a thesis:

- 1) In the case of textual material (e.g., using short quotes or referring to the work within these papers) users must give full credit to the original source (author, paper, publication) followed by the IEEE copyright line © 2011 IEEE.
- 2) In the case of illustrations or tabular material, we require that the copyright line © [Year of original publication] IEEE appear prominently with each reprinted figure and/or table.
- 3) If a substantial portion of the original paper is to be used, and if you are not the senior author, also obtain the senior author's approval.

Requirements to be followed when using an entire IEEE copyrighted paper in a thesis:

- 1) The following IEEE copyright/ credit notice should be placed prominently in the references: © [year of original publication] IEEE. Reprinted, with permission, from [author names, paper title, IEEE publication title, and month/year of publication]
- 2) Only the accepted version of an IEEE copyrighted paper can be used when posting the paper or your thesis on-line.
- 3) In placing the thesis on the author's university website, please display the following message in a prominent place on the website: In reference to IEEE copyrighted material which is used with permission in this thesis, the IEEE does not endorse any of [university/educational entity's name goes here]'s products or services. Internal or personal use of this material is permitted. If interested in reprinting/republishing IEEE copyrighted material for advertising or promotional purposes or for creating new collective works for resale or redistribution, please go to http://www.ieee.org/publications_standards/publications/rights/rights_link.html to learn how to obtain a License from RightsLink.

If applicable, University Microfilms and/or ProQuest Library, or the Archives of Canada may supply single copies of the dissertation.

[BACK](#)
[CLOSE WINDOW](#)

Copyright © 2015 [Copyright Clearance Center, Inc.](#) All Rights Reserved. [Privacy statement](#). [Terms and Conditions](#). Comments? We would like to hear from you. E-mail us at customer@copyright.com

10/26/2015

Re: Rights Request - efc

>>

>> Please see the attached application to reproduce Figure 1 from [K. Ema and F. Shimizu, "Optical Pulse Shaping Using a Fourier-Transformed Hologram," Japanese Journal of Applied Physics 29, L631-L633 (1990).] in my PhD dissertation.

>>

>> Thank you for your time and consideration,

>> ~Eric Cunningham

>> Institute for the Frontier of Attosecond Science and Technology

>> University of Central Florida

>>

>

> --

> Michiya Takekawa (Dr.)

> Manager, Publishing Development The Japan Society of Applied Physics (JSAP)

> 2-31-22-5F, Yushima, Bunkyo-ku, Tokyo 113-0034, Japan

> Tel: +81-3-5844-3291 Fax: +81-3-5844-3290

> E-mail: takekawa@jsap.or.jp

(Notice)

If you are the one of the authors of the paper, you don't have to apply for a permission with the following conditions.

1. Follow the Copyright Policy of the Japan Society of Applied Physics
2. A credit line of "Copyright (published year) The Japan Society of Applied Physics" should be added to the end of the figure caption in the Content.
3. The Content must be cited as a reference in the Publication.

To: President of the Japan Society of Applied Physics

24 / 10 / 2015
Day Month Year

Submit to:

Publication Center for Pure and Applied Physics, The Japan Society of Applied Physics
2-31-22-5F, Yushima, Bunkyo-ku, Tokyo 113-0034, Japan
TEL: +81-3-5844-3291 FAX: +81-3-5844-3290 E-mail address: permission@jsap.or.jp

Application for Permission to Reproduce Material

I request permission to reproduce the following material, copyrighted by the Japan Society of Applied Physics.

Publication where material is reproduced (the Publication)

Name of the Publication (e.g., journal title, book title): Towards High-Flux Isolated Attosecond Pulses with a 200 TW CPA
Publisher (e.g., publishing company): none (PhD dissertation)
Planned date of publication: November 2015
Number of copies: 10

Content of reproduction (the Content)


Journal title: Japanese Journal of Applied Physics
Volume/Year/ID(starting page): 29 / 1990 / L631
Article title: Optical Pulse Shaping Using a Fourier-Transformed Hologram
Author(s): Kazuhiro Ema and Fujio Shimizu
Content to be reproduced (please specify): Figure 1

Applicant (only to be completed by the author of the Publication)

Name: Eric Cunningham
Affiliation (e.g., university, company, organization):
University of Central Florida
E-mail address: efc@knights.ucf.edu

I will abide by the following conditions of reproduction.

1. A credit line "Copyright *publication year* The Japan Society of Applied Physics" must be added to the Content (in the figure caption(s)). The material containing the Content, copyrighted by the Japan Society of Applied Physics, must be cited in the references of the Publication.
2. The Content will not be modified.
3. The Content will not be reproduced in other materials.

Signature of applicant: 

* The purpose of reproduction will be considered before permission is granted.

ENDORSEMENT

Dr. Eric Cunningham

I permit the reproduction of the Content in the Publication.

26 / Oct / 2015

Publication Center for Pure and Applied Physics, The Japan Society of Applied Physics
2-31-22-5F, Yushima, Bunkyo-ku, Tokyo 113-0034, Japan / TEL: +81-3-5844-3291 / FAX: +81-3-5844-3290 / E-mail address: permission@jsap.or.jp

Released March 2014

**AIP PUBLISHING LLC LICENSE
TERMS AND CONDITIONS**

Oct 23, 2015

All payments must be made in full to CCC. For payment instructions, please see information listed at the bottom of this form.

License Number	3734781171157
Order Date	Oct 23, 2015
Publisher	AIP Publishing LLC
Publication	Applied Physics Letters
Article Title	Generation of high-flux attosecond extreme ultraviolet continuum with a 10 TW laser
Author	Y. Wu,E. Cunningham,H. Zang, et al.
Online Publication Date	May 21, 2013
Volume number	102
Issue number	20
Type of Use	Thesis/Dissertation
Requestor type	Author (original article)
Format	Print and electronic
Portion	Figure/Table
Number of figures/tables	5
Title of your thesis / dissertation	Towards High-Flux Isolated Attosecond Pulses with a 200 TW CPA
Expected completion date	Nov 2015
Estimated size (number of pages)	150
Total	0.00 USD

Terms and Conditions

AIP Publishing LLC -- Terms and Conditions: Permissions Uses

AIP Publishing LLC ("AIPP") hereby grants to you the non-exclusive right and license to use and/or distribute the Material according to the use specified in your order, on a one-time basis, for the specified term, with a maximum distribution equal to the number that you have ordered. Any links or other content accompanying the Material are not the subject of this license.

1. You agree to include the following copyright and permission notice with the reproduction of the Material:"Reprinted with permission from [FULL CITATION]. Copyright [PUBLICATION YEAR], AIP Publishing LLC." For an article, the copyright and permission notice must be printed on the first page of the article or book chapter. For photographs, covers, or tables, the copyright and permission notice may appear with the Material, in a footnote, or in the reference list.
2. If you have licensed reuse of a figure, photograph, cover, or table, it is your responsibility to ensure that the material is original to AIPP and does not contain the copyright of another entity, and that the copyright notice of the figure, photograph, cover, or table does not indicate that it was reprinted by AIPP, with permission, from another source. Under no circumstances does AIPP, purport or intend to grant permission to reuse material to which it does not hold copyright.
3. You may not alter or modify the Material in any manner. You may translate the Material into another language only if you have licensed translation rights. You may not use the Material

- for promotional purposes. AIPP reserves all rights not specifically granted herein.
4. The foregoing license shall not take effect unless and until AIPP or its agent, Copyright Clearance Center, receives the Payment in accordance with Copyright Clearance Center Billing and Payment Terms and Conditions, which are incorporated herein by reference.
 5. AIPP or the Copyright Clearance Center may, within two business days of granting this license, revoke the license for any reason whatsoever, with a full refund payable to you. Should you violate the terms of this license at any time, AIPP, AIP Publishing LLC, or Copyright Clearance Center may revoke the license with no refund to you. Notice of such revocation will be made using the contact information provided by you. Failure to receive such notice will not nullify the revocation.
 6. AIPP makes no representations or warranties with respect to the Material. You agree to indemnify and hold harmless AIPP, AIP Publishing LLC, and their officers, directors, employees or agents from and against any and all claims arising out of your use of the Material other than as specifically authorized herein.
 7. The permission granted herein is personal to you and is not transferable or assignable without the prior written permission of AIPP. This license may not be amended except in a writing signed by the party to be charged.
 8. If purchase orders, acknowledgments or check endorsements are issued on any forms containing terms and conditions which are inconsistent with these provisions, such inconsistent terms and conditions shall be of no force and effect. This document, including the CCC Billing and Payment Terms and Conditions, shall be the entire agreement between the parties relating to the subject matter hereof.

This Agreement shall be governed by and construed in accordance with the laws of the State of New York. Both parties hereby submit to the jurisdiction of the courts of New York County for purposes of resolving any disputes that may arise hereunder.

Questions? customer@copyright.com or +1-855-239-3415 (toll free in the US) or +1-978-646-2777.

efc

From: Nicole Harris <nicoleh@spie.org>
Sent: Monday, October 26, 2015 11:41 AM
To: efc
Subject: RE: Request to reprint figure in PhD dissertation

Dear Mr. Cunningham,

Thank you for seeking permission from SPIE to reprint material from our publications. Publisher's permission is hereby granted under the following conditions:

- (1) you obtain permission of one of the authors;
 - (2) the material to be used has appeared in our publication without credit or acknowledgment to another source;
- and
- (3) you credit the original SPIE publication. Include the authors' names, title of paper, volume title, SPIE volume number, and year of publication in your credit statement.

Sincerely,

Nicole Harris
Administrative Editor, SPIE Publications
1000 20th St.
Bellingham, WA 98225
+1 360 685 5586 (office)
nicoleh@spie.org

SPIE is the international society for optics and photonics. <http://SPIE.org>



SPIE.

From: efc [mailto:efc@knights.ucf.edu]
Sent: Saturday, October 24, 2015 6:42 AM
To: reprint_permission <reprint_permission@spie.org>
Subject: Request to reprint figure in PhD dissertation

Title: Polarization gratings for non-mechanical beam steering applications.
Author: J. Buck ; S. Serati ; L. Hosting ; R. Serati ; H. Masterson ; M. Escuti ; J. Kim ; M. Miskiewicz;
Volume, issue, and page numbers: Proc. SPIE 8395, Acquisition, Tracking, Pointing, and Laser Systems Technologies XXVI, 83950F (June 8, 2012); doi:10.1117/12.921688.

I would like to reproduce Figure 3.

I would like to republish the requested material in my PhD dissertation.

Thank you for your time,
~Eric Cunningham
University of Central Florida
efc@knights.ucf.edu

efc

From: Chris Hoy <CHoy@bnonlinear.com>
Sent: Monday, October 26, 2015 6:34 PM
To: efc
Subject: RE: Figure re-use permission

Follow Up Flag: Follow up
Flag Status: Flagged

Hi Eric,

Of course, you have the authors' permission to include the figure in your dissertation. If you need to show permission, you can include something like "Courtesy of Boulder Nonlinear Systems". Best of luck with your dissertation!

Chris Hoy

Christopher L. Hoy, PhD
Research Scientist
Boulder Nonlinear Systems, Inc.
450 Courtney Way, Unit 107
Lafayette, CO 80026
303-604-0077
303-604-0066-Fax
choy@bnonlinear.com
www.bnonlinear.com

From: efc [mailto:efc@knights.ucf.edu]
Sent: Monday, October 26, 2015 12:04 PM
To: Info Recipients <info@bnonlinear.com>
Subject: Figure re-use permission

Hello –

I am writing a PhD dissertation ("Towards High-Flux Isolated Attosecond Pulses from a 200 TW CPA"), and I am including a section highlighting our BNS Model CP12288-700-900 LCoS-SLM used to compress our 100 TW-level beam.

To aid the reader, I would like to include in my dissertation, with appropriate crediting, the unaltered representation of Figure 3 from the publication "Polarization gratings for non-mechanical beam steering applications" appearing in Proc. SPIE 8395, Acquisition, Tracking, Pointing, and Laser Systems Technologies XXVI, 83950F (June 8, 2012) (doi:10.1117/12.921688).

According to SPIE policy for reuse of copyrighted materials, I must "obtain permission of one of the authors". For this publication, the list of authors is as follows: Dr. Joseph Buck, Mr. Steve Serati, Mr. Lance Hosting, Ms. RoyInn Serati, Mr. Hugh Masterson, Dr. Michael Escuti, Dr. Jihwan Kim, and Mr. Matthew Miskiewicz.

I understand that a number of these individuals are affiliated with Boulder Nonlinear Systems. Would it be possible to be put into contact with at least one of these individuals in order to seek her/his permission?

I appreciate your time and consideration in this regard.

Thank you,
~Eric Cunningham
Institute for the Frontier of Attosecond Science and Technology
University of Central Florida
efc@knights.ucf.edu

American Physical Society License Details

Oct 24, 2015

This is an Agreement between Eric Cunningham ("You") and American Physical Society ("Publisher"). It consists of your order details, the terms and conditions provided by American Physical Society, and the payment instructions.

License Number	3735190477588
License date	Oct 24, 2015
Licensed content publisher	American Physical Society
Licensed content publication	Physical Review Letters
Licensed content title	Isolated Attosecond Pulse Generation without the Need to Stabilize the Carrier-Envelope Phase of Driving Lasers
Licensed copyright line	© 2010 The American Physical Society
Licensed content author	Steve Gilbertson et al.
Licensed content date	Aug 24, 2010
Volume number	105
Type of Use	Thesis/Dissertation
Requestor type	Student
Format	Print, Electronic
Portion	image/photo
Number of images/photos requested	2
Portion description	Fig. 1a&b
Rights for	Main product
Duration of use	Life of current edition
Creation of copies for the disabled	no
With minor editing privileges	no
For distribution to	United States
In the following language(s)	Original language of publication
With incidental promotional use	no
The lifetime unit quantity of new product	0 to 499
The requesting person/organization is:	Eric Cunningham
Order reference number	None
Title of your thesis / dissertation	Towards High-Flux Isolated Attosecond Pulses with a 200 TW CPA
Expected completion date	Nov 2015
Expected size (number of	150

pages)

Total 0.00 USD

[Terms and Conditions](#)

Terms and Conditions

The American Physical Society (APS) is pleased to grant the Requestor of this license a non-exclusive, non-transferable permission, limited to [**print** and/or **electronic** format, depending on what they chose], provided all criteria outlined below are followed.

1. For electronic format permissions, Requestor agrees to provide a hyperlink from the reprinted APS material using the source material's DOI on the web page where the work appears. The hyperlink should use the standard DOI resolution URL, <http://dx.doi.org/{DOI}>. The hyperlink may be embedded in the copyright credit line.
2. For print format permissions, Requestor agrees to print the required copyright credit line on the first page where the material appears: "Reprinted (abstract/excerpt/figure) with permission from [(FULL REFERENCE CITATION) as follows: Author's Names, APS Journal Title, Volume Number, Page Number and Year of Publication.] Copyright (YEAR) by the American Physical Society."
3. Permission granted in this license is for a one-time use and does not include permission for any future editions, updates, databases, formats or other matters. Permission must be sought for any additional use.
4. Use of the material does not and must not imply any endorsement by APS.
5. Under no circumstance does APS purport or intend to grant permission to reuse materials to which it does not hold copyright. It is the requestors sole responsibility to ensure the licensed material is original to APS and does not contain the copyright of another entity, and that the copyright notice of the figure, photograph, cover or table does not indicate that it was reprinted by APS, with permission from another source.
6. The permission granted herein is personal to the Requestor for the use specified and is not transferable or assignable without express written permission of APS. This license may not be amended except in writing by APS.
7. You may not alter, edit or modify the material in any manner.
8. You may translate the materials only when translation rights have been granted.
9. You may not use the material for promotional, sales, advertising or marketing purposes.
10. The foregoing license shall not take effect unless and until APS or its agent, Copyright Clearance Center (CCC), receives payment in full in accordance with CCC Billing and Payment Terms and Conditions, which are incorporated herein by reference.
11. Should the terms of this license be violated at any time, APS or CCC may revoke the license with no refund to you and seek relief to the fullest extent of the laws of the USA. Official written notice will be made using the contact information provided with the permission request. Failure to receive such notice will not nullify revocation of the permission.
12. APS reserves all rights not specifically granted herein.
13. This document, including the CCC Billing and Payment Terms and Conditions, shall be the entire agreement between the parties relating to the subject matter hereof.

Other Terms and Conditions

Questions? customer@copyright.com or +1-855-239-3415 (toll free in the US) or +1-978-646-2777.

**JOHN WILEY AND SONS LICENSE
TERMS AND CONDITIONS**

Oct 24, 2015

This Agreement between Eric Cunningham ("You") and John Wiley and Sons ("John Wiley and Sons") consists of your license details and the terms and conditions provided by John Wiley and Sons and Copyright Clearance Center.

License Number	3735191335367
License date	Oct 24, 2015
Licensed Content Publisher	John Wiley and Sons
Licensed Content Publication	Laser & Photonics Reviews
Licensed Content Title	Advances in carrier-envelope phase stabilization of grating-based chirped-pulse amplifiers
Licensed Content Author	E. Moon,H. Wang,S. Gilbertson,H. Mashiko,M. Chini,Z. Chang
Licensed Content Date	Jun 17, 2009
Pages	18
Type of use	Dissertation/Thesis
Requestor type	University/Academic
Format	Print and electronic
Portion	Figure/table
Number of figures/tables	1
Original Wiley figure/table number(s)	Figure 5
Will you be translating?	No
Title of your thesis / dissertation	Towards High-Flux Isolated Attosecond Pulses with a 200 TW CPA
Expected completion date	Nov 2015
Expected size (number of pages)	150
Requestor Location	Eric Cunningham University of Central Florida 4111 Libra Dr. PS-430 ORLANDO, FL 32816 United States Attn: Eric Cunningham
Billing Type	Invoice
Billing Address	Eric Cunningham University of Central Florida 4111 Libra Dr. PS-430 ORLANDO, FL 32816 United States Attn: Eric Cunningham

Total 0.00 USD

[Terms and Conditions](#)

TERMS AND CONDITIONS

This copyrighted material is owned by or exclusively licensed to John Wiley & Sons, Inc. or one of its group companies (each a "Wiley Company") or handled on behalf of a society with which a Wiley Company has exclusive publishing rights in relation to a particular work (collectively "WILEY"). By clicking "accept" in connection with completing this licensing transaction, you agree that the following terms and conditions apply to this transaction (along with the billing and payment terms and conditions established by the Copyright Clearance Center Inc., ("CCC's Billing and Payment terms and conditions"), at the time that you opened your RightsLink account (these are available at any time at <http://myaccount.copyright.com>).

Terms and Conditions

- The materials you have requested permission to reproduce or reuse (the "Wiley Materials") are protected by copyright.
- You are hereby granted a personal, non-exclusive, non-sub licensable (on a stand-alone basis), non-transferable, worldwide, limited license to reproduce the Wiley Materials for the purpose specified in the licensing process. This license, **and any CONTENT (PDF or image file) purchased as part of your order**, is for a one-time use only and limited to any maximum distribution number specified in the license. The first instance of republication or reuse granted by this license must be completed within two years of the date of the grant of this license (although copies prepared before the end date may be distributed thereafter). The Wiley Materials shall not be used in any other manner or for any other purpose, beyond what is granted in the license. Permission is granted subject to an appropriate acknowledgement given to the author, title of the material/book/journal and the publisher. You shall also duplicate the copyright notice that appears in the Wiley publication in your use of the Wiley Material. Permission is also granted on the understanding that nowhere in the text is a previously published source acknowledged for all or part of this Wiley Material. Any third party content is expressly excluded from this permission.
- With respect to the Wiley Materials, all rights are reserved. Except as expressly granted by the terms of the license, no part of the Wiley Materials may be copied, modified, adapted (except for minor reformatting required by the new Publication), translated, reproduced, transferred or distributed, in any form or by any means, and no derivative works may be made based on the Wiley Materials without the prior permission of the respective copyright owner. **For STM Signatory Publishers clearing permission under the terms of the [STM Permissions Guidelines](#) only, the terms of the license are extended to include subsequent editions and for editions in other languages, provided such editions are for the work as a whole in situ and does not involve the separate exploitation of the permitted figures or extracts**, You may not alter, remove or suppress in any manner any copyright, trademark or other notices displayed by the Wiley Materials. You may not license, rent, sell, loan, lease, pledge, offer as security, transfer or assign the Wiley Materials on a stand-alone basis, or any of the rights granted to you hereunder to any other person.

- The Wiley Materials and all of the intellectual property rights therein shall at all times remain the exclusive property of John Wiley & Sons Inc, the Wiley Companies, or their respective licensors, and your interest therein is only that of having possession of and the right to reproduce the Wiley Materials pursuant to Section 2 herein during the continuance of this Agreement. You agree that you own no right, title or interest in or to the Wiley Materials or any of the intellectual property rights therein. You shall have no rights hereunder other than the license as provided for above in Section 2. No right, license or interest to any trademark, trade name, service mark or other branding ("Marks") of WILEY or its licensors is granted hereunder, and you agree that you shall not assert any such right, license or interest with respect thereto
- NEITHER WILEY NOR ITS LICENSORS MAKES ANY WARRANTY OR REPRESENTATION OF ANY KIND TO YOU OR ANY THIRD PARTY, EXPRESS, IMPLIED OR STATUTORY, WITH RESPECT TO THE MATERIALS OR THE ACCURACY OF ANY INFORMATION CONTAINED IN THE MATERIALS, INCLUDING, WITHOUT LIMITATION, ANY IMPLIED WARRANTY OF MERCHANTABILITY, ACCURACY, SATISFACTORY QUALITY, FITNESS FOR A PARTICULAR PURPOSE, USABILITY, INTEGRATION OR NON-INFRINGEMENT AND ALL SUCH WARRANTIES ARE HEREBY EXCLUDED BY WILEY AND ITS LICENSORS AND WAIVED BY YOU.
- WILEY shall have the right to terminate this Agreement immediately upon breach of this Agreement by you.
- You shall indemnify, defend and hold harmless WILEY, its Licensors and their respective directors, officers, agents and employees, from and against any actual or threatened claims, demands, causes of action or proceedings arising from any breach of this Agreement by you.
- IN NO EVENT SHALL WILEY OR ITS LICENSORS BE LIABLE TO YOU OR ANY OTHER PARTY OR ANY OTHER PERSON OR ENTITY FOR ANY SPECIAL, CONSEQUENTIAL, INCIDENTAL, INDIRECT, EXEMPLARY OR PUNITIVE DAMAGES, HOWEVER CAUSED, ARISING OUT OF OR IN CONNECTION WITH THE DOWNLOADING, PROVISIONING, VIEWING OR USE OF THE MATERIALS REGARDLESS OF THE FORM OF ACTION, WHETHER FOR BREACH OF CONTRACT, BREACH OF WARRANTY, TORT, NEGLIGENCE, INFRINGEMENT OR OTHERWISE (INCLUDING, WITHOUT LIMITATION, DAMAGES BASED ON LOSS OF PROFITS, DATA, FILES, USE, BUSINESS OPPORTUNITY OR CLAIMS OF THIRD PARTIES), AND WHETHER OR NOT THE PARTY HAS BEEN ADVISED OF THE POSSIBILITY OF SUCH DAMAGES. THIS LIMITATION SHALL APPLY NOTWITHSTANDING ANY FAILURE OF ESSENTIAL PURPOSE OF ANY LIMITED REMEDY PROVIDED HEREIN.
- Should any provision of this Agreement be held by a court of competent jurisdiction to be illegal, invalid, or unenforceable, that provision shall be deemed amended to achieve as nearly as possible the same economic effect as the original provision, and the legality, validity and enforceability of the remaining provisions of this Agreement shall not be affected or impaired thereby.

- The failure of either party to enforce any term or condition of this Agreement shall not constitute a waiver of either party's right to enforce each and every term and condition of this Agreement. No breach under this agreement shall be deemed waived or excused by either party unless such waiver or consent is in writing signed by the party granting such waiver or consent. The waiver by or consent of a party to a breach of any provision of this Agreement shall not operate or be construed as a waiver of or consent to any other or subsequent breach by such other party.
- This Agreement may not be assigned (including by operation of law or otherwise) by you without WILEY's prior written consent.
- Any fee required for this permission shall be non-refundable after thirty (30) days from receipt by the CCC.
- These terms and conditions together with CCC's Billing and Payment terms and conditions (which are incorporated herein) form the entire agreement between you and WILEY concerning this licensing transaction and (in the absence of fraud) supersedes all prior agreements and representations of the parties, oral or written. This Agreement may not be amended except in writing signed by both parties. This Agreement shall be binding upon and inure to the benefit of the parties' successors, legal representatives, and authorized assigns.
- In the event of any conflict between your obligations established by these terms and conditions and those established by CCC's Billing and Payment terms and conditions, these terms and conditions shall prevail.
- WILEY expressly reserves all rights not specifically granted in the combination of (i) the license details provided by you and accepted in the course of this licensing transaction, (ii) these terms and conditions and (iii) CCC's Billing and Payment terms and conditions.
- This Agreement will be void if the Type of Use, Format, Circulation, or Requestor Type was misrepresented during the licensing process.
- This Agreement shall be governed by and construed in accordance with the laws of the State of New York, USA, without regards to such state's conflict of law rules. Any legal action, suit or proceeding arising out of or relating to these Terms and Conditions or the breach thereof shall be instituted in a court of competent jurisdiction in New York County in the State of New York in the United States of America and each party hereby consents and submits to the personal jurisdiction of such court, waives any objection to venue in such court and consents to service of process by registered or certified mail, return receipt requested, at the last known address of such party.

WILEY OPEN ACCESS TERMS AND CONDITIONS

Wiley Publishes Open Access Articles in fully Open Access Journals and in Subscription journals offering Online Open. Although most of the fully Open Access journals publish open access articles under the terms of the Creative Commons Attribution (CC BY) License only, the subscription journals and a few of the Open Access Journals offer a choice of

Creative Commons Licenses. The license type is clearly identified on the article.

The Creative Commons Attribution License

The [Creative Commons Attribution License \(CC-BY\)](#) allows users to copy, distribute and transmit an article, adapt the article and make commercial use of the article. The CC-BY license permits commercial and non-

Creative Commons Attribution Non-Commercial License

The [Creative Commons Attribution Non-Commercial \(CC-BY-NC\)License](#) permits use, distribution and reproduction in any medium, provided the original work is properly cited and is not used for commercial purposes.(see below)

Creative Commons Attribution-Non-Commercial-NoDerivs License

The [Creative Commons Attribution Non-Commercial-NoDerivs License](#) (CC-BY-NC-ND) permits use, distribution and reproduction in any medium, provided the original work is properly cited, is not used for commercial purposes and no modifications or adaptations are made. (see below)

Use by commercial "for-profit" organizations

Use of Wiley Open Access articles for commercial, promotional, or marketing purposes requires further explicit permission from Wiley and will be subject to a fee.

Further details can be found on Wiley Online Library

<http://olabout.wiley.com/WileyCDA/Section/id-410895.html>

Other Terms and Conditions:

v1.10 Last updated September 2015

Questions? customercare@copyright.com or +1-855-239-3415 (toll free in the US) or +1-978-646-2777.



RightsLink®

[Home](#)
[Account Info](#)
[Help](#)


Title: Optical Gating With Asymmetric Field Ratios for Isolated Attosecond Pulse Generation

Author: Cunningham, E.; Zenghu Chang

Publication: Selected Topics in Quantum Electronics, IEEE Journal of

Publisher: IEEE

Date: Sept.-Oct. 2015

Logged in as:
Eric Cunningham
Account #:
3000968473

[LOGOUT](#)

Copyright © 2015, IEEE

Thesis / Dissertation Reuse

The IEEE does not require individuals working on a thesis to obtain a formal reuse license, however, you may print out this statement to be used as a permission grant:

Requirements to be followed when using any portion (e.g., figure, graph, table, or textual material) of an IEEE copyrighted paper in a thesis:

- 1) In the case of textual material (e.g., using short quotes or referring to the work within these papers) users must give full credit to the original source (author, paper, publication) followed by the IEEE copyright line © 2011 IEEE.
- 2) In the case of illustrations or tabular material, we require that the copyright line © [Year of original publication] IEEE appear prominently with each reprinted figure and/or table.
- 3) If a substantial portion of the original paper is to be used, and if you are not the senior author, also obtain the senior author's approval.

Requirements to be followed when using an entire IEEE copyrighted paper in a thesis:

- 1) The following IEEE copyright/ credit notice should be placed prominently in the references: © [year of original publication] IEEE. Reprinted, with permission, from [author names, paper title, IEEE publication title, and month/year of publication]
- 2) Only the accepted version of an IEEE copyrighted paper can be used when posting the paper or your thesis on-line.
- 3) In placing the thesis on the author's university website, please display the following message in a prominent place on the website: In reference to IEEE copyrighted material which is used with permission in this thesis, the IEEE does not endorse any of [university/educational entity's name goes here]'s products or services. Internal or personal use of this material is permitted. If interested in reprinting/republishing IEEE copyrighted material for advertising or promotional purposes or for creating new collective works for resale or redistribution, please go to http://www.ieee.org/publications_standards/publications/rights/rights_link.html to learn how to obtain a License from RightsLink.

If applicable, University Microfilms and/or ProQuest Library, or the Archives of Canada may supply single copies of the dissertation.

[BACK](#)
[CLOSE WINDOW](#)

Copyright © 2015 [Copyright Clearance Center, Inc.](#) All Rights Reserved. [Privacy statement](#). [Terms and Conditions](#).
Comments? We would like to hear from you. E-mail us at customer@copyright.com



Home

Create Account

Help



Title: Frequency domain optical parametric amplification

Author: Bruno E. Schmidt, Nicolas Thiré, Maxime Boivin, Antoine Laramée, François Poitras, Guy Lebrun

Publication: Nature Communications

Publisher: Nature Publishing Group

Date: May 7, 2014

[LOGIN](#)

If you're a [copyright.com user](#), you can login to RightsLink using your [copyright.com](#) credentials. Already **a [RightsLink user](#)** or want to [learn more?](#)

Copyright © 2014, Rights Managed by Nature Publishing Group

Creative Commons

The request you have made is considered to be non-commercial/educational. As the article you have requested has been distributed under a Creative Commons license (Attribution-Noncommercial), you may reuse this material for non-commercial/educational purposes without obtaining additional permission from Nature Publishing Group, providing that the author and the original source of publication are fully acknowledged (please see the article itself for the license version number). You may reuse this material without obtaining permission from Nature Publishing Group, providing that the author and the original source of publication are fully acknowledged, as per the terms of the license. For license terms, please see <http://creativecommons.org/>

[BACK](#)

[CLOSE WINDOW](#)

Copyright © 2015 [Copyright Clearance Center, Inc.](#) All Rights Reserved. [Privacy statement](#). [Terms and Conditions](#). Comments? We would like to hear from you. E-mail us at customer@copyright.com

LIST OF REFERENCES

- [1] H. W. Melville, "The labile molecule. Introductory Address," *Discuss. Faraday Soc.* **2**, 2–6 (1947).
- [2] G. Porter, "Flash photolysis and some of its applications," presented at the 1967 Nobel Lecture, (Stockholm, Sweden, Dec. 11, 1967).
- [3] R. G. W. Norrish and G. Porter, "Chemical Reactions Produced by Very High Light Intensities," *Nature* **164**, 658 (1949).
- [4] G. Porter, "Flash Photolysis and Spectroscopy. A New Method for the Study of Free Radical Reactions," *Proc. Roy. Soc. A* **200**, 284–300 (1950).
- [5] G. Porter and F. J. Wright, "Studies of free radical reactivity by the methods of flash photolysis. The photochemical reaction between chlorine and oxygen," *Discuss. Faraday Soc.* **14**, 23–34 (1953).
- [6] "The Nobel Prize in Chemistry 1967," http://www.nobelprize.org/nobel_prizes/chemistry/laureates/1967/ (Accessed April 1, 2014).
- [7] J. P. Gordon, H. J. Zeiger, and C. H. Townes, "Molecular Microwave Oscillator and New Hyperfine Structure in the Microwave Spectrum of NH_3 ," *Phys. Rev.* **95**, 282–284 (1954).
- [8] N. Basov and A. Prokhorov, "Application of molecular beams for the radiospectroscopic study of rotational molecular spectra," *Zh. Eksp. Teor. Fiz.* **27**, 431–438 (1954).
- [9] C. Townes, *How the Laser Happened: Adventures of a Scientist* (OUP USA, 1999), pp. 96–97.
- [10] A. Schawlow, "Infrared and optical masers," In *Quantum Electronics*, **1**, 553 (1960).

- [11] T. H. Maiman, “Optical and Microwave-Optical Experiments in Ruby,” *Phys. Rev. Lett.* **4**, 564–566 (1960).
- [12] T. H. Maiman, “Stimulated Optical Radiation in Ruby,” *Nature* **187**, 493–494 (1960).
- [13] T. H. Maiman, R. H. Hoskins, I. J. D’Haenens, C. K. Asawa, and V. Evtuhov, “Stimulated Optical Emission in Fluorescent Solids. II. Spectroscopy and Stimulated Emission in Ruby,” *Phys. Rev.* **123**, 1151–1157 (1961).
- [14] M. Bertolotti, *The History of the Laser* (Taylor & Francis, 2004), pp. 230–231.
- [15] “The Nobel Prize in Physics 1981,” http://www.nobelprize.org/nobel_prizes/physics/laureates/1981/ (Accessed April 1, 2014).
- [16] A. Schawlow, “Twenty-five years of Lasers,” 1987 Yearbook of Science and the Future (1987).
- [17] F. J. McClung and R. W. Hellwarth, “Giant Optical Pulsations from Ruby,” *Appl. Opt.* **1**, 103–105 (1962).
- [18] L. E. Hargrove, R. L. Fork, and M. A. Pollack, “LOCKING OF He-Ne LASER MODES INDUCED BY SYNCHRONOUS INTRACAVITY MODULATION,” *Appl. Phys. Lett.* **5**, 4–5 (1964).
- [19] A. H. Zewail, “Femtochemistry: Atomic-Scale Dynamics of the Chemical Bond,” *The Journal of Physical Chemistry A* **104**, 5660–5694 (2000).
- [20] “The Nobel Prize in Chemistry 1999,” http://www.nobelprize.org/nobel_prizes/chemistry/laureates/1999/ (Accessed April 1, 2014).

- [21] M. Hentschel, R. Kienberger, C. Spielmann, G. A. Reider, N. Milosevic, T. Brabec, P. Corkum, U. Heinzmann, M. Drescher, and F. Krausz, “Attosecond metrology,” *Nature* **414**, 509–513 (2001).
- [22] F. Krausz and M. Ivanov, “Attosecond physics,” *Rev. Mod. Phys.* **81**, 163–234 (2009).
- [23] M. Chini, X. Wang, Y. Cheng, Y. Wu, D. Zhao, D. A. Telnov, S.-I. Chu, and Z. Chang, “Sub-cycle oscillations in virtual states brought to light,” *Sci. Rep.* **3**, 1105 (2013).
- [24] R. H. Dicke, “Object detection system,” U.S. Patent No. 2624876 (1953).
- [25] C. Cook, “Pulse Compression-Key to More Efficient Radar Transmission,” *PIRE* **48**, 310–316 (1960).
- [26] F. Gires and P. Tournois, “Interféromètre utilisable pour la compression d’impulsions lumineuses modulées en fréquence,” *C. R. Acad. Sc. Paris* **258**, 6112–6115 (1964).
- [27] P. Tournois and F. Gires, “WAVE COMPRESSION DEVICE,” U.S. Patent No. 3551034 (1965).
- [28] M. A. Duguay and J. W. Hansen, “COMPRESSION OF PULSES FROM A MODE-LOCKED HeNe LASER,” *Appl. Phys. Lett.* **14**, 14–16 (1969).
- [29] J. H. Collins, E. G. H. Lean, and H. J. Shaw, “PULSE COMPRESSION BY BRAGG DIFFRACTION OF LIGHT WITH MICROWAVE SOUND,” *Appl. Phys. Lett.* **11**, 240–242 (1967).
- [30] J. Giordmaine, M. Duguay, and J. Hansen, “Compression of optical pulses,” *IEEE J. Quantum Electron.* **4**, 252–255 (1968).
- [31] E. Treacy, “Optical pulse compression with diffraction gratings,” *IEEE J. Quantum Electron.* **5**, 454–458 (1969).

- [32] B. Y. Zeldovich and I. I. Sobelman, “Possibility of Shortening Light Pulses in Alkali-Metal Vapor,” *Sov. Phys. JETP* **13**, 129–131 (1971).
- [33] Z. Bor and B. Rácz, “Group velocity dispersion in prisms and its application to pulse compression and travelling-wave excitation,” *Opt. Commun.* **54**, 165–170 (1985).
- [34] R. Szipöcs, K. Ferencz, C. Spielmann, and F. Krausz, “Chirped multilayer coatings for broadband dispersion control in femtosecond lasers,” *Opt. Lett.* **19**, 201–203 (1994).
- [35] R. A. Fisher, P. L. Kelley, and T. K. Gustafson, “SUBPICOSECOND PULSE GENERATION USING THE OPTICAL KERR EFFECT,” *Appl. Phys. Lett.* **14**, 140–143 (1969).
- [36] A. Laubereau, “External frequency modulation and compression of picosecond pulses,” *Phys. Lett. A* **29**, 539–540 (1969).
- [37] H. Nakatsuka, D. Grischkowsky, and A. C. Balant, “Nonlinear Picosecond-Pulse Propagation through Optical Fibers with Positive Group Velocity Dispersion,” *Phys. Rev. Lett.* **47**, 910–913 (1981).
- [38] C. V. Shank, R. L. Fork, R. Yen, R. H. Stolen, and W. J. Tomlinson, “Compression of femtosecond optical pulses,” *Appl. Phys. Lett.* **40**, 761–763 (1982).
- [39] B. Nikolaus and D. Grischkowsky, “90-fs tunable optical pulses obtained by two-stage pulse compression,” *Appl. Phys. Lett.* **43**, 228–230 (1983).
- [40] W. J. Tomlinson, R. H. Stolen, and C. V. Shank, “Compression of optical pulses chirped by self-phase modulation in fibers,” *J. Opt. Soc. Am. B* **1**, 139–149 (1984).
- [41] T. Damm, M. Kaschke, F. Noack, and B. Wilhelmi, “Compression of picosecond pulses from a solid-state laser using self-phase modulation in graded-index fibers,” *Opt. Lett.* **10**, 176–178 (1985).

- [42] W. Dietel, E. Döpel, V. Petrov, C. Rempel, W. Rudolph, B. Wilhelmi, G. Marowsky, and F. P. Schäfer, “Self phase modulation in a femtosecond pulse amplifier with subsequent compression,” *Appl. Phys. B* **46**, 183–184 (1988).
- [43] C. Rolland and P. B. Corkum, “Compression of high-power optical pulses,” *J. Opt. Soc. Am. B* **5**, 641–647 (1988).
- [44] M. Nisoli, S. D. Silvestri, and O. Svelto, “Generation of high energy 10 fs pulses by a new pulse compression technique,” *Appl. Phys. Lett.* **68**, 2793–2795 (1996).
- [45] I. Durfee, C.G., S. Backus, M. Murnane, and H. Kapteyn, “Design and implementation of a TW-class high-average power laser system,” *IEEE J. Sel. Topics Quantum Electron.* **4**, 395–406 (1998).
- [46] K. Yamane, Z. Zhang, K. Oka, R. Morita, M. Yamashita, and A. Suguro, “Optical pulse compression to 3.4fs in the monocycle region by feedback phase compensation,” *Opt. Lett.* **28**, 2258–2260 (2003).
- [47] A. Verhoef, J. Seres, K. Schmid, Y. Nomura, G. Tempea, L. Veisz, and F. Krausz, “Compression of the pulses of a Ti:sapphire laser system to 5 femtoseconds at 0.2 terawatt level,” *Appl. Phys. B* **82**, 513–517 (2006).
- [48] D. Strickland and G. Mourou, “Compression of amplified chirped optical pulses,” *Opt. Commun.* **55**, 447–449 (1985).
- [49] R. L. Fork, O. E. Martinez, and J. P. Gordon, “Negative dispersion using pairs of prisms,” *Opt. Lett.* **9**, 150–152 (1984).
- [50] O. E. Martinez, J. P. Gordon, and R. L. Fork, “Negative group-velocity dispersion using refraction,” *J. Opt. Soc. Am. A* **1**, 1003–1006 (1984).

- [51] O. E. Martinez, "Grating and prism compressors in the case of finite beam size," *J. Opt. Soc. Am. B* **3**, 929–934 (1986).
- [52] O. Martinez, "3000 times grating compressor with positive group velocity dispersion: Application to fiber compensation in 1.3-1.6 μm region," *IEEE J. Quantum Electron.* **23**, 59–64 (1987).
- [53] O. Martinez, "Design of high-power ultrashort pulse amplifiers by expansion and recompression," *IEEE J. Quantum Electron.* **23**, 1385–1387 (1987).
- [54] P. Maine, D. Strickland, P. Bado, M. Pessot, and G. Mourou, "Generation of ultrahigh peak power pulses by chirped pulse amplification," *IEEE J. Quantum Electron.* **24**, 398–403 (1988).
- [55] M. Pessot, J. Squier, G. Mourou, and D. J. Harter, "Chirped-pulse amplification of 100-fsec pulses," *Opt. Lett.* **14**, 797–799 (1989).
- [56] P. F. Moulton, "Ti-doped sapphire: tunable solid-state laser," *Opt. News* **8**, 9 (1982).
- [57] P. F. Moulton, "Spectroscopic and laser characteristics of Ti:Al₂O₃," *J. Opt. Soc. Am. B* **3**, 125–133 (1986).
- [58] A. Yariv and R. C. C. Leite, "Super Radiant Narrowing in Fluorescence Radiation of Inverted Populations," *J. Appl. Phys.* **34**, 3410–3411 (1963).
- [59] D. F. Hotz, "Gain Narrowing in a Laser Amplifier," *Appl. Opt.* **4**, 527–530 (1965).
- [60] L. Casperson and A. Yariv, "Spectral narrowing in high-gain lasers," *IEEE J. Quantum Electron.* **8**, 80–85 (1972).
- [61] J. Zhou, C.-P. Huang, M. M. Murnane, and H. C. Kapteyn, "Amplification of 26-fs, 2-TW pulses near the gain-narrowing limit in Ti:sapphire," *Opt. Lett.* **20**, 64–66 (1995).

- [62] C. Fiorini, C. Sauteret, C. Rouyer, N. Blanchot, S. Seznec, and A. Migus, “Temporal aberrations due to misalignments of a stretcher-compressor system and compensation,” *IEEE J. Quantum Electron.* **30**, 1662–1670 (1994).
- [63] M. Stern, J. Heritage, and E. Chase, “Grating compensation of third-order fiber dispersion,” *IEEE J. Quantum Electron.* **28**, 2742–2748 (1992).
- [64] W. E. White, F. G. Patterson, R. L. Combs, D. F. Price, and R. L. Shepherd, “Compensation of higher-order frequency-dependent phase terms in chirped-pulse amplification systems,” *Opt. Lett.* **18**, 1343–1345 (1993).
- [65] B. E. Lemoff and C. P. J. Barty, “Quintic-phase-limited, spatially uniform expansion and recompression of ultrashort optical pulses,” *Opt. Lett.* **18**, 1651–1653 (1993).
- [66] C. P. J. Barty, C. L. G. III, and B. E. Lemoff, “Multiterawatt 30-fs Ti:sapphire laser system,” *Opt. Lett.* **19**, 1442–1444 (1994).
- [67] Y. Nabekawa, Y. Kuramoto, T. Togashi, T. Sekikawa, and S. Watanabe, “Generation of 0.66-TW pulses at 1 kHz by a Ti:sapphire laser,” *Opt. Lett.* **23**, 1384–1386 (1998).
- [68] K. Yamakawa, M. Aoyama, S. Matsuoka, T. Kase, Y. Akahane, and H. Takuma, “100-TW sub-20-fs Ti:sapphire laser system operating at a 10-Hz repetition rate,” *Opt. Lett.* **23**, 1468–1470 (1998).
- [69] K. Yamakawa, M. Aoyama, S. Matsuoka, H. Takuma, C. P. J. Barty, and D. Fittinghoff, “Generation of 16-fs, 10-TW pulses at a 10-Hz repetition rate with efficient Ti:sapphire amplifiers,” *Opt. Lett.* **23**, 525–527 (1998).
- [70] K. Yamakawa, M. Aoyama, S. Matsuoka, H. Takuma, D. Fittinghoff, and C. Barty, “Ultrahigh-peak and high-average power chirped-pulse amplification of sub-20-fs pulses with Ti:sapphire amplifiers,” *IEEE J. Sel. Topics Quantum Electron.* **4**, 385–394 (1998).

- [71] V. Bagnoud and F. Salin, “Amplifying laser pulses to the terawatt level at a 1-kilohertz repetition rate,” *Appl. Phys. B* **70**, S165–S170 (2000).
- [72] P. Tournois, “New diffraction grating pair with very linear dispersion for laser pulse compression,” *Electron. Lett.* **29**, 1414–1415 (1993).
- [73] S. Kane and J. Squier, “Grism-pair stretcher–compressor system for simultaneous second- and third-order dispersion compensation in chirped-pulse amplification,” *J. Opt. Soc. Am. B* **14**, 661–665 (1997).
- [74] S. Kane and J. Squier, “Fourth-order-dispersion limitations of aberration-free chirped-pulse amplification systems,” *J. Opt. Soc. Am. B* **14**, 1237–1244 (1997).
- [75] M. Aoyama, K. Yamakawa, Y. Akahane, J. Ma, N. Inoue, H. Ueda, and H. Kiriyama, “0.85-PW, 33-fs Ti:sapphire laser,” *Opt. Lett.* **28**, 1594–1596 (2003).
- [76] J. Squier, C. P. J. Barty, F. Salin, C. L. Blanc, and S. Kane, “Use of Mismatched Grating Pairs in Chirped-Pulse Amplification Systems,” *Appl. Opt.* **37**, 1638–1641 (1998).
- [77] A. Offner, “UNIT POWER IMAGING CATOPTRIC ANASTIGMAT,” U.S. Patent No. 2748015 (1973).
- [78] A. Suzuki, “Complete analysis of a two-mirror unit magnification system. Part 1,” *Appl. Opt.* **22**, 3943–3949 (1983).
- [79] G. Cheriaux, P. Rousseau, F. Salin, J. P. Chambaret, B. Walker, and L. F. Dimauro, “Aberration-free stretcher design for ultrashort-pulse amplification,” *Opt. Lett.* **21**, 414–416 (1996).
- [80] M. Hentschel, Z. Cheng, F. Krausz, and C. Spielmann, “Generation of 0.1-TW optical pulses with a single-stage Ti:sapphire amplifier at a 1-kHz repetition rate,” *Appl. Phys. B* **70**, 161–164 (2000).

- [81] M. B. Danailov and I. P. Christov, “Ultrabroadband laser using prism-based “spatially-dispersive” resonator,” *Appl. Phys. B* **51**, 300–302 (1990).
- [82] I. P. Christov, “Amplification of femtosecond pulses in a spatially dispersive scheme,” *Opt. Lett.* **17**, 742–744 (1992).
- [83] J. Faure, J. Itatani, S. Biswal, G. Cheriaux, L. R. Bruner, G. C. Templeton, and G. Mourou, “A spatially dispersive regenerative amplifier for ultrabroadband pulses,” *Opt. Commun.* **159**, 68–73 (1999).
- [84] C. P. Hauri, M. Bruck, W. Kornelis, J. Biegert, and U. Keller, “Generation of 14.8-fs pulses in a spatially dispersed amplifier,” *Opt. Lett.* **29**, 201–203 (2004).
- [85] M. P. Kalashnikov, K. Osvay, I. M. Lachko, H. Schönagel, and W. Sandner, “Suppression of gain narrowing in multi-TW lasers with negatively and positively chirped pulse amplification,” *Appl. Phys. B* **81**, 1059–1062 (2005).
- [86] M. D. Perry, F. G. Patterson, and J. Weston, “Spectral shaping in chirped-pulse amplification,” *Opt. Lett.* **15**, 381–383 (1990).
- [87] F. G. Patterson and M. D. Perry, “Design and performance of a multiterawatt, subpicosecond neodymium:glass laser,” *J. Opt. Soc. Am. B* **8**, 2384–2391 (1991).
- [88] Y. H. Cha, Y. I. Kang, and C. H. Nam, “Generation of a broad amplified spectrum in a femtosecond terawatt Ti:sapphire laser by a long-wavelength injection method,” *J. Opt. Soc. Am. B* **16**, 1220–1223 (1999).
- [89] J. P. Heritage, A. M. Weiner, and R. N. Thurston, “Picosecond pulse shaping by spectral phase and amplitude manipulation,” *Opt. Lett.* **10**, 609–611 (1985).
- [90] A. M. Weiner, J. P. Heritage, and E. M. Kirschner, “High-resolution femtosecond pulse shaping,” *J. Opt. Soc. Am. B* **5**, 1563–1572 (1988).

- [91] C. P. J. Barty, G. Korn, F. Raksi, C. Rose-Petruck, J. Squier, A.-C. Tien, K. R. Wilson, V. V. Yakovlev, and K. Yamakawa, “Regenerative pulse shaping and amplification of ultrabroad-band optical pulses,” *Opt. Lett.* **21**, 219–221 (1996).
- [92] A. M. Weiner, D. E. Leaird, J. S. Patel, and J. R. Wullert, “Programmable femtosecond pulse shaping by use of a multielement liquid-crystal phase modulator,” *Opt. Lett.* **15**, 326–328 (1990).
- [93] A. Weiner, D. Leaird, J. Patel, and I. Wullert, J.R., “Programmable shaping of femtosecond optical pulses by use of 128-element liquid crystal phase modulator,” *IEEE J. Quantum Electron.* **28**, 908–920 (1992).
- [94] M. M. Wefers and K. A. Nelson, “Programmable phase and amplitude femtosecond pulse shaping,” *Opt. Lett.* **18**, 2032–2034 (1993).
- [95] M. M. Wefers and K. A. Nelson, “Generation of high-fidelity programmable ultrafast optical waveforms,” *Opt. Lett.* **20**, 1047–1049 (1995).
- [96] T. Brixner and G. Gerber, “Femtosecond polarization pulse shaping,” *Opt. Lett.* **26**, 557–559 (2001).
- [97] T. Baumert, T. Brixner, V. Seyfried, M. Strehle, and G. Gerber, “Femtosecond pulse shaping by an evolutionary algorithm with feedback,” *Appl. Phys. B* **65**, 779–782 (1997).
- [98] D. Yelin, D. Meshulach, and Y. Silberberg, “Adaptive femtosecond pulse compression,” *Opt. Lett.* **22**, 1793–1795 (1997).
- [99] A. Efimov and D. H. Reitze, “Programmable dispersion compensation and pulse shaping in a 26-fs chirped-pulse amplifier,” *Opt. Lett.* **23**, 1612–1614 (1998).
- [100] T. Brixner, M. Strehle, and G. Gerber, “Feedback-controlled optimization of amplified femtosecond laser pulses,” *Appl. Phys. B* **68**, 281–284 (1999).

- [101] Y. Nabekawa, Y. Shimizu, and K. Midorikawa, "Development of an ultrabroad-band regenerative amplifier with a mirrorless cavity and generation of sub-20 fs pulses in terawatt regime with an adaptive phase controller," *RIKEN Rev.*, 3–6 (2002).
- [102] H. Takada, M. Kakehata, and K. Torizuka, "High-repetition-rate 12fs pulse amplification by a Ti:sapphire regenerative amplifier system," *Opt. Lett.* **31**, 1145–1147 (2006).
- [103] Y. Nabekawa, A. Amani Eilanlou, Y. Furukawa, K. Ishikawa, H. Takahashi, and K. Midorikawa, "Multi-terawatt laser system generating 12-fs pulses at 100 Hz repetition rate," *Appl. Phys. B* **101**, 523–534 (2010).
- [104] J. J. Field, T. A. Planchon, W. Amir, C. G. Durfee, and J. A. Squier, "Characterization of a high efficiency, ultrashort pulse shaper incorporating a reflective 4096-element spatial light modulator," *Opt. Commun.* **278**, 368–376 (2007).
- [105] C. Dorrer, F. Salin, F. Verluise, and J. P. Huignard, "Programmable phase control of femtosecond pulses by use of a nonpixelated spatial light modulator," *Opt. Lett.* **23**, 709–711 (1998).
- [106] K. Mahoney and A. Weiner, "A femtosecond pulse-shaping apparatus containing microlens arrays for use with pixelated spatial light modulators," *IEEE J. Quantum Electron.* **32**, 2071–2077 (1996).
- [107] K. Ema and F. Shimizu, "Optical Pulse Shaping Using a Fourier-Transformed Hologram," *Jpn. J. Appl. Phys.* **29**, L631–L633 (1990).
- [108] C. W. Hillegas, J. X. Tull, D. Goswami, D. Strickland, and W. S. Warren, "Femtosecond laser pulse shaping by use of microsecond radio-frequency pulses," *Opt. Lett.* **19**, 737–739 (1994).

- [109] M. A. Dugan, J. X. Tull, and W. S. Warren, “High-resolution acousto-optic shaping of unamplified and amplified femtosecond laser pulses,” *J. Opt. Soc. Am. B* **14**, 2348–2358 (1997).
- [110] E. Zeek, K. Maginnis, S. Backus, U. Russek, M. Murnane, G. Mourou, H. Kapteyn, and G. Vdovin, “Pulse compression by use of deformable mirrors,” *Opt. Lett.* **24**, 493–495 (1999).
- [111] E. Zeek, R. Bartels, M. M. Murnane, H. C. Kapteyn, S. Backus, and G. Vdovin, “Adaptive pulse compression for transform-limited 15-fs high-energy pulse generation,” *Opt. Lett.* **25**, 587–589 (2000).
- [112] G. Chériaux, O. Albert, V. Wänman, J. P. Chambaret, C. Félix, and G. Mourou, “Temporal control of amplified femtosecond pulses with a deformable mirror in a stretcher,” *Opt. Lett.* **26**, 169–171 (2001).
- [113] K.-H. Hong and C. H. Nam, “Adaptive Pulse Compression of Femtosecond Laser Pulses Using a Low-Loss Pulse Shaper,” *Jpn. J. Appl. Phys.* **43**, 5289 (2004).
- [114] M. Hacker, G. Stobrawa, R. Sauerbrey, T. Buckup, M. Motzkus, M. Wildenhain, and A. Gehner, “Micromirror SLM for femtosecond pulse shaping in the ultraviolet,” *Appl. Phys. B* **76**, 711–714 (2003).
- [115] S. M. Weber, J. Extermann, L. Bonacina, W. Noell, D. Kiselev, S. Waldis, N. F. de Rooij, and J.-P. Wolf, “Ultraviolet and near-infrared femtosecond temporal pulse shaping with a new high-aspect-ratio one-dimensional micromirror array,” *Opt. Lett.* **35**, 3102–3104 (2010).
- [116] J. Extermann, S. M. Weber, D. Kiselev, L. Bonacina, S. Lani, F. Jutzi, W. Noell, N. F. de Rooij, and J.-P. Wolf, “Spectral phase, amplitude, and spatial modulation from ultraviolet to infrared with a reflective MEMS pulse shaper,” *Opt. Express* **19**, 7580–7586 (2011).
- [117] J. Itatani, Y. Nabekawa, K. Kondo, and S. Watanabe, “Generation of 13-TW, 26-fs pulses in a Ti:sapphire laser,” *Optics Communications* **134**, 134–138 (1997).

- [118] B. Walker, C. Toth, D. Fittinghoff, T. Guo, D.-E. Kim, C. Rose-Petruck, J. Squier, K. Yamakawa, K. Wilson, and C. Barty, “A 50 EW/cm² Ti:sapphire laser system for studying relativistic light-matter interactions,” *Opt. Express* **5**, 196–202 (1999).
- [119] Y. Nabekawa, Y. Shimizu, and K. Midorikawa, “Sub-20-fs terawatt-class laser system with a mirrorless regenerative amplifier and an adaptive phase controller,” *Opt. Lett.* **27**, 1265–1267 (2002).
- [120] S. Ito, H. Ishikawa, T. Miura, K. Takasago, A. Endo, and K. Torizuka, “Seven-terawatt Ti:sapphire laser system operating at 50 Hz with high beam quality for laser Compton femtosecond X-ray generation,” *Appl. Phys. B* **76**, 497–503 (2003).
- [121] X. Lu, C. Li, Y. Leng, C. Wang, C. Zhang, X. Liang, R. Li, and Z. Xu, “Birefringent plate design for broadband spectral shaping in a Ti:sapphire regenerative amplifier,” *Chin. Opt. Lett.* **5**, 493–496 (2007).
- [122] H. Takada, M. Kakehata, and K. Torizuka, “Study on Design of 10 TW Class 10 fs Ti:sapphire Laser,” *Rev. Laser Eng.* **27**, 341–345 (1999).
- [123] H. Takada, M. Kakehata, and K. Torizuka, “Broadband high-energy mirror for ultrashort pulse amplification system,” *Appl. Phys. B* **70**, S189–S192 (2000).
- [124] H. Takada, M. Kakehata, and K. Torizuka, “Broadband Regenerative Amplifier Using a Gain-Narrowing Compensator with Multiple Dielectric Layers,” *Jpn. J. Appl. Phys.* **43**, L1485–L1487 (2004).
- [125] F. Giambruno, C. Radier, G. Rey, and G. Chériaux, “Design of a 10 PW (150-J/15-fs) peak power laser system with Ti:sapphire medium through spectral control,” *Appl. Opt.* **50**, 2617–2621 (2011).

- [126] A. A. Eilanlou, Y. Nabekawa, K. L. Ishikawa, H. Takahashi, and K. Midorikawa, “Direct amplification of terawatt sub-10-fs pulses in a CPA system of Ti:sapphire laser,” *Opt. Express* **16**, 13431–13438 (2008).
- [127] L. Antonucci, J. P. Rousseau, A. Jullien, B. Mercier, V. Laude, and G. Cheriaux, “14-fs high temporal quality injector for ultra-high intensity laser,” *Opt. Commun.* **282**, 1374–1379 (2009).
- [128] P. Tournois, “Acousto-optic programmable dispersive filter for adaptive compensation of group delay time dispersion in laser systems,” *Opt. Commun.* **140**, 245–249 (1997).
- [129] F. Verluise, V. Laude, Z. Cheng, C. Spielmann, and P. Tournois, “Amplitude and phase control of ultrashort pulses by use of an acousto-optic programmable dispersive filter: pulse compression and shaping,” *Opt. Lett.* **25**, 575–577 (2000).
- [130] F. Verluise, V. Laude, J.-P. Huignard, P. Tournois, and A. Migus, “Arbitrary dispersion control of ultrashort optical pulses with acoustic waves,” *J. Opt. Soc. Am. B* **17**, 138–145 (2000).
- [131] M. Pittman, S. Ferré, J. Rousseau, L. Notebaert, J. Chambaret, and G. Chériaux, “Design and characterization of a near-diffraction-limited femtosecond 100-TW 10-Hz high-intensity laser system,” *Appl. Phys. B* **74**, 529–535 (2002).
- [132] H. S. Peng *et al.*, “SILEX-I: 300-TW Ti:sapphire laser,” *Laser Phys.* **16**, 244–247 (2006).
- [133] A. Trisorio, P. M. Paul, F. Ple, C. Ruchert, C. Vicario, and C. P. Hauri, “Ultrabroadband TW-class Ti:sapphire laser system with adjustable central wavelength, bandwidth and multi-color operation,” *Opt. Express* **19**, 20128–20140 (2011).

- [134] T. Oksenhendler, D. Kaplan, P. Tournois, G. M. Greetham, and F. Estable, “Intracavity acousto-optic programmable gain control for ultra-wide-band regenerative amplifiers,” *Appl. Phys. B* **83**, 491–494 (2006).
- [135] L. Canova, O. Albert, R. Lopez-Martens, P. Giacomini, and P.-M. Paul, “Ultrashort Pulses Generation with the Mazzer Active Spectral Broadening and the XPW Pulse Shortening Technique,” In *Conference on Lasers and Electro-Optics/Quantum Electronics and Laser Science Conference and Photonic Applications Systems Technologies*, p. JTuA39 (Optical Society of America, 2008).
- [136] D. B. Joyce and F. Schmid, “Progress in the growth of large scale Ti:sapphire crystals by the heat exchanger method (HEM) for petawatt class lasers,” *J. Crys. Growth* **312**, 1138–1141 (2010).
- [137] J. E. Swain, R. E. Kidder, K. Pettipiece, F. Rainer, E. D. Baird, and B. Loth, “Large Aperture Glass Disk Laser System,” *J. Appl. Phys.* **40**, 3973–3977 (1969).
- [138] J. McMahon, J. Emmett, J. Holzrichter, and J. Trenholme, “A glass-disk-laser amplifier,” *IEEE J. Quantum Electron.* **9**, 992–999 (1973).
- [139] D. C. Brown, S. D. Jacobs, and N. Nee, “Parasitic oscillations, absorption, stored energy density and heat density in active-mirror and disk amplifiers,” *Appl. Opt.* **17**, 211–224 (1978).
- [140] P. Labudde, W. Seka, and H. P. Weber, “Gain increase in laser amplifiers by suppression of parasitic oscillations,” *Appl. Phys. Lett.* **29**, 732–734 (1976).
- [141] S. Guch, “Parasitic suppression in large aperture disk lasers employing liquid edge claddings,” *Appl. Opt.* **15**, 1453–1457 (1976).

- [142] F. G. Patterson, J. Bonlie, D. Price, and B. White, “Suppression of parasitic lasing in large-aperture Ti:sapphire laser amplifiers,” *Opt. Lett.* **24**, 963–965 (1999).
- [143] V. Chvykov and K. Krushelnick, “Large aperture multi-pass amplifiers for high peak power lasers,” *Opt. Commun.* **285**, 2134–2136 (2012).
- [144] J. Bonlie, F. Patterson, D. Price, B. White, and P. Springer, “Production of $<10^{21}$ W/cm² from a large-aperture Ti:sapphire laser system,” *Appl. Phys. B* **70**, S155–S160 (2000).
- [145] K. Ertel, C. Hooker, S. J. Hawkes, B. T. Parry, and J. L. Collier, “ASE suppression in a high energy Titanium sapphire amplifier,” *Opt. Express* **16**, 8039–8049 (2008).
- [146] Y. Chu, X. Liang, Z. Gan, L. Yu, L. Xu, R. Li, and Z. Xu, “Suppression of transverse parasitic lasing and amplified spontaneous emission in Ti:sapphire amplifier by polarization-selection pump,” *Appl. Opt.* **54**, 6291–6296 (2015).
- [147] F. Ple, M. Pittman, F. Canova, J.-P. Chambaret, G. Mourou, and T. Planchon, “Suppression of Parasitic Lasing in Large-Aperture Ti: Sapphire Amplifiers: Amplifying Strategies for High Rep-Rate Petawatt Class Ti:sapphire Systems,” In *Conference on Lasers and Electro-Optics/Quantum Electronics and Laser Science and Photonic Applications Systems Technologies*, p. JThE97 (Optical Society of America, 2005).
- [148] Y. Wu, E. Cunningham, H. Zang, J. Li, M. Chini, X. Wang, Y. Wang, K. Zhao, and Z. Chang, “Generation of high-flux attosecond extreme ultraviolet continuum with a 10 TW laser,” *Appl. Phys. Lett.* **102**, 201104 (2013).
- [149] F. Ferrari, F. Calegari, M. Lucchini, C. Vozzi, S. Stagira, G. Sansone, and M. Nisoli, “High-energy isolated attosecond pulses generated by above-saturation few-cycle fields,” *Nat. Photon.* **4**, 875–879 (2010).

- [150] X. Feng, S. Gilbertson, H. Mashiko, H. Wang, S. D. Khan, M. Chini, Y. Wu, K. Zhao, and Z. Chang, “Generation of Isolated Attosecond Pulses with 20 to 28 Femtosecond Lasers,” *Phys. Rev. Lett.* **103**, 183901 (2009).
- [151] J. Seres, A. Müller, E. Seres, K. O’Keeffe, M. Lenner, R. F. Herzog, D. Kaplan, C. Spielmann, and F. Krausz, “Sub-10-fs, terawatt-scale Ti:sapphire laser system,” *Opt. Lett.* **28**, 1832–1834 (2003).
- [152] H. Takada and K. Torizuka, “Design and construction of a TW-class 12-fs Ti:Sapphire chirped-pulse amplification system,” *IEEE J. Sel. Topics Quantum Electron.* **12**, 201–212 (2006).
- [153] D. Kane and R. Trebino, “Characterization of arbitrary femtosecond pulses using frequency-resolved optical gating,” *IEEE J. Quantum Electron.* **29**, 571–579 (1993).
- [154] E. Takahashi, Y. Nabekawa, H. Mashiko, H. Hasegawa, A. Suda, and K. Midorikawa, “Generation of strong optical field in soft X-ray region by using high-order harmonics,” *IEEE J. Sel. Topics Quantum Electron.* **10**, 1315–1328 (2004).
- [155] X. Wang, M. Chini, Y. Cheng, Y. Wu, and Z. Chang, “In situ calibration of an extreme ultraviolet spectrometer for attosecond transient absorption experiments,” *Appl. Opt.* **52**, 323–329 (2013).
- [156] A. Suda, M. Hatayama, K. Nagasaka, and K. Midorikawa, “Generation of 9-fs 5-mJ pulses using a hollow fiber with pressure gradient,” In *Conference on Lasers and Electro-Optics/Quantum Electronics and Laser Science Conference*, p. CThPDA1 (Optical Society of America, 2003).

- [157] S. Laux, F. Lureau, C. Radier, O. Chalus, F. Caradec, O. Casagrande, E. Pourtal, C. Simon-Boisson, F. Soyer, and P. Lebarney, “Suppression of parasitic lasing in high energy, high repetition rate Ti:sapphire laser amplifiers,” *Opt. Lett.* **37**, 1913–1915 (2012).
- [158] J. Buck, S. Serati, L. Hosting, R. Serati, H. Masterson, M. Escuti, J. Kim, and M. Miskiewicz, “Polarization gratings for non-mechanical beam steering applications,” In *Society of Photo-Optical Instrumentation Engineers (SPIE) Conference Series*, Society of Photo-Optical Instrumentation Engineers (SPIE) Conference Series 8395 (2012).
- [159] W. Yang, X. Song, S. Gong, Y. Cheng, and Z. Xu, “Carrier-Envelope Phase Dependence of Few-Cycle Ultrashort Laser Pulse Propagation in a Polar Molecule Medium,” *Phys. Rev. Lett.* **99**, 133602 (2007).
- [160] K. Y. Kim, I. Alexeev, and H. M. Milchberg, “Single-shot supercontinuum spectral interferometry,” *Appl. Phys. Lett.* **81**, 4124–4126 (2002).
- [161] S. E. Irvine, P. Dombi, G. Farkas, and A. Y. Elezzabi, “Influence of the Carrier-Envelope Phase of Few-Cycle Pulses on Ponderomotive Surface-Plasmon Electron Acceleration,” *Phys. Rev. Lett.* **97**, 146801 (2006).
- [162] G. G. Paulus, F. Grasbon, H. Walther, P. Villoresi, M. Nisoli, S. Stagira, E. Priori, and S. De Silvestri, “Absolute-phase phenomena in photoionization with few-cycle laser pulses,” *Nature* **414**, 182–184 (2001).
- [163] G. G. Paulus, F. Lindner, H. Walther, A. Baltuška, E. Goulielmakis, M. Lezius, and F. Krausz, “Measurement of the Phase of Few-Cycle Laser Pulses,” *Phys. Rev. Lett.* **91**, 253004 (2003).

- [164] C. Lemell, X.-M. Tong, F. Krausz, and J. Burgdörfer, “Electron Emission from Metal Surfaces by Ultrashort Pulses: Determination of the Carrier-Envelope Phase,” *Phys. Rev. Lett.* **90**, 076403 (2003).
- [165] A. Apolonski *et al.*, “Observation of Light-Phase-Sensitive Photoemission from a Metal,” *Phys. Rev. Lett.* **92**, 073902 (2004).
- [166] M. Kreß *et al.*, “Determination of the carrier-envelope phase of few-cycle laser pulses with terahertz-emission spectroscopy,” *Nat. Phys.* **2**, 327–331 (2006).
- [167] P. B. Corkum, “Plasma perspective on strong field multiphoton ionization,” *Phys. Rev. Lett.* **71**, 1994–1997 (1993).
- [168] M. Lewenstein, P. Balcou, M. Y. Ivanov, A. L’Huillier, and P. B. Corkum, “Theory of high-harmonic generation by low-frequency laser fields,” *Phys. Rev. A* **49**, 2117–2132 (1994).
- [169] M. Lewenstein, P. Salières, and A. L’Huillier, “Phase of the atomic polarization in high-order harmonic generation,” *Phys. Rev. A* **52**, 4747–4754 (1995).
- [170] P. Salières, P. Antoine, A. de Bohan, and M. Lewenstein, “Temporal and Spectral Tailoring of High-Order Harmonics,” *Phys. Rev. Lett.* **81**, 5544–5547 (1998).
- [171] G. Sansone, E. Benedetti, J.-P. Caumes, S. Stagira, C. Vozzi, M. Pascolini, L. Poletto, P. Villorosi, S. De Silvestri, and M. Nisoli, “Measurement of Harmonic Phase Differences by Interference of Attosecond Light Pulses,” *Phys. Rev. Lett.* **94**, 193903 (2005).
- [172] C. A. Haworth, L. E. Chipperfield, J. S. Robinson, P. L. Knight, J. P. Marangos, and J. W. G. Tisch, “Half-cycle cutoffs in harmonic spectra and robust carrier-envelope phase retrieval,” *Nat. Phys.* **3**, 52–57 (2007).
- [173] P. Antoine, A. L’Huillier, and M. Lewenstein, “Attosecond Pulse Trains Using High-Order Harmonics,” *Phys. Rev. Lett.* **77**, 1234–1237 (1996).

- [174] P. Antoine, B. Piraux, D. B. Milošević, and M. Gajda, “Generation of ultrashort pulses of harmonics,” *Phys. Rev. A* **54**, R1761–R1764 (1996).
- [175] G. Sansone *et al.*, “Isolated Single-Cycle Attosecond Pulses,” *Science* **314**, 443–446 (2006).
- [176] P. B. Corkum, N. H. Burnett, and M. Y. Ivanov, “Subfemtosecond pulses,” *Opt. Lett.* **19**, 1870–1872 (1994).
- [177] M. Ivanov, P. B. Corkum, T. Zuo, and A. Bandrauk, “Routes to Control of Intense-Field Atomic Polarizability,” *Phys. Rev. Lett.* **74**, 2933–2936 (1995).
- [178] V. T. Platonenko and V. V. Strelkov, “Single attosecond soft-x-ray pulse generated with a limited laser beam,” *J. Opt. Soc. Am. B* **16**, 435–440 (1999).
- [179] A. Baltuska *et al.*, “Attosecond control of electronic processes by intense light fields,” *Nature* **421**, 611–615 (2003).
- [180] P. Agostini and L. F. DiMauro, “The physics of attosecond light pulses,” *Rep. Prog. Phys.* **67**, 813 (2004).
- [181] S. Gilbertson, S. D. Khan, Y. Wu, M. Chini, and Z. Chang, “Isolated Attosecond Pulse Generation without the Need to Stabilize the Carrier-Envelope Phase of Driving Lasers,” *Phys. Rev. Lett.* **105**, 093902 (2010).
- [182] Z. Chang, “Carrier-envelope phase shift caused by grating-based stretchers and compressors,” *Appl. Opt.* **45**, 8350–8353 (2006).
- [183] T. Wittmann, B. Horvath, W. Helml, M. G. Schatzel, X. Gu, A. L. Cavalieri, G. G. Paulus, and R. Kienberger, “Single-shot carrier-envelope phase measurement of few-cycle laser pulses,” *Nat. Phys.* **5**, 357–362 (2009).

- [184] M. Moller, A. M. Sayler, T. Rathje, M. Chini, Z. Chang, and G. G. Paulus, “Precise, real-time, single-shot carrier-envelope phase measurement in the multi-cycle regime,” *Appl. Phys. Lett.* **99**, 121108 (2011).
- [185] A. M. Sayler, T. Rathje, W. Müller, K. Rühle, R. Kienberger, and G. G. Paulus, “Precise, real-time, every-single-shot, carrier-envelope phase measurement of ultrashort laser pulses,” *Opt. Lett.* **36**, 1–3 (2011).
- [186] P. Dietrich, F. Krausz, and P. B. Corkum, “Determining the absolute carrier phase of a few-cycle laser pulse,” *Opt. Lett.* **25**, 16–18 (2000).
- [187] M. Kakehata, H. Takada, Y. Kobayashi, K. Torizuka, Y. Fujihira, T. Homma, and H. Takahashi, “Single-shot measurement of carrier-envelope phase changes by spectral interferometry,” *Opt. Lett.* **26**, 1436–1438 (2001).
- [188] M. Mehendale, S. A. Mitchell, J.-P. Likforman, D. M. Villeneuve, and P. B. Corkum, “Method for single-shot measurement of the carrier envelope phase of a few-cycle laser pulse,” *Opt. Lett.* **25**, 1672–1674 (2000).
- [189] A. Ishizawa and H. Nakano, “Measurement of the True Value of the Carrier-Envelope Phase of a Few-Cycle Laser Pulse by the Interference between Second and Third Harmonics from the Surface of a Solid,” *Jpn. J. Appl. Phys.* **45**, 4087–4089 (2006).
- [190] T. Fuji, A. Apolonski, and F. Krausz, “Self-stabilization of carrier-envelope offset phase by use of difference-frequency generation,” *Opt. Lett.* **29**, 632–634 (2004).
- [191] P. A. Roos, X. Li, R. P. Smith, J. A. Pipis, T. M. Fortier, and S. T. Cundiff, “Solid-state carrier-envelope phase stabilization via quantum interference control of injected photocurrents,” *Opt. Lett.* **30**, 735–737 (2005).

- [192] Y. S. Lee, J. Sung, C. Nam, T. Yu, and K.-H. Hong, “Novel method for carrier-envelope phase stabilization of femtosecond laser pulses,” *Opt. Express* **13**, 2969–2976 (2005).
- [193] S. B. P. Radnor, P. Kinsler, and G. H. C. New, “Proposal for absolute CEP measurement using 0-to-f self-referencing,” ArXiv e-prints (2009).
- [194] H. Telle, G. Steinmeyer, A. Dunlop, J. Stenger, D. Sutter, and U. Keller, “Carrier-envelope offset phase control: A novel concept for absolute optical frequency measurement and ultrashort pulse generation,” *Appl. Phys. B* **69**, 327–332 (1999).
- [195] A. Apolonski, A. Poppe, G. Tempea, C. Spielmann, T. Udem, R. Holzwarth, T. W. Hänsch, and F. Krausz, “Controlling the Phase Evolution of Few-Cycle Light Pulses,” *Phys. Rev. Lett.* **85**, 740–743 (2000).
- [196] D. J. Jones, S. A. Diddams, J. K. Ranka, A. Stentz, R. S. Windeler, J. L. Hall, and S. T. Cundiff, “Carrier-Envelope Phase Control of Femtosecond Mode-Locked Lasers and Direct Optical Frequency Synthesis,” *Science* **288**, 635–639 (2000).
- [197] A. Poppe, R. Holzwarth, A. Apolonski, G. Tempea, C. Spielmann, T. Hänsch, and F. Krausz, “Few-cycle optical waveform synthesis,” *Appl. Phys. B* **72**, 373–376 (2001).
- [198] E. Gagnon, I. Thomann, A. Paul, A. L. Lytle, S. Backus, M. M. Murnane, H. C. Kapteyn, and A. S. Sandhu, “Long-term carrier-envelope phase stability from a grating-based, chirped pulse amplifier,” *Opt. Lett.* **31**, 1866–1868 (2006).
- [199] F. Helbing, G. Steinmeyer, J. Stenger, H. Telle, and U. Keller, “Carrier-envelope-offset dynamics and stabilization of femtosecond pulses,” *Appl. Phys. B* **74**, S35–S42 (2002).
- [200] F. W. Helbing, G. Steinmeyer, U. Keller, R. S. Windeler, J. Stenger, and H. R. Telle, “Carrier-envelope offset dynamics of mode-locked lasers,” *Opt. Lett.* **27**, 194–196 (2002).

- [201] T. M. Fortier, D. J. Jones, J. Ye, S. T. Cundiff, and R. S. Windeler, “Long-term carrier-envelope phase coherence,” *Opt. Lett.* **27**, 1436–1438 (2002).
- [202] A. Baltuska, M. Uiberacker, E. Goulielmakis, R. Kienberger, V. Yakovlev, T. Udem, T. Hansch, and F. Krausz, “Phase-controlled amplification of few-cycle laser pulses,” *IEEE J. Sel. Topics Quantum Electron.* **9**, 972–989 (2003).
- [203] R. Holzwarth, T. Udem, T. W. Hänsch, J. C. Knight, W. J. Wadsworth, and P. S. J. Russell, “Optical Frequency Synthesizer for Precision Spectroscopy,” *Phys. Rev. Lett.* **85**, 2264–2267 (2000).
- [204] H. Wang, M. Chini, Y. Wu, E. Moon, H. Mashiko, and Z. Chang, “Carrier-envelope phase stabilization of 5-fs, 0.5-mJ pulses from adaptive phase modulator,” *Appl. Phys. B* **98**, 291–294 (2010).
- [205] E. Moon, H. Wang, S. Gilbertson, H. Mashiko, M. Chini, and Z. Chang, “Advances in carrier-envelope phase stabilization of grating-based chirped-pulse amplifiers,” *Laser & Photon. Rev.* **4**, 160–177 (2010).
- [206] L. Canova, X. Chen, A. Trisorio, A. Jullien, A. Assion, G. Tempea, N. Forget, T. Oksenhendler, and R. Lopez-Martens, “Carrier-envelope phase stabilization and control using a transmission grating compressor and an AOPDF,” *Opt. Lett.* **34**, 1333–1335 (2009).
- [207] S. Koke, C. Grebing, H. Frei, A. Anderson, A. Assion, and G. Steinmeyer, “Direct frequency comb synthesis with arbitrary offset and shot-noise-limited phase noise,” *Nat. Photon.* **4**, 462–465 (2010).
- [208] J.-F. Hergott *et al.*, “Carrier-Envelope Phase stabilization of a 20 W, grating based, chirped-pulse amplified laser, using Electro-Optic effect in a LiNbO₃ crystal,” *Opt. Express* **19**, 19935–19941 (2011).

- [209] M. Takeda, H. Ina, and S. Kobayashi, “Fourier-transform method of fringe-pattern analysis for computer-based topography and interferometry,” *J. Opt. Soc. Am.* **72**, 156–160 (1982).
- [210] M. Kakehata, Y. Fujihira, H. Takada, Y. Kobayashi, K. Torizuka, T. Homma, and H. Takahashi, “Measurements of carrier-envelope phase changes of 100-Hz amplified laser pulses,” *Appl. Phys. B* **74**, 43–50 (2002).
- [211] H. Wang, M. Chini, E. Moon, H. Mashiko, C. Li, and Z. Chang, “Coupling between energy and phase in hollow-core fiber based f-to-2f interferometers,” *Opt. Express* **17**, 12082–12089 (2009).
- [212] C. Li, E. Moon, H. Mashiko, H. Wang, C. M. Nakamura, J. Tackett, and Z. Chang, “Mechanism of phase-energy coupling in f-to-2f interferometry,” *Appl. Opt.* **48**, 1303–1307 (2009).
- [213] H. Wang, C. Li, J. Tackett, H. Mashiko, C. M. Nakamura, E. Moon, and Z. Chang, “Power locking of high-repetition-rate chirped pulse amplifiers,” *Appl. Phys. B* **89**, 275–279 (2007).
- [214] O. Tcherbakoff, E. Mével, D. Descamps, J. Plumridge, and E. Constant, “Time-gated high-order harmonic generation,” *Phys. Rev. A* **68**, 043804 (2003).
- [215] Z. Chang, “Single attosecond pulse and xuv supercontinuum in the high-order harmonic plateau,” *Phys. Rev. A* **70**, 043802 (2004).
- [216] J. Mauritsson, P. Johnsson, E. Gustafsson, A. L’Huillier, K. J. Schafer, and M. B. Gaarde, “Attosecond Pulse Trains Generated Using Two Color Laser Fields,” *Phys. Rev. Lett.* **97**, 013001 (2006).
- [217] Y. Oishi, M. Kaku, A. Suda, F. Kannari, and K. Midorikawa, “Generation of extreme ultraviolet continuum radiation driven by a sub-10-fs two-color field,” *Opt. Express* **14**, 7230–7237 (2006).

- [218] T. Pfeifer, L. Gallmann, M. J. Abel, D. M. Neumark, and S. R. Leone, “Single attosecond pulse generation in the multicycle-driver regime by adding a weak second-harmonic field,” *Opt. Lett.* **31**, 975–977 (2006).
- [219] Z. Chang, “Controlling attosecond pulse generation with a double optical gating,” *Phys. Rev. A* **76**, 051403 (2007).
- [220] H. Mashiko, S. Gilbertson, C. Li, S. D. Khan, M. M. Shakya, E. Moon, and Z. Chang, “Double Optical Gating of High-Order Harmonic Generation with Carrier-Envelope Phase Stabilized Lasers,” *Phys. Rev. Lett.* **100**, 103906 (2008).
- [221] E. Cunningham and Z. Chang, “Optical Gating With Asymmetric Field Ratios for Isolated Attosecond Pulse Generation,” *IEEE J. Sel. Topics Quantum Electron.* **21**, 1–6 (2015).
- [222] M. Ammosov, N. Delone, and V. Krainov, “Tunnel ionization of complex atoms and of atomic ions in an alternating electromagnetic field,” *Sov. Phys. JETP* **64**, 1191–1194 (1986).
- [223] Z. Chang, *Fundamentals of Attosecond Optics*, 1st ed. (CRC Press, 2011), pp. 182.
- [224] Z. Chang, *Fundamentals of Attosecond Optics*, 1st ed. (CRC Press, 2011), pp. 288.
- [225] J. L. Krause, K. J. Schafer, and K. C. Kulander, “High-order harmonic generation from atoms and ions in the high intensity regime,” *Phys. Rev. Lett.* **68** (1992).
- [226] C. Jin, A.-T. Le, and C. D. Lin, “Retrieval of target photorecombination cross sections from high-order harmonics generated in a macroscopic medium,” *Phys. Rev. A* **79**, 053413 (2009).
- [227] P.-C. Li and S.-I. Chu, “Effects of macroscopic propagation on spectra of broadband supercontinuum harmonics and isolated-attosecond-pulse generation: Coherent control of the electron quantum trajectories in two-color laser fields,” *Phys. Rev. A* **86**, 013411 (2012).

- [228] Z. Chang, “Chirp of the single attosecond pulse generated by a polarization gating,” *Phys. Rev. A* **71**, 023813 (2005).
- [229] K. T. Kim, C. M. Kim, M.-G. Baik, G. Umesh, and C. H. Nam, “Single sub-50-attosecond pulse generation from chirp-compensated harmonic radiation using material dispersion,” *Phys. Rev. A* **69**, 051805 (2004).
- [230] B. E. Schmidt, N. Thiré, M. Boivin, A. Laramée, F. Poitras, G. Lebrun, T. Ozaki, H. Ibrahim, and F. Légaré, “Frequency domain optical parametric amplification,” *Nat. Commun.* **5**, 1–8 (2014).
- [231] J. Peatross and M. Ware, *Physics of Light and Optics* (2015), pp. 56–57.
- [232] J. Peatross and M. Ware, *Physics of Light and Optics* (2015), pp. 145–147.
- [233] J. Peatross and M. Ware, *Physics of Light and Optics* (2015), pp. 180–182.